Flexible well patterns and Net Present Value (NPV) optimisation on large scale geothermal field development

Master thesis

to obtain the Master degree
at Delft University of Technology,
To be defended in public on the authority of the the thesis committee
on 25 May 2021 at 14:30 pm

by

Entela Kane

MSc in Applied Earth Sciences,
Track of Petroleum Engineering and Geosciences,
Department of Geosciences and Engineering,
Faculty of Civil Engineering and Geosciences
Delft University of Technology
Delft, The Netherlands

TU Delft Delft University of Technology

Student number: 4943104
Project duration: March, 2020 – May, 2021

This thesis has been approved by the thesis committee:

Prof. Dr. **David Bruhn**	Supervisor and Committee Chair	Professor	Delft University of Technology
Dr. Ir. **Olwijn Leeuwenburgh**	Daily supervisor	Senior Research Associate	Delft University of Technology
Ir. **Gerard Joosten**	Daily supervisor	Researcher	Shell Global Solutions International
Dr. **Rick Donselaar**	Supervisor	Associate Professor	Delft University of Technology

Keywords: Flexible Well Pattern, Global Optimisation, Large Scale Geothermal Development, Objective Function, Well Density Function

Keep Ithaca always in your mind.
Arriving there is what you're destined for.
But don't hurry the journey at all.
Better if it lasts for years,
so you're old by the time you reach the island,
wealthy with all you've gained on the way,
not expecting Ithaca to make you rich.
Konstantinos Kavafis

Dedicated to my parents, Vladimir and Majlinda, who taught me the values of education..

Contents

Acknowledgement

With this thesis I am walking towards the end of my studies at the Delft University of Technology. It started on a day of April 2018, when I received the acceptance letter for the Master studies and it finishes almost 3 years later....

To begin with I would like to address that this final project would have not came to a success without the contribution of several persons. First and foremost I want to thank my daily supervisors **Olwijn Leeuwenburgh** and **Gerard Joosten** who both have been so engaged during the entire process. Both of them gave me a great guidance, but also daily challenges and discussions to tackle different problems. The most important lesson from them was to me how to push my limits, communicate and collaborate and further develop my engineering skills. The COVID-19 conditions proved to be not an obstacle for my mentors trying always their best to assist and guide me with the clear goal being the quality of the research outcome.

I would like to thank **David Bruhn** for accepting my thesis and being the Chair of the Committee. I received a lot of knowledge from our discussions and your expertise on the geothermal field always impressed and motivated me. Special thanks go also to the geologist of my committee **Rick Donselaar** who assisted and motivated the geological aspect of this geothermal project.

I would also to express my gratitude to **Alexandros Daniilidis** for actively being engaged in my project and offering his comments on the economical model. His knowledge and advice enriched and improved the quality of this project. For this project also contributed **Denis Voskov** and his PhD student **Xiaoming Tian** who were always there to answer my questions regarding the DARTS reservoir simulator.

My family, my stepping stone, mother and father, and sister, a big thank you for giving everything you had in your life to ensure that your child will acquire qualifications with the hope to be a productive person in this society, as you are. You showed me that great work never comes in a comfort zone. Thank you for supporting me financially and ethically in these difficult times.

I would like to express gratitude to my friends here in the Netherlands as well as in Greece for keeping in touch and staying connected. It was a challenging period that staying connected was really important. Martijn, I have to thank you as well for the time we spent together working and having all the scientific discussions.

Abstract

The Netherlands has set the ambitious goal to be CO2 neutral by 2050 and signed the Paris Treaty in 2015. The contribution of geothermal energy to reaching this goal are outlined in the Masterplan in 2018 which attempts to reduce CO2 emissions. It is imperative to enhance geothermal participation in renewable energy resources, so this thesis proposes a consideration of large scale geothermal field development in order to meet these requirements. For these large scale projects, large scale geological heterogeneities must be taken into account in order to propose a development strategy that honours subsurface variability in properties like porosity or permeability of an aquifer. Furthermore, the nature of the large scale operations, inherently requires the consideration and application of well patterns typically used in oil and gas developments. Operating in these extensive domains, carries a lot of uncertainty in the final economical output of the project, so modelling the process could indicate the optimal conditions that would deliver the best possible operational outcome. Conceptual 2D model approaches were adopted to demonstrate the main ideas behind large-scale geothermal well pattern optimisation.

The main objective of this project is to model, evaluate and optimise the performance of large scale geothermal field development. The proposed strategy is based on the use of well patterns as are frequently used in the oil industry. The heterogeneity in geological properties that may be expected to be encountered at larger spatial scales is addressed by the concept of a flexible well density function. This density function allows the well patterns to be resized (or ultimately, reshaped) and adapt to spatial variations in geological characteristics. The flexible well pattern is fed to an objective function created with embedded simulator. The output of the function is the net present value (NPV) of the project. Four test cases are created, starting with a homogeneous static model and building up more heterogeneous aquifer models, aiming to test the performance of the flexible well density function. The aquifer property models are representative of the West Netherlands Basin and specifically the Delft Sandstone Member. Per each aquifer model, line drive and 5-spot development strategies are assessed. Each development scenario is modeled in an objective function and optimised. The optimisation algorithm chosen is the Simplicial Homology Global Optimisation, suitable for black-box functions that show multiple local optimum solution and among them, a global optimum pattern size is found. The NPV of each project realisation is calculated based on the energy recovered and an economic model under Dutch fiscal conditions.

The results suggest that, the flexible well placement is successfully aligning with the different aquifer geological properties. Pattern size is inversely correlated to porosity which corresponds to higher volume of pore fluid from which heat can be recovered. The optimisation algorithm managed to identify the global optimum solution of pattern size that delivers the highest possible positive NPV. The most efficient in terms of profitable strategy, is suggested to be the 5-spot pattern. The optimal pattern size ranges between 500 - 2160m depending on the aquifer model. The sweep efficiency, in terms of energy recovery, is also assessed per aquifer model and development strategy. The most efficient is the 5-spot pattern.

The performance of the adopted optimisation algorithm, on the fully homogeneous aquifer, is tested with an exhaustive response curve of NPV. It is confirmed that the algorithm manages to identify the global optimum. The character of the NPV as a function of well pattern size/density proved the complexity of the system with respect to the amount and well types introduced. Different sensitivity analyses in the context of the uncertainty of the aquifer thickness, thermal conductivity property and full economic model are conducted in order to show the impact on the optimal patter size. The performance of the optimisation algorithm is assessed as well, indicating that further investigation on the tuning meta-parameters could potentially lead to better global optimum solutions in more heterogeneous aquifer models.

List of Figures

List of Tables

Chapter 1

Introduction

1.1 Geothermal Energy in the Netherlands

Geothermal energy is on the rise and is a promising, renewable energy source that can deliver baseload energy for industrial, domestic usage (Ministry of Economic Affairs and Climate Policy 2021). Hot water can be exploited at a temperature of 45-120 °C, by pumping it out of the aquifers—depths of exploitation range between 1.5 to 4 kilometres. As of January 2020, the Ministry of Economic Affairs and Climate Policy declared 58 Exploration licences for geothermal energy, 22 production licences for geothermal energy in the Netherlands (Figure 1.1).

In 2015, 195 countries agreed to reduce greenhouse gasses emissions and maintain the maximum rise of the average temperature on Earth below 1.5-2°C. The Dutch government (Schoots & Hammingh 2019) pledged to reduce greenhouse gas emissions by 40% in 2030 and 95%in 2050. The contribution from geothermal energy is planned to deliver a total CO2 reduction of 3 megatons in 2030 and 12 megatons in 2050. Between now and 2030, geothermal energy contribution is expected to increase from 0.5% of total heat production to 5%, increasing to 23% by 2050 . This implies the necessity of bringing more and more areas with geothermal potential in production to meet the preset requirements.

The annual primary energy consumption in the Netherlands is around 3000 PJ. Currently, 91% of the Netherlands' energy comes from fossil fuels combustion, and 36% comes from natural gas. Renewable energy covers 5% of that amount (ING 2018), as shown in Figure 1.3. 2.0 % (3.7 PJ) of that is covered by geothermal heat. As shown in Figure 1.4, 30% of coal, oil and gas shares are utilised in industry, 35% of gas counts for domestic heating, 65% of oil in transportation and 75% of coal in the sector of electricity. It is inferred that there is a need to reduce these conventional energy sources and replace them later with cleaner forms.

Current geothermal sources in the Netherlands emit on average 13 kg CO2/GJ, which is an 80% reduction compared to 66 kg CO2/GJ emissions from hydrocarbon sources (Stichting Platform Geothermie 2019). This makes geothermal energy a source with high potential for the Dutch government to accelerate the energy transition and reduce CO2 emissions. A master plan was set in 2018 by a collaboration of geothermal organisations EBN, DAGO, Stichting Platform Geothermie, Stichting Warmtenetwerk to stimulate the acceleration of sustainable energy production in the Netherlands and accelerate geothermal energy applications' development (Schoof et al. 2018). One PJ per year can provide heat to approximately 20,000 households in the Netherlands. To meet this target, geothermal developments in the Netherlands need to be accelerated and extended to produce many more geothermal wells. More than 20 geothermal well doublets are currently operating in the Netherlands, almost all used for providing heat to greenhouses. The average temperature gradient in the Netherlands is about 30°C/km. Based on this fact, in depths greater than 1 km, temperatures can be found up to 100 . Thus, the heat extracted from pore fluid should be utilised by bringing it into geothermal production fields with many more wells.

There are three types of heat applications from the subsurface (Schoof et al. 2018). The present geothermal production wells per depth are also shown in Fig. 1.2. Types of geothermal applications:

- Shallow geothermal: everything up to 500m deep. It is primarily used for excess heat cold storage (HCS), also known as Aquifer Thermal Energy Storage (ATES). It is the most common type in the Netherlands, with around 2500 projects (Provoost et al. 2018). This type is often used for buildings during high demand for heat in the winters or cold in the summers.

- Deep geothermal: projects that target between 500-4000m depth, but often reaching 2-3 km depth. At depths up to 1,000 metres, the temperatures (30-40 °C) are not always high enough for direct use with current technology; a fact that requires a heat pump is to increase the temperature to a certain level. From 2,000 metres, temperatures between 70-100 °C can be reached. It can be used for geothermal heat production in greenhouses or urban heat-networks for domestic heating. This type of geothermal installations provides geothermal heat generated in the Netherlands nowadays (3.7 PJ) (CBS Statline 2021).

- Ultra-deep geothermal: UDG energy is planned to be extracted at depths of more than 4,000 metres. Heat is produced with temperatures above 130 °C. This type can be used in industry and for electricity production. It

has not yet been developed in the Netherlands; therefore, more research needs to be conducted on this kind of projects.

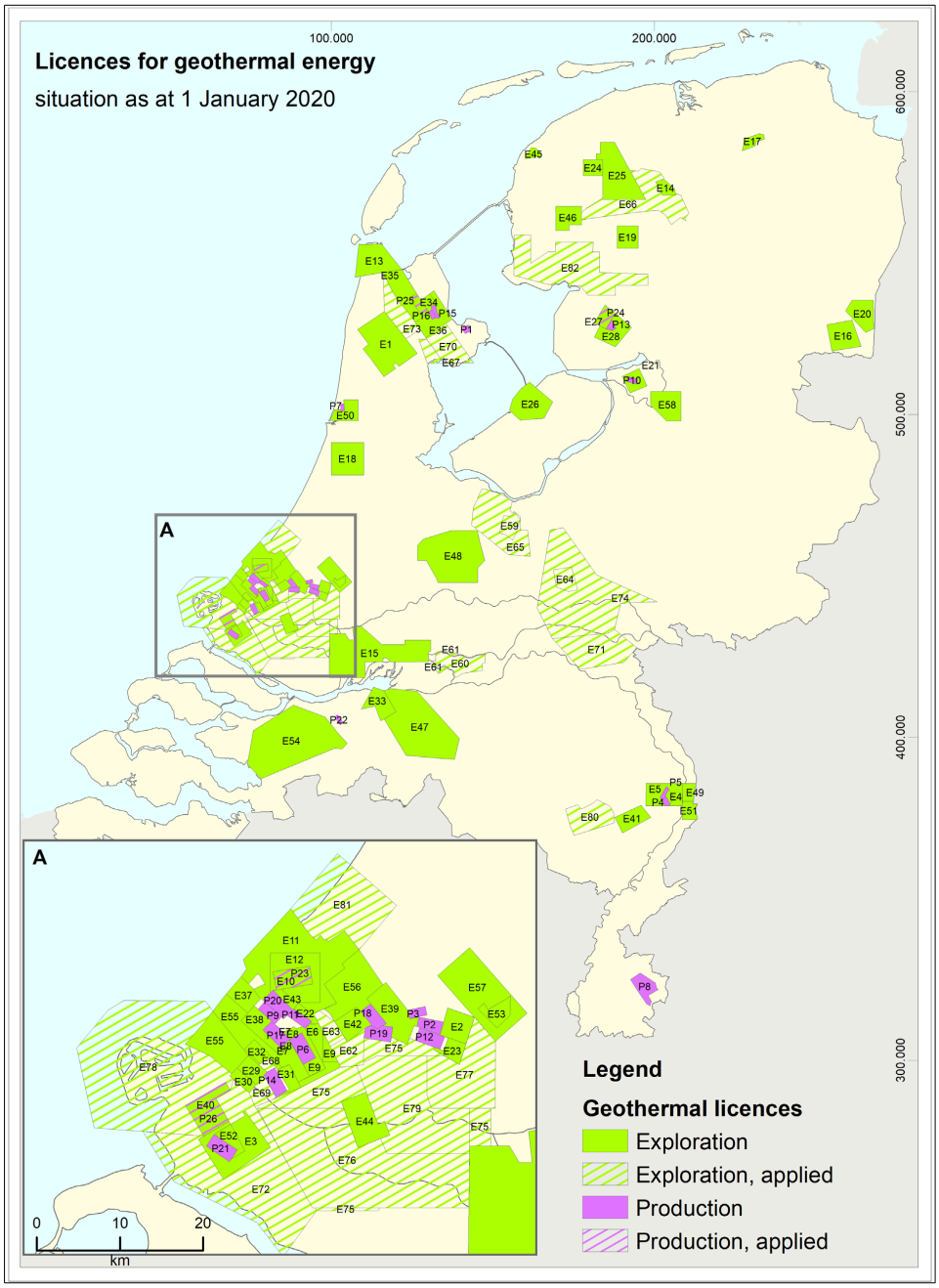

Figure 1.1: Licences for geothermal energy as 1 January 2020 (Ministry of Economic Affairs and Climate Policy 2021).

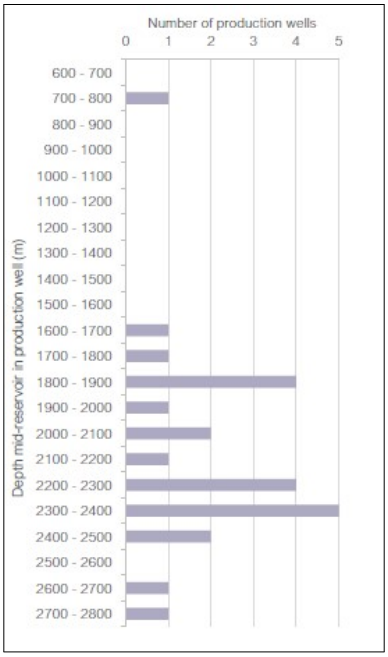

Figure 1.2: Depth to mid of aquifer and corresponding number of geothermal production wells (Ministry of Economic Affairs and Climate Policy 2020).

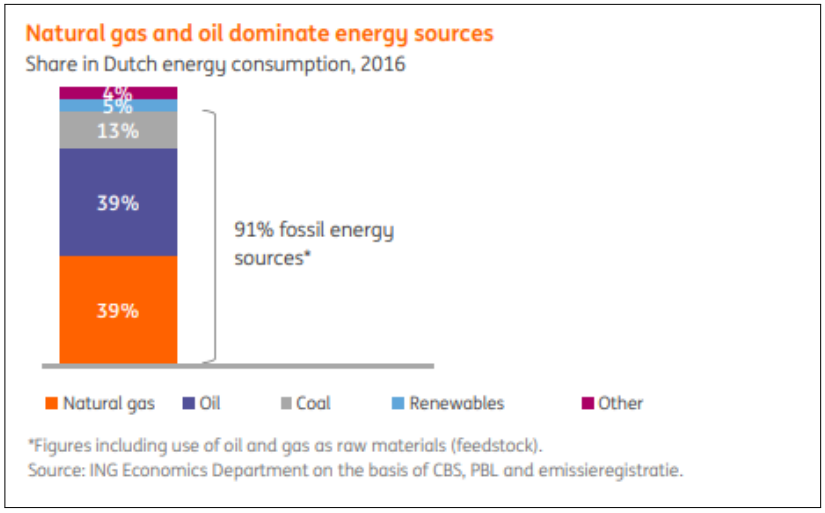

Figure 1.3: Share in Dutch energy consumption (ING Economics Department 2018).

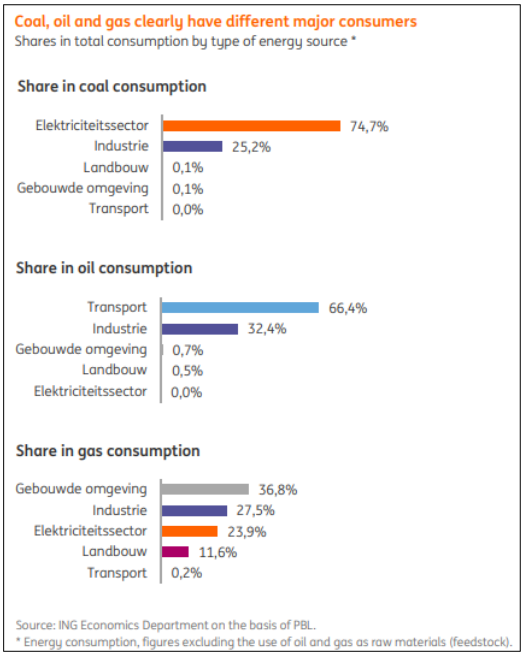

Figure 1.4: Shares in total consumption by type of energy source (ING Economics Department 2018).

1.2 From oil and gas to extensive scale geothermal development strategies

Field development for oil and gas purposes so far have adopted specific strategies in terms of well placement. The injection pattern for an operating field or part of a field is based on the location of existing wells, size of reservoir and shape, expenditures of new wells and the oil or gas recovery increase associated with various injection patterns. The flood pattern can be changed during the life of a field to alter the direction of flow in a reservoir to contact unswept oil. It is a common strategy to reduce the pattern size by infill drilling, which improves oil recovery by increasing reservoir continuity between injectors and producers. Common injection patterns (Figure. 1.6Are direct line drive, staggered line drive, two-spot, three-spot, four-spot, five-spot, seven-spot and nine-spot. Normally, the two-spot and three-spot patterns are meant to be used for pilot testing purposes. The patterns are called normal or regular when they include only one production well per pattern. Patterns are called inverted when they include only one injection well per pattern.

In the geothermal energy domain, the common practice is to drill a doublet (an injection and production well pair) system for subsurface heat production (Figure 1.5). The injector-producer spacing at the surface may be very close to each other (just a few meters apart), while the spacing at depth typically varies between 1 to 2 km. One well produces hot water from a water-bearing geological formation. This is normally supported by an Electric Submersible Pump (ESP) located in the production well. First, a separator separates the geo-gas from the water. This gas can be transported to a boiler which supplies extra heat to the warm freshwater used in a secondary network providing consumers with heat. There are also cases where geo-gas is used to generate electricity. After the separator, production filters capture solids suspended in water formation to protect the heat exchanger against damage and clogging. After that, heat exchangers transfer heat from water formation to the freshwater network that goes to consumers. Pumps re-inject the cooled water through the second well into the same reservoir. This way, the reservoir pressure is maintained. If it remains in the reservoir, the water temperature can be restored to almost its original value after several decades. Still, the surrounding aquifer rock is cooled, such that a cold front develops and propagates with increasing time and injection.

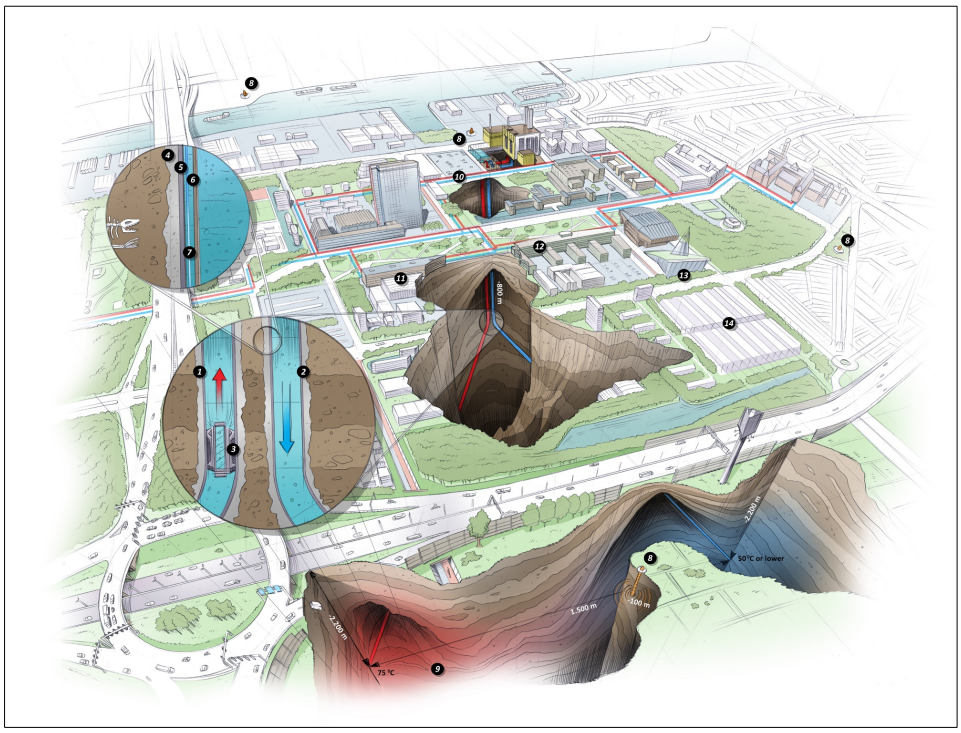

Figure 1.5: Visual representation of doublet that will be drilled at TU Delft campus (Stichting DAP 2021).

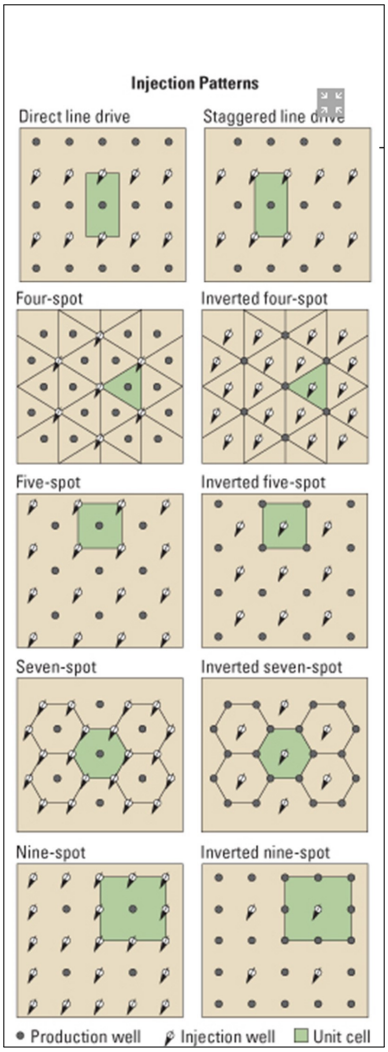

Figure 1.6: Regular and inverted pattern types used in oil and gas development (Schlumberger Oilfield Glossary 2021).

1.3 Large scale geothermal field developments

Field development strategies for hydrocarbons, as discussed above, adopt regular pattern sizes with or without any coordination in pattern sizes. When the well spacing is adapted and brought to an optimal value, the exploitation of the field is conducted in the optimal conditions, meaning that the possible heat is extracted in the given project lifetime, at the lowermost cost, and without any early cold water breakthrough in the producing wells. Any other uncoordinated strategy could lead to sub-optimal use of subsurface resources.

Willems (2017) in his doctorate thesis, suggested that the current geothermal policy in the Netherlands leads to an individual 'first come, first served' deployment. This means that a coordinated deployment could lead to increased heat production. Specifically, in one of the suggested development strategies of the Delft sandstone member, it was proven that an extension of the concept of doublets is necessary to bring a larger scale of geothermal field development. The specific field dimensions are restricted on the scale of 1 x 2 km and already implies that multiple doublets should be introduced to sweep the aquifer in a time frame of more than $\tilde{1}00$ years (Figure 1.7). Moreover, a suggestion is made to lower the well spacing to 800 m, which directly translates to more energy recovered in a time frame of 40 years.

Keeping this result in mind and the goal of this specific project which is to propose larger-scale field developments than the previously addressed, it is inferred that more wells should be brought into production to sweep extensive aquifers. The aquifers that will be brought into production need to be investigated in terms of heterogeneity. Willems 2017 suggested that when exploiting the area of Delft sandstone Member, it was critical to place the doublets aligned with the individual channels' paleo flow direction. When zooming out of these geological formations, a more upscaled framework should be applied. Generally, channels are restricted in their dimensions, on the scale of 10's-100's of meters but spatially can create formations extensive in width and length. These are channel belts and can be encountered at a larger scale of field development. The West Netherlands basin could be approached as a channel belt with a paleo flow direction of SE-NW, instead of single meandering channels that Willems showed in his work.

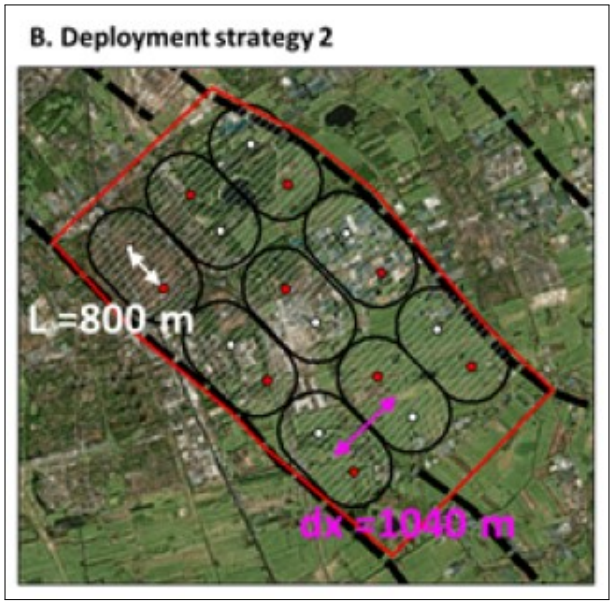

Figure 1.7: Delft Sandstone proposed development strategy with multiple doublets (Willems 2017).

But what is the scope of considering these large scale field developments? Again, the same author proved that from his much smaller investigated field, in different development strategies, a production heat rate in the range of 0.83 - 2.5 PJ/year translated to 230,56 - 694,44 GWh/year. Expanding production in much larger exploiting areas could shoot up the produced energy and significantly impact geothermal energy participation in renewable energy and the overall contribution (Fig 1.3). If the same field is repeated ten times, the energy produced would potentially also increase ten times. Another aspect that could be encountered when applying exploitation in large scale fields is the impact of faults and fractures. Most fractures could act both as flow barriers or flow paths. This directly affects the flow patterns altering the flow paths and delaying the cold front arrival. On the other hand, it could accelerate cold water breakthrough in producer wells if faults are aligned with the injector - producer direction or diverging the cold waterfront from its original pathway if the faults are not aligned with the injector-producer direction. In the Delft Sandstone scale, faults are proved to be present, creating blocks like Delft-Pijnacker and the Westland block. Thus, these kinds of geological structures should also be taken into consideration. Here, to demonstrate the concept of (flexible) well pattern development, we focus exclusively on the heterogeneity introduced in rock properties by variations in depositional processes.

1.4 Flexible Well Pattern application

The doublets concept can cover a limited production area since doublet spacing is limited to 1-2 km in the greater depths drilled. There have been applied strategies of repeated doublets (Willems, Nick, Goense & Bruhn 2017, Willems & Nick 2019), that can be translated as a line drive (Willems, Nick, Weltje & Bruhn 2017, Mijnlieff et al. 2009). The question is, what would be the most appropriate strategy to deal with more significantly greater areas than those produced so far?

The necessity of larger fields to be operated in order to cover the demand in different sectors like heating or electricity generation is already discussed. Based on this idea, the concept of individual and uncoordinated placement of doublets in geothermal applications is expected to lead to sub-optimal recovery of heat, and therefore cover this great energy demand. The transition from small to large scale fields can be implemented with the application of well patterns similar to oil and gas field development (Willems, Nick, Goense & Bruhn 2017, Kahrobaei et al. 2019). The main goal behind such an approach is to find which combinations of initial reservoir and production conditions and well development strategy will maximise production in a given field, taking into account the geological properties of an aquifer like porosity, permeability and thickness.

Adding a hint of complexity to the concept of large scale geothermal developments, flexible well patterns can be considered a basis of adapting current practices applied concerning heterogeneity in the subsurface. This is a crucial aspect of the significant impact of heterogeneity and high uncertainty of geological structures and formations present in the subsurface on flow paths and injectivity and productivity. The concept is that geological formations with higher porosity imply a higher volume of warm brine to be swept and extracted; thus, more wells could be introduced for a given flow rate capacity and field life expectancy. A balance between the pattern size and timing of cold water breakthrough is also considered given a lifetime of a project, and no early breakthrough should be observed before that. As far as the field permeability and pattern size are concerned, they should be positively correlated. Hence, higher permeability fields should be developed with larger pattern sizes to avoid early cold water breakthrough before the end of the project lifetime. The impact of each geological property (porosity, permeability) on pattern size is

described, but what about when both properties are coexisting, and what should the result look like? The approach of taking into account both porosity and permeability is the most realistic given that permeability is inherently correlated to porosity. So higher porosity leads to a higher permeability. The timing of cold water breakthrough has the greatest impact on a geothermal project life time. The timing of breakthrough is directly linked to the geological properties of the aquifer. Higher porosity would require smaller pattern sizes, to delay the cold from arrival on the producer wells, but higher permeability should balance the pattern size not to be that small that would cause early cold water breakthrough.

Flexible well patterns with global parameters (squeeze, shear, rotate) have already been applied in oil and gas field development but not with parameters impacting locally varying density and specifically in geothermal. The term of flexibility encompasses the freedom of changing the locations of the injectors and producers to accomplish a given goal (maximising production, extending project lifetime etc.) This was addressed by **??**, who proved that applying this concept could optimise heat recovered. The flexibility and optimisation of pattern sizes are two different terms but strongly related since the first term reveals room for improvement. An introduction to the concept of optimisation is going to be described in the following subsection.

1.5 Well pattern optimisation

Fixed well pattern development is defined as the repeated placement of a well pattern of constant size. Flexible well pattern development will is defined as a repeated application of a base pattern with a spatial adaptation of the pattern sizes or shapes to local geological heterogeneity. Both concepts have been considered in the oil field development literature. Optimisation methods, gradient-based and derivative-free techniques, have been used to determine optimal location of wells in an oil field (well-placement optimisation). However, because reservoir heterogeneity gives rise to non-regular objective function surfaces, with multiple local optima with significantly different objective function values (Onwunalu & Durlofsky 2010), the well-placement optimization problems have been frequently solved using stochastic derivative-free methods which are able to avoid getting trapped in a local optima, because they do not strongly depend on the initial guess of the optimisation like the gradient-based method. Other methodologies like Genetic Algorithm (Badru & Kabir 2003), Particle Swarm Optimization (Onwunalu & Durlofsky 2009, 2010, 2011) or Covariance Matrix Adaptation Evolution Strategy (Bouzarkouna et al. 2013), have also been used to solve the well-placement optimization problem. Some authors have considered the use of gradient-based algorithms to determine optimal well locations (Sarma et al. 2008, Forouzanfar et al. 2010, Zhang et al. 2010). These methodologies have been considered for the context of this project.

As previously stated, introducing flexibility in a well pattern is motivated by the fact that some room for improvement of energy recovery or the lifetime of a project is required. So flexibility in a well pattern and lifetime of a project is a relationship between cause and effect. This concept can be described in the context of mathematics as a model; therefore, creating a function that would take as input a well pattern size and output energy recovered can deliver that: a pattern should be flexible to improve its target. The concept of optimisation is introduced to mathematically describe the conditions and input of the model under which it will deliver the optimal solution. This process has been extensively described and utilised in oil and gas field developments (Chen et al. 2017) and geothermal alike (Kahrobaei et al. 2019). The detailed concept is explained in the Methodology chapter.

1.6 Research questions

These are the main ideas and questions that will be addressed in this project :

- Is geothermal field development feasible at larger scales than the already applied, feasible? What is the development scale that needs to be considered to reach the contribution of geothermal energy cover the regional or national heat demand?
- What conditions make developments beyond well doublets desirable? Are well patterns used for oil and gas fields also applicable to geothermal field exploitation, and to what extent?
- Is well placement, in the forms of standard well patterns used for oil and gas field development, flexible for geothermal field development? If yes, how should the pattern size adapt to local geological features?
- How should the automatic distortion of well pattern be modelled? What is the term that should be set as the output, and what is an input in the defined modelling process?
- Can this model or so-called objective function be optimised? Which type of optimisation technique would be suited to address the well pattern optimisation problem, and how will it perform in selected test cases?
- Is there still room for improvements in the optimal development decision proposed by the optimisation algorithm in different development strategies?

1.7 Research approach description

Since the research questions are set, it is necessary to propose a workflow that will explain in detail which steps need to be accomplished and develop a working methodology that will address the answers to the research questions. A proposed detailed workflow is presented below. A schematic diagram is presented in figure1.8.

Starting from scratch, different geological models will be constructed with increasing complexity. For the first basic model, is proposed a homogeneous porosity and permeability equal in both horizontal directions and significantly smaller in the third dimension, so horizontal flow is enhanced. This model can be generated in Python, and different permeability values are assigned. This model is then used as the basis for simulations in a dynamic model. As the study is developed with reservoir conditions typical for the Netherlands, fully saturated with brine, so steam (vapour) is not included in fluid flow. In addition to the fluid flow, the thermal term will be taken into account. So brine saturation and temperature are modelled both in time and space. A reservoir simulator chosen for this study, is DARTS (Delft Advanced Research Terra Simulator). It is based on the Operator-Based Linearization (OBL) approach, utilised for forward and inverse problems in petroleum engineering, low- and high-enthalpy geothermal applications, subsurface storage and subsurface integrity (Voskov 2017). Well patterns used for oil and gas field development projects will be introduced and placed in the present reservoir. For geometrical reasons, the wells should be firstly placed in a larger field. In that field, filled with wells, the license area for production will be placed. When the well pattern is stretched and squeezed during the optimisation process, wells will cover the whole licence block. Restrictions for the well placed next to the licence area borders have been applied if the wells produce from the same reservoir. This way, the well communication between neighbouring license is restricted or ideally eliminated. For the construction of the objective function, well density or the pattern size will be used as input for the model. Several terms can be considered as an output of that function. The DARTS simulator will be embedded in the objective function. Total energy recovered is the output of the simulation. In addition, the net present value is calculated with all costs contributing to the expenses, extra revenues from subsidies or well drilling and completion. A detailed economic model will be presented with the most updated market values incorporated in the desired function. After setting an objective function, the next step is the optimisation part. The number of input parameters, the continuous or discrete nature of those parameters, the ability to extract gradients from the objective function will determine the optimisation type. The optimisation starts with one control at the objective function like the well spacing equal in both horizontal directions. Such a pattern is appropriate if geological homogeneity is present in both horizontal directions. The next step is to consider the well spacing flexible in both horizontal directions. This strategy is proposed when the geological model entails different permeability spatially. Based on the optimisation type that is implemented, it must be ensured that the optimum of the function is the global optimum and the optimisation procedure is not trapped in local optima that might be present. A pre-screening of the output of the function is proposed to ensure robust results. If the termination criteria of the function are met, then work is finished. For example, if the function output is the NPV of the project, then the optimiser should output a positive value to make sure the project is profitable. If not, a loop is needed that redirects the workflow to step 1. There might be significant numbers of loops needed until the goal is met.

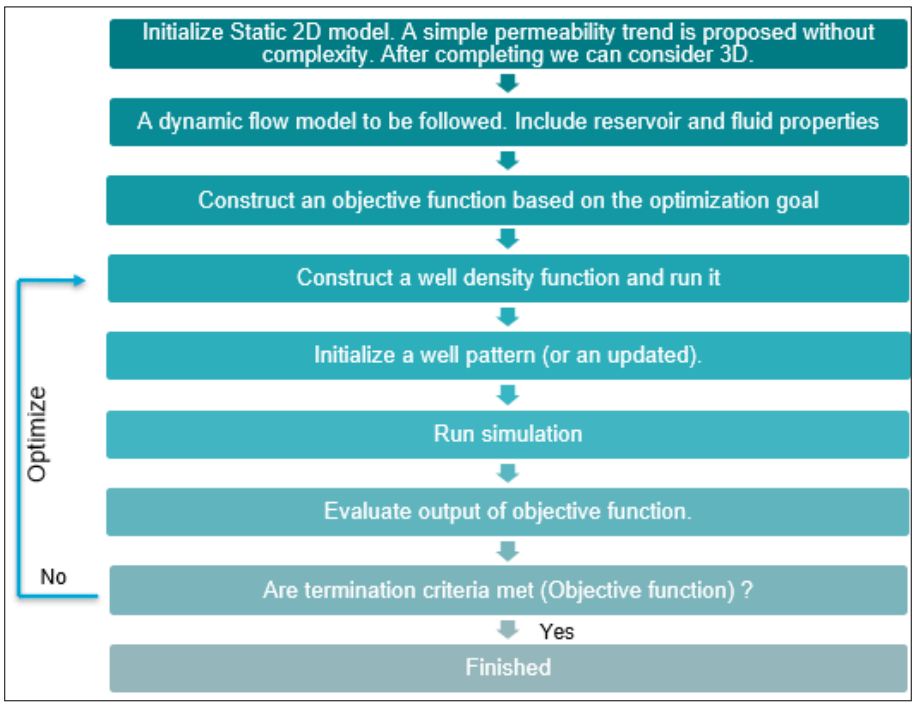

Figure 1.8: Proposed workflow diagram.

1.8 Proof of concept

This study attempts to combine the concept of NPV optimisation of large scale geothermal development with a realistic geological background. The main concept to be proven in this project, is the concept of optimisability of flexible well patterns, and that given the complexity of this multi-well system, we've chosen to make the physical system (both concerning wells and reservoir) as simple as possible.

Every kind of reservoir-aquifer development requires to be modelled under the highest possible realistic basis of both subsurface and development conditions. As far as the **subsurface conditions** are concerned, for the sake of this project, there are generated synthetic models that attempt to approximate some of the geothermal targets from the Dutch subsurface. Therefore a realistic basis is created in terms of property modeling and dimensions of the geothermal aquifers. Albeit the realistic background, some concept modifications, for sake of proving the basic concept of NPV optimisation on large scale geothermal developments, is required. Hence, some aspects on property modelling are deviating from typical range of values of Dutch subsurface, in order to prove and fully grasp the results of the project and make interpretation easier, given the imposed injection and production constraints. For a realistic field case, all the essential realism should be built in bit by bit (well rate and pressure constraints; model boundary conditions; etc.)

As far as the **development conditions** are concerned, reservoir production and injection constrains is a fundamental aspect that needs to be defined before the production starts. In this project, a fixed injection flow rate and fixed production pressure is imposed. There are other possibilities also, but we chose this owing to keeping the the production dependent to the facies, therefore porosity and permeability spatial distribution. Discrepancies in porosity-permeability, would create discrepancies of pressure distribution if production was done under fixed rate. To avoid this, a fixed bottom hole production pressure will be imposed and the flow rates will be flexible to tune with the pressure.

Chapter 2

Well density function

2.1 Well pattern definition

Well patterns are the particular arrangement of production and injection wells typical for oil and gas field development to maximise production. Common patterns are direct line drive, staggered line drive, two-spot, three-spot, four-spot, five-spot, seven-spot and nine-spot. The patterns are called normal or regular when they include only one production well per pattern. Patterns are described as inverted when they have only one injection well per pattern. This project aims to adopt this technique and use it for geothermal field development.

Typically well doublets are used for geothermal exploitation. As of 1 January 2020, there were a total of 24 geothermal production installations in the Netherlands that (will) produce heat from the deep subsurface (Figure 2.1). In general, these installations are named doublets as they consist of two wells (Ministry of Economic Affairs and Climate Policy 2020). So the next indicated step is well pattern application.

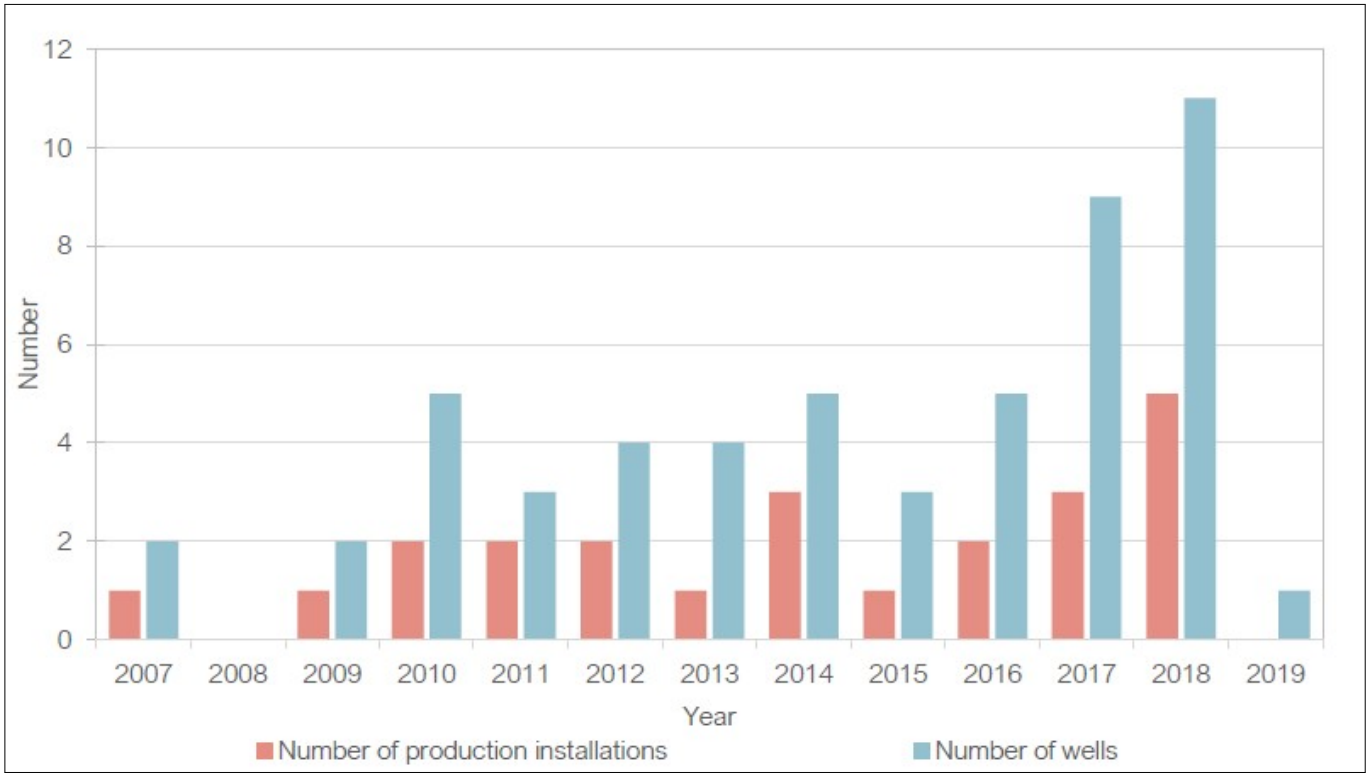

Figure 2.1: Number of geothermal wells completed (side-tracks excluded) per calendar year and the number of installations completed since 2007. All of the active facilities operate under a formal production licence (as of 1 January 2020). At the end of 2019, not all producing operators owned a formal production licence or had applied for one (Ministry of Economic Affairs and Climate Policy 2020).

2.2 Regular well pattern size

Well pattern operators define the geometric operations that can be implemented in well patterns to change their shape, size, orientation, type, and well locations. (Onwunalu & Durlofsky 2009, 2011) proposed these global operators for application in oil and gas field development:

- Scaling operator that increases the size of the pattern.
- Rotation operator that rotates the pattern.
- Switching operator changes the pattern type from standard to inverted by changing the location of producer wells with one of the injection wells and vice versa.
- Shearing operator that skews the shape of the well pattern.

These operators generally require a reference well whose location will remain unchanged after the application of operators. Moreover, when changing the shape of the pattern, angles can be used for this purpose. The value of an angle is positive for a change in a clockwise direction (+) and negative for an anticlockwise direction (-).

For this project, only the **scaling operator** will be implemented for geothermal field development. Initially, a Cartesian rectangle field is created, which will be covered with wells. It is going to be named the testing field. This testing field does not correspond to the license area that is going to be exploited. A reference well- per well type (injector-producer), is defined and fit with an offset of preference from the origin x,y = 0,0 principal axis. Considering the first injector and producer location (x,y), the following well locations are extrapolated and placed every N grid blocks, which correspond to a step or well spacing between adjacent wells of a similar type (adjacent injectors and neighbouring producers). This extrapolation is implemented in both, the x and y direction to fill the whole domain with wells. When the wells fill the entire testing field, the operator is applied based on the horizontal and vertical injector-producer distance components.

Defining a pattern size as regular means that an original pattern size is repeated with the same value and fills the operating domain. The pattern size is described in x, y-directions. An isotropic pattern size can be with the x value = y value or x value ≠ y value. The latter, where the x value ≠ y value, refers to the shape size of the pattern and is adjusted based on the geology of the operated field.

Scaling operator ($O_{scaling}$) increases or decreases the size of a well pattern (Figure 2.2). The operator begins placing production and injection wells with different offsets from the origin of the x, y-axis (0,0) as defined by the geometric requirements of each well pattern. The actual arguments of this operator are the horizontal and vertical spacing between two injectors or two producers. This way, the flexibility of assigning different scaling of well spacing per direction or keeping it fixed in both directions, is ensured. The actual distance between producers or injectors plus the scaling factor(s) serve as the components of calculating the genuine injector - producer distance per well pair.

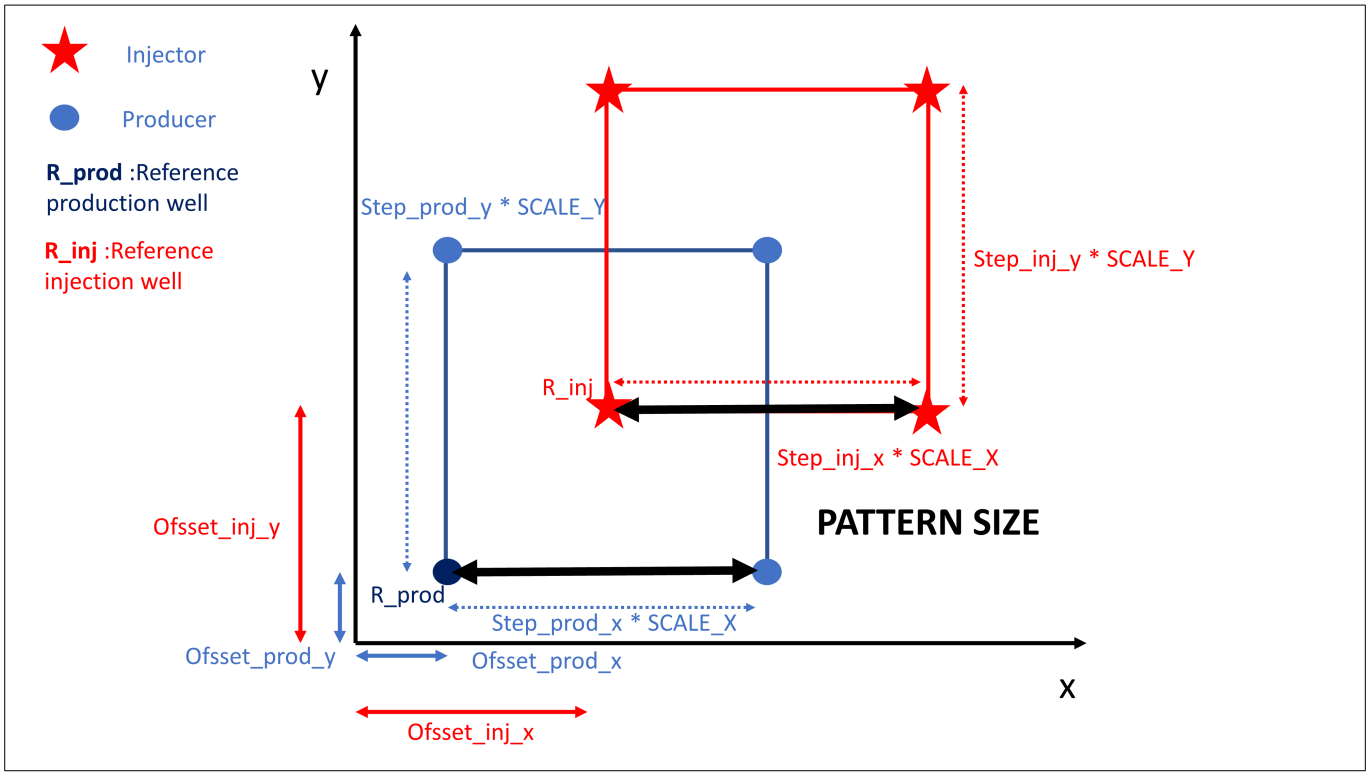

Figure 2.2: Well pattern initialization with scaling factor $Scale_x$ and $Scale_y$ [1,1] for both injectors and producers.

When the whole testing field is filled with the well pattern, scaling factors per direction can be applied and are shown in the following figures 2.3, 2.4.

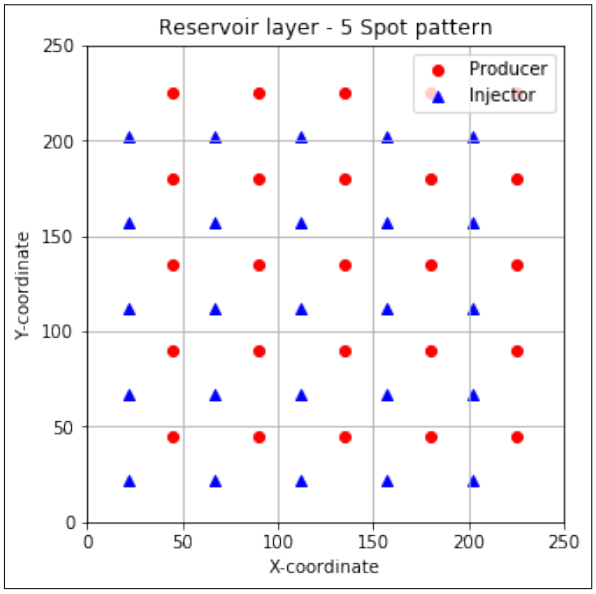

Figure 2.3: Isotropic 5 spot well pattern with scaling factor $Scale_x$ and $Scale_y$ [x,y] with x=y, for both injectors and producers, with respect to the initial inter-producers and inter-injector distances.

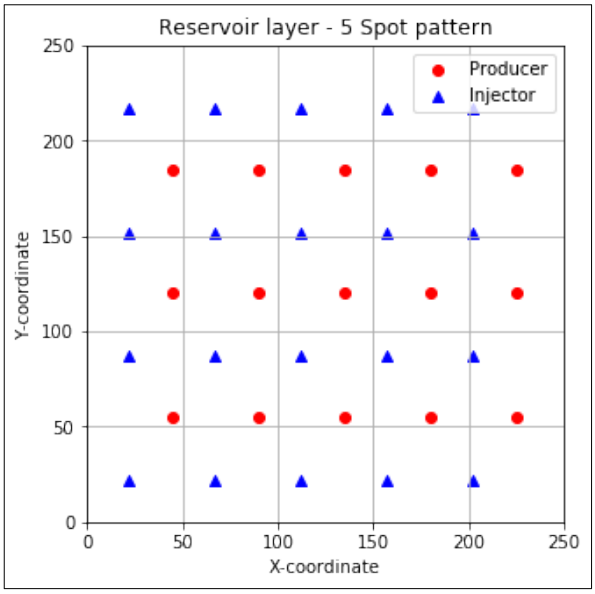

Figure 2.4: Isotropic 5 spot well pattern with scaling factor $Scale_x$ and $Scale_y$ [x,y] with x $\neq$ y, for both injectors and producers, with respect to the initial inter-producers and inter-injector distances.

2.3 Flexible well pattern size

More complex cases than a uniform aquifer property distribution need to develop a more flexible strategy in placing wells. A flexible well pattern concept requires a heterogeneous geological realisation that will be the input to the simulator. This heterogeneity may refer to either porosity or permeability. The property is needed to be modelled with a function. This property distribution could be a natural trend or a channelized feature observed in field data. Still, for the sake of this proof of concept study, we will describe the property trend with a function, thus making a synthetic property field. So a prior knowledge of property distribution is necessary. This function addresses the spatial variation of the modelled property. This implies that the property can be described with a different function per direction (x,y,z). Only 1D (x or y) or 2D (x,y directions) are taken into account in this project. When a function describes the property trend in the x-direction and y-direction, it is constant, and then only one function is required to describe the geological system. When the property is not consistent also in the y-direction, then another function needs to be introduced. All type of functions can be considered since they describe a realistic geological model.

2.3.1 Porosity modelling with linear function

The first property to be described is porosity by the model/function, with a linear distribution in the x-direction. Porosity in the y-direction is not changing. Then a function in the form of Equation 2.5 is used. Parameters a,b are used to manipulate the output of the porosity model.

$$\phi = -a * x + b \tag{2.1}$$

where:

- $a = \frac{\phi_{max} - \phi_{min}}{nx}$ where nx is the x-dimension of the field in grid blocks.
- b is minimum porosity (ϕ_{min}) of the field

Figure 2.5 represents the output of the porosity function with a = 0.00064, b = 0.12. Figure 2.6 is a 2D representation of the porosity field.

After the function that describes the geological model is adopted, a modification is required to transform it into a function that would introduce flexible well placement. For example, the area with higher porosity corresponds to a higher volume of warm water than the area with lower porosity. It is important impose constraints of isotropic permeability in all geological formations, if the focus in om warm water volume swept. Normally higher porosity implies higher permeability; thus, fewer wells are necessary to sweep the area. The adopted concept is counter-intuitive, but it serves the concept of well density function in simple synthetic models. Building up the complexity of the problem, permeability for a real case has to be included.

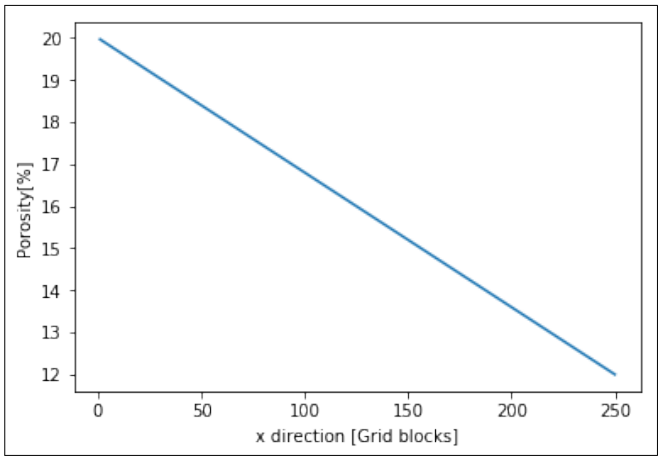

Figure 2.5: Porosity distribution of a field in x-direction, modeled with a linear function.

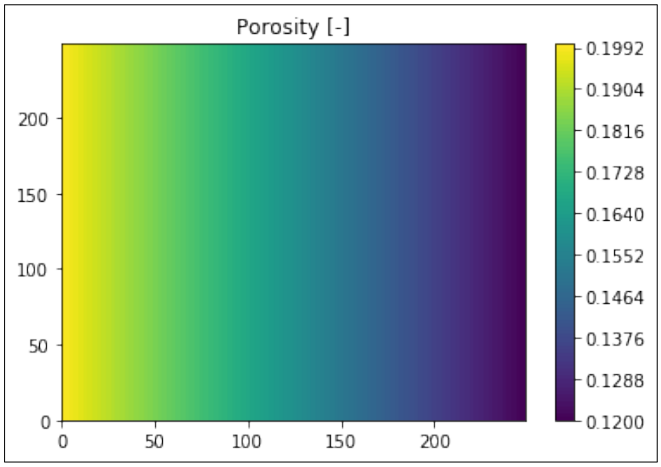

Figure 2.6: Porosity distribution of a field in x-direction, modeled with a linear function.

The adopted concept directly implies that more wells are needed in the high porosity area. Thus the pattern size should be smaller. The relationship between porosity and well spacing is negative, and the function should have a minus in the control of gradient a. Taking this into account, the flexible well placement function is written in Equation 2.6.

$$Pattern - size = \frac{a}{x} * x + b \tag{2.2}$$

where:

- a is the rate of pattern size-reduction receiving values $0 \leq$ a ≤ 250.
- b is the minimum pattern size receiving values smaller than the actual field x-dimension (nx).

The function starts placing the first injector with a distance of $a/2$ from the origin of the x-axis. At that given location, the injector holds a value based on the linear function. That value will be added to the first injector location and thus produce the second injector location. The process continues until an injector location falls out of the field boundaries and that injector is disregarded. As far as producer placement is concerned, they do not follow the same function. The producer is placed in the middle of the distance of two first injectors based on Equation 2.7.

$$Prod(i)_{loc} = \frac{Inj(i)_{loc} + Inj(i+1)_{loc}}{2} \tag{2.3}$$

The following producers are placed based on Equation 2.8 to ensure that one producer is always placed between two injectors and honours the 5-spot pattern. If the last producer falls out of the field boundaries, it is disregarded.

$$Prod(i)_{loc} - Inj(i)_{loc} = [Inj(i+1)_{loc} - Inj(i)_{loc}] * \frac{Inj(i)_{loc}}{Inj(i)_{loc} + Inj(i+1)_{loc}} \tag{2.4}$$

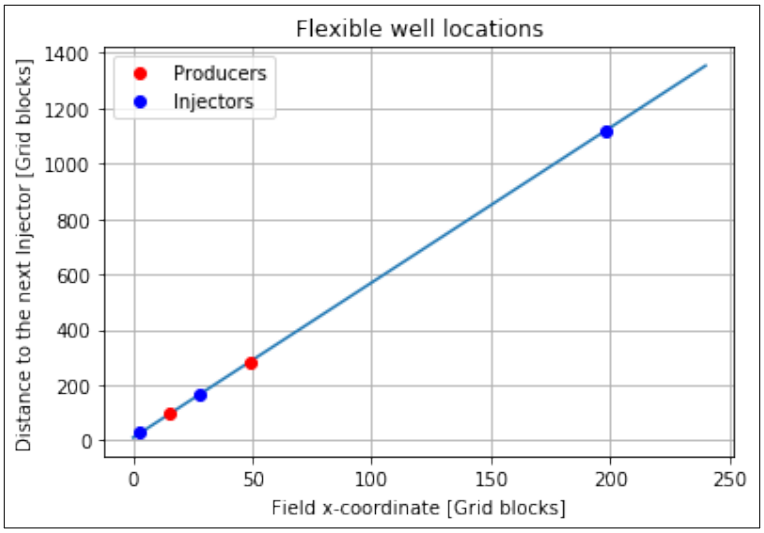

Figure 2.7: Flexible well placement given a linear trend distribution.

Figure 2.7 shows an example of a flexible well placement with parameters a = 40, b = 0.3, c = 125, d = 30 of equation 2.6. These values are assigned within a specific range. The boundaries depend on the licence area dimensions (nx * ny grid blocks). Summarising, the x location of the wells follows the well density function contrary to the y location. In this case, the y component of the location, follows the principles of scaling operator that would place injectors and producers in equidistant spacings, as described in section 2.2.

2.3.2 Porosity modelling with a Gaussian function

The first example to be described is porosity, with a Gaussian distribution in the x-direction, describing a channel belt with a higher porosity compared to an adjacent shale formation. Porosity in the y-direction is not changing. Then a function in the form of Equation 2.1 is used. Parameters a,b,c,d are used to manipulate the output of the porosity model:

$$\phi = a + b * e^{(-\frac{(x-c)^2}{d^2})} \tag{2.5}$$

Where:

- a is the minimum porosity of the field.
- b is the fractional increase from the minimum porosity of the area.
- c is the location in x-direction where the maximum porosity value is encountered (i.e., the location of the channel).
- d represents the standard deviation of the Gaussian curve.

Figure 2.8 represents the output of the porosity function with a = 12, b = 16, c = 125, d = 30. Figure 2.9 is a 2D representation of the porosity field.

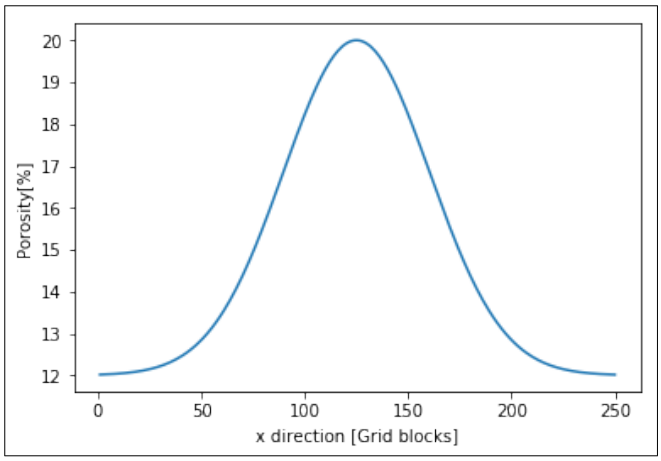

Figure 2.8: Porosity distribution of a field in x-direction, modeled with a Gaussian function.

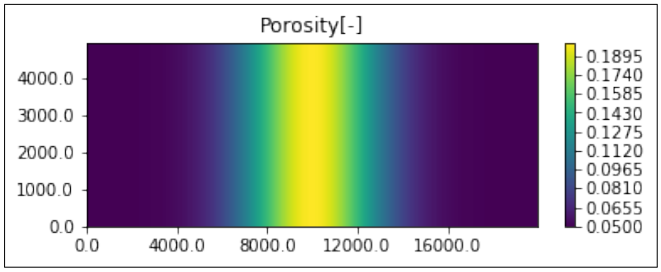

Figure 2.9: Porosity distribution of a field in x-direction, modeled with a Gaussian function.

After the function that describes the geological model is adopted, a modification is required to transform it into a function that would introduce flexible well placement. For example, the area with higher porosity corresponds to a higher volume of warm water than the area with lower porosity. This directly implies that more wells are needed in the high porosity area. Thus the well spacing should be smaller. The relationship between porosity and well spacing is inverted, and the function should follow an inverted trend. Taking this into account, the flexible well placement function is written in Equation 2.2.

$$Pattern - size = a - a * b * e^{\left(-\frac{(x-c)^2}{d^2}\right)} \tag{2.6}$$

Where:

- a is the standard or maximum well spacing in the x-direction.
- a*b is the fractional deduction of well spacing in the x-direction from the normal well spacing.
- c is the location in x-direction where the Gaussian distribution peak is encountered (i.e., the location of the channel).
- d represents the standard deviation of the Gaussian curve.

The function starts placing the first injector with a distance of $a/2$ from the origin of the x-axis. At that given location, the injector holds a value based on the Gaussian function. That value will be added to the first injector location and thus produce the second injector location. The process continues until an injector location falls out of the field boundaries and that injector is disregarded. As far as producer placement is concerned, they do not follow the same function. The producer is placed in the middle of the distance of the two first injectors based on Equation 2.3

$$Prod(i)_{loc} = \frac{Inj(i)_{loc} + Inj(i+1)_{loc}}{2} \tag{2.7}$$

where i=1

The following producers are placed based on Equation 2.4 to ensure that one producer is always placed between two injectors and honour the chosen optimisation pattern (5-spot in the example shown here). If the last producer falls out of the field boundaries, it is disregarded. The equation returns the spacing between the previous injector and the following producer.

$$Prod(i)_{loc} - Inj(i)_{loc} = [Inj(i+1)_{loc} - Inj(i)_{loc}] * \frac{Inj(i)_{loc}}{Inj(i)_{loc} + Inj(i+1)_{loc}} \tag{2.8}$$

Figure 2.10 shows an example of a flexible well placement with parameters a = 40, b = 0.3, c = 125, d = 30. These values are assigned within a specific range. The boundaries depend on the licence area dimensions (nx * ny grid blocks). When introducing the wells, the operator assigning the y location wells also needs to be specified. This is the scaling operator that would place injectors and producers with equidistant spacing.

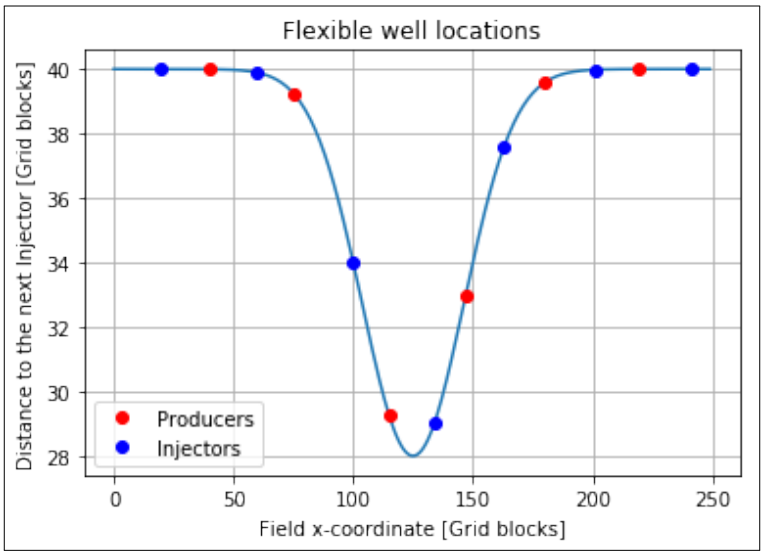

Figure 2.10: Flexible well placement given a Gaussian distribution.

Chapter 3

Objective function definition

3.1 Introduction

The initial thought of setting the objective function is to feed it with a pattern size (well density function) between one producer and one injector. The pattern size either is directly assigned as an input in the case of a regular pattern or is the result of a flexible well density function. This pattern size can be identical in both horizontal directions (x,y) of the Euclidean surface or different. When the well spacing or pattern size is different in the two directions, two input variables are created for the same objective function. When they are the well spacing is the same in both x,y directions, only one argument is set. These arguments hold for the scaling operator. When introducing the well density function, the number of input arguments becomes higher, since it includes the tuning parameters that subsequently generate the pattern size.

The next step is to understand the nature of the function controls and if the same input could result in multiple realisations. All the input values are rational numbers, and the objective function creates results with a unique corresponding output. For example, introducing an A pattern size to the objective function would give a unique B energy recovery output. The set of input variables, should be clarified as being continuous or discrete. The scaling factors in both directions present a continuous character. The tuning parameters of the well density function are of the same nature. The constraints for the input arguments need to correspond to reality and cannot exceed testing field limitations. For example, a singe pattern size cannot exceed the field size of 10 or 20 km because the field cannot be operated with half a pattern. Therefore, minimum and maximum threshold values are assigned to the input variables of the objective function. The objective function is non-linear, as the net present value calculated entails the exponential term of time.

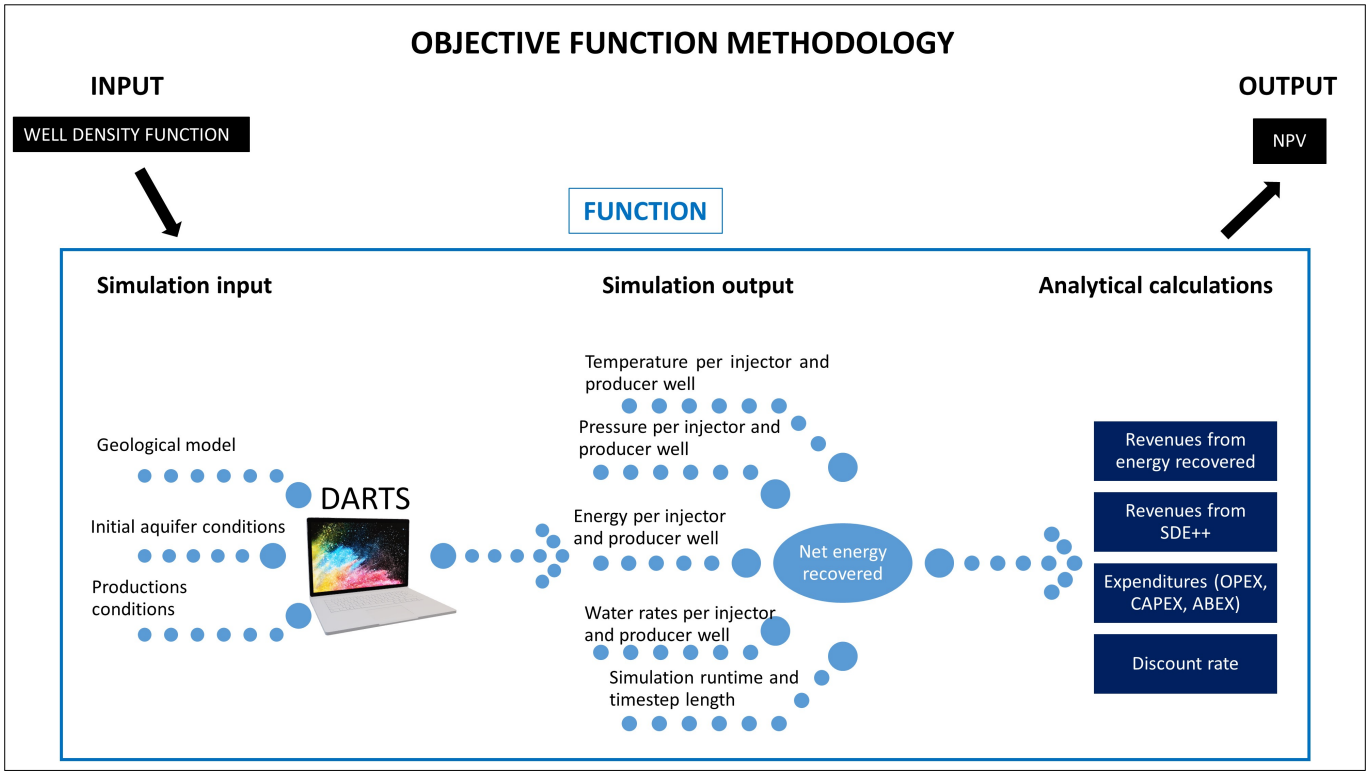

Figure 3.1: Definition and methodology of the objective function

The objective function is fed with the arguments: scaling operator in x,y directions or the well density function. The objective function initialises with the simulation input criteria. These are the initial reservoir conditions, production conditions, well pattern placement with the corresponding scaling operator or well density function. The simulation runs and produces a database for every injector and producer set within the license area. Among a dataset declared, for this project temperature, pressure, energy, water flow rate data were used. The energy data per producer and injector well are used for the calculation of revenues in the economic model. The number of wells included in the model contributes to the total expenses. The rest of the expenses are calculated based on current Dutch fiscal conditions. The Net Present Value of the running project is given as an output in the constructed objective function. The methodology followed is depicted in the figure 3.1.

3.2 Delft Advanced Research Terra Simulator (DARTS)

3.2.1 Governing equations for flow and transport in porous media

Geothermal simulations follow a fundamentally different approach, from those of oil and gas reservoirs and groundwater, as they consider the flow of energy and mass in the reservoir. This introduces an element of complexity to geothermal reservoir simulation since a thermal term is included. Three fundamental equations are the base for geothermal reservoir simulation. Conservation of mass, conservation of energy and Darcy's Law for fluid flow in porous media (O'Sullivan et al. 2001). Conservation of mass states that a system mass should remain constant with time for a closed system. It is inferred that any change in the mass of a system is balanced by mass coming into or out of the system for an open system. The mass balance for fluid with multiple phases and multiple porous media components can be written as shown in equation 3.1. The first term is the change in mass with time. The second term states the flux of mass in and out of the system due to flow, and the third term introduces a source term in case any mass is added to or removed from the system, for example, at a well (Voskov 2017).

$$\frac{\mathrm{d}}{\mathrm{d}t}\left(\phi x_{cj}\rho_j s_j\right) - \boldsymbol{\nabla}\cdot\left(x_{cj}\rho_j u_j\right) + \left(x_{cj}\rho_j q_j\right) = 0 \tag{3.1}$$

where:

- c = 1....n_c
- n_c = number of components
- t = time
- ϕ = porosity
- x_{cj} = mole fraction of component c in phase j
- ρ_j = density of phase j
- s_j = saturation of phase j
- q_j = source term for phase j
- u_j = Darcy velocity of phase j

Darcy's Law (equation 3.2) is used to introduce the velocity of a fluid through porous media given a fluid viscosity, permeability and a pressure gradient. Relative permeability is one since there is a single-phase flowing in the geothermal application of this study (Voskov 2017).

$$u_j = -K\frac{k_{rj}}{\mu_j}\left(\boldsymbol{\nabla}\cdot p_j - g_j\boldsymbol{\nabla}\cdot d\right) \tag{3.2}$$

where:

- K = permeability tensor
- k_{rj} = the relative permeability
- μ_j = viscosity of phase j
- p_j = vector of pressure of phase j
- g_j = gravity term
- $\boldsymbol{\nabla}\cdot d$ = the vector of depths

Conservation of energy can be described similarly to the conservation of mass. It introduces the energy term, a flow term and source term, the only difference being that energy moves through the subsurface by two transport mechanisms: conduction and convection. The flow of heat by convection is controlled again by Darcy's law (equation 2.6), while conduction is fundamentally controlled by the temperature gradient and the thermal conductivity of the rock type the heat is conducted through (Khait & Voskov 2018*b*) (equation 3.3)

$$\frac{\mathrm{d}}{\mathrm{d}t}\left(\phi U_j \rho_j s_j + (1-\phi)U_r\right) - \boldsymbol{\nabla}\cdot\left(x_{cj}\rho_j u_j h_j\right) + \boldsymbol{\nabla}\cdot\left(\kappa\boldsymbol{\nabla}\cdot T\right)\left(x_{cj}\rho_j q_j h_j\right) = 0 \tag{3.3}$$

where:

- U_j = internal energy of phase j
- U_r = internal energy of the rock
- h_j = enthalpy of phase j
- κ = thermal conductivity of rock

For reservoir simulation, the last two equations have to be in the discretised formulation. In DARTS, a backwards Euler approximation in time is used for discretisation (Khait & Voskov 2018*b*, Voskov 2017). Equations 3.4 and 3.5 show the finite volume discretised form of the conservation equations.

$$\begin{aligned} &V\left[\phi\left(\left(x_{cj}\rho_j s_j\right)^{n+1} + \left(x_{cj}\rho_j s_j\right)^{n}\right)\right] - \Delta t\sum_l\left(\phi\left(x^l_{cj}\rho^l_j\Gamma^l_j\boldsymbol{\nabla}\cdot p^l_j\right)\right) \\ &+\Delta t\left(x_{cj}\rho_j q_j\right) = 0 \end{aligned} \tag{3.4}$$

$$\begin{aligned} &V\left[\left(\phi U_j\rho_j s_j + (1-\phi)U_r\right)^{n+1} - \left(\phi U_j\rho_j s_j + (1-\phi)U_r\right)^{n}\right] \\ &- \Delta t\sum_l\left(x^l_{cj}\rho^l_j\Gamma^l_j\boldsymbol{\nabla}\cdot p^l_j + \Gamma^l_j\boldsymbol{\nabla}\cdot T^l\right) + \Delta t\rho^l_j h^l_j q^l_j = 0 \end{aligned} \tag{3.5}$$

where:

- V is volume
- Δt is the time step
- l = connection l in the grid
- $\Gamma^l_j = \frac{\Gamma^l}{\mu_j}$ where Γ^L s the harmonic average of permeability between two grids cells
- $\Gamma^l_K = K\Gamma^l$
- n = time step
- $q_j = \tilde{q_j}V$

Both equations 3.4 and 3.5 are approximated using a fully implicit method, which introduces non-linearity to the system modelled. Solving this non-linear system is typically done using a conventional linearisation approach called the Newton-Raphson method (Khait & Voskov 2018*b*). However, this system holds more complex combinations of non-linear properties and relations and therefore linearising this with Newton-Rhapson may lead to various errors (Voskov 2017). Linearisation in DARTS is done using the Operator-Based Linearization approach (OBL) developed by Voskov (2017).

The traditional way proposed to solve these systems of equations is the Newton-Raphson method. This method delivers the linearisation of the non-linear equations using the Newton method, constructing a Jacobian matrix at each non-linear iteration, solving the linear equations and finally obtaining a residual. The residual should be below a given tolerance of the solution before the next time step is introduced. The Newton-Raphson method solves the linearised equations in the following formulation:

$$J(\omega^k)(\omega^{k+1} - \omega^k) = -r(\omega^k) \tag{3.6}$$

where:

- J is a Jacobian matrix that is assembled in each iteration
- ω is the value you are trying to attain
- k is a non-linear iteration number
- r is the residual

3.2.2 Operator-Based Linearization (OBL)

When a system is complex, with numerous phases and components, the system becomes very complicated and leads to various potential error sources (Voskov 2017). DARTS uses a novel method for linearisation developed by Voskov (2017), known as operator-based linearisation (OBL). The OBL approach was proposed recently for generalised complex multi-phase flow and transport applications and improved simulation performance (Wang et al. 2019, Khait & Voskov 2018*a*,*b*). For a detailed explanation of the methodology DARTS uses, please refer to Denis Voskov.

OBL simplifies the complicated non-linear physics by parameterising the different operators in physical space with a limited number of supporting points, allowing it to represent the operators piece-wise (Khait & Voskov 2018*a*,*b*, Wang et al. 2019). During simulations, the operators are evaluated based on multi-linear interpolations, which reduces the non-linear trend of the system. The successful application of OBL in thermal multi-component and multi-phase flow simulations has been conducted by researchers like Voskov (2017), Khait & Voskov (2018*a*,*b*), Wang et al. (2019, 2020). Further discussion of the mathematics governing DARTS is outside the scope of this thesis.

3.2.3 Simulation input

The simulation requires some input data to be able to perform the simulation of a geothermal project and can be found in table 3.1. These are:

- Aquifer property modelling, more specifically the porosity and permeability matrices in the actual numerical field size. This means that, a porosity and permeability number should be defined per grid block. The size of the property models should correspond to the size of the numerical field. Thus, a field modelled in 100 * 100 grid blocks requires porosity and permeability matrices of 100 * 100 elements. Detailed information about the geothermal aquifers is mentioned in geothermal aquifer model Chapter 5.
- Initial aquifer conditions and production conditions are required for the simulator. These are presented in detail in Table. 3.1

For the purpose of this study, it is necessary to imitate an aquifer that has constant input and output flow. Therefore, the volume of surrounding and boundary grid blocks of the simulated reservoir is increased by a factor of 10^6 compared to the grid blocks located in the reservoir. Subsequently, a difference in volume therefore mass present is created which is impacting the sweep of warm water. In the following figure 3.2 is presented the difference in the cold front speed with (right) and without inflated boundaries (left). Apparently when the boundaries are non-inflated (left), the system imitates an closed to flow aquifer, thus the cold front is restricted within the boundaries of the geothermal field. When the boundaries are inflated (right), the presence of large volume of water on the boundaries, is actually extending the radius of the cold front.

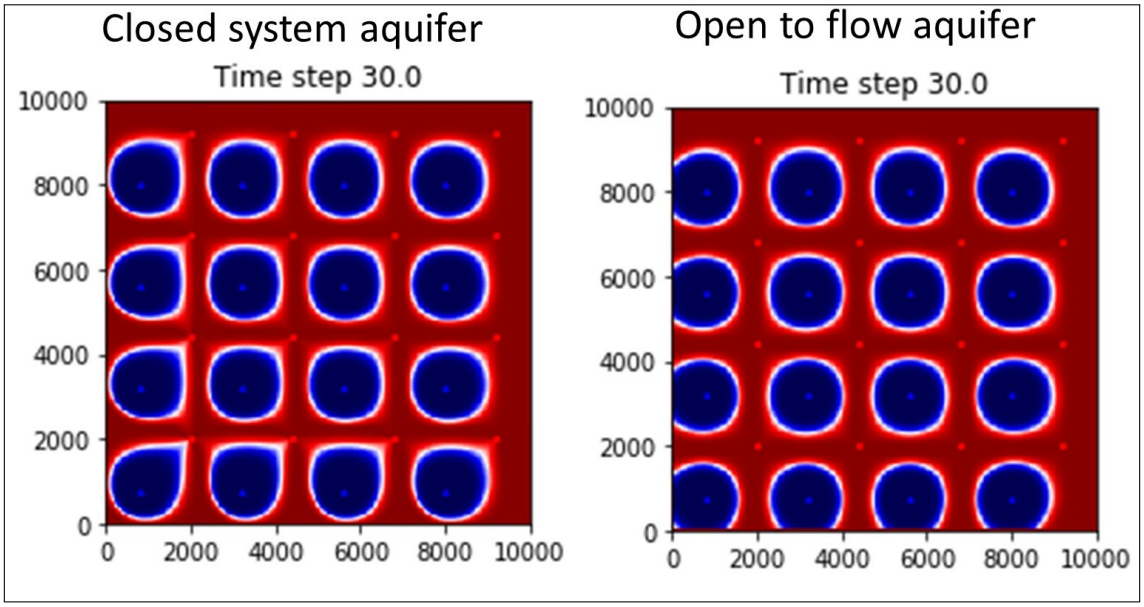

Figure 3.2: Aquifer status after 30 years of production under same constraints, with the difference of inflated and non-inflated boundaries.

Table 3.1: Constant parameters used as simulation inputs, in all models

Constant		Value	Unit
Aquifer x-discretization	nx	250	Grid blocks
Aquifer y-discretization	ny	250	Grid blocks
Aquifer z-discretization	nz	1	Grid blocks
Grid x-dimension	dx	40,80	m
Grid x-dimension	dy	40	m
Grid x-dimension	dz	10	m
Fluid density	ρ_f	1021	Kg/m^3
Fluid heat capacity	C_f	4,184	J/Kg*K
Fluid heat conductivity	κ_f	700	W/m*K
Rock density	ρ_r	2680	Kg/m^3
Rock heat capacity	C_r	2200	J/Kg*K
Rock heat conductivity	κ_r	450	W/m*K
Aquifer top depth	d	2200	m
Aquifer temperature	T_{res}	349.15	K
Aquifer pressure	P_{res}	242	bar
Injection temperature	T_{inj}	308.15	K
Injection rate	Q_{inj}	1500	m^3/day
Production pressure	BHP_{prod}	237	bar
Geothermal gradient	$Grad_{geoth}$	0.03	C/m
Pore fluid pressure gradient	Pr_f	0. 11	bar/m
Project lifetime	t	30*365	days

3.2.4 Simulation output

The reservoir simulator has an embedded report of several parameters. Not all of them are necessary for this project. The retrieved data are:

- Time series of temperature per injector and producer well reported in Kelvin [K].
- Time series of bottom hole pressure [BHP] per injector and producer well reported in bar.
- Time series of flow rate per injector and producer well reported in $\frac{m^3}{day}$.
- Time series of energy rate per injector and producer well reported in $\frac{KJ}{day}$.
- Reported time-steps reported in days.

After receiving these data sets, a modification is made to calculate the required net energy recovered based on the principle of subtracting the total injected energy from the total produced energy. First, the energy rates have to be translated to energy recovered. This is achieved by multiplying the energy value per time-step with the difference between the corresponding and previous time-step. The time series (t) of net energy recovered is calculated as the per time-step difference between the sum of wells (n) of energy produced and the sum over wells (n) of energy injected. This is going to be fed in the algorithm that comes up with the economic model calculation.

$$E_{net} = \sum_{t=0}^{t} \left(\sum_{n=0}^{n} E_{prod} - \sum_{n=0}^{n} E_{inje} \right) \tag{3.7}$$

3.3 The economic model under Dutch fiscal conditions

Geothermal project costs rely on multiple factors such as the costs of different phases of the project, geological uncertainties, government policies, and heat demand in the area that the geothermal project is going to supply energy. This subsection describes the development of the economic model and its parameters based on the TU Delft thesis of Zaal Caroline (2020).

The economic model is designed to evaluate the feasibility of geothermal projects in the Netherlands. The model inputs are all based on Dutch financial regulations and, therefore, only simulate Dutch geothermal projects. The information used in the model is given in Table 3.2.

Table 3.2: Input for the economic model

Base case Parameters	Value	Unit	Reference
Heat price	66	€/MWh	Daniilidis et al. (2020)
Discount rate	7	%	Daniilidis et al. (2020)
€/$ conversion	0.85	-	-
Capex			
Surface facilities	1.5-3	M€/km	van den Bosch et al. (2013)
Well costs	Depth dependent		TNO (2019)
Cost of ESP	0.80	M€	van't Spijker (2016)
Opex			
Fixed OPEX	5	% of CapEx	Daniilidis et al. (2020)
Electricity price	0.78	€/kWh	CBS Statline (2021)
Variable Opex	0.5	M€	Daniilidis et al. (2020)
Abex	1.084175	M€/well	Osundare et al. (2018)
Revenues			
Contribution SDE++	0.033	€/kWh	Rijksoverheid (2019*a*)

3.4 Project Expenditures

3.4.1 Capital Expenditures

This phase includes installation of the drilling site, required equipment and drilling of the doublet. These different elements all contribute to the total investments costs of the project and are further discussed in the drilling location, well drilling and equipment sections.

The **drilling location** is the place at the surface where the production facilities and buildings will be placed. The drilling location costs depend mainly and highly on the purpose of the geothermal project, the used drilling rig, and on the type of wells drilled (deviated or not). Earlier geothermal projects in the Netherlands have indicated that total drilling location costs are between €150.000 and €300.000 (van den Bosch et al. 2013). These refer to costs from the time of site preparation to the end of drilling operations. As mentioned, the exact amount depends on different factors, so the most conservative case of cost amount is taken into consideration in the economic model (150.000 €) in order to conclude to a deterministic output of drilling and not a probabilistic (Low estimate, Mid estimate and High estimate case).

Geothermal doublets consist of production and injection wells. The costs of drilling these wells can vary depending on the depth, given in equation 3.8 TNO (2019).

$$Well_{costs} = 375000 + 1150 * depth + 0.3 * depth^2 \tag{3.8}$$

All costs are given in Euros, and the output of the equation is the well and installation costs of a single well. In our project, the well-doublet concept is not followed, so the above equation is multiplied by the total number of wells drilled. Dutch geothermal projects consist of some standard necessary **equipment**. These include equipment for water circulation, filters and screens, an injection pump, an Electrical Submersible Pump (ESP), and a heat exchanger. The ESP is installed in the production well and lifts the water to the surface. Most geothermal production wells in the Netherlands are equipped with a Baker Hughes ESP (van't Spijker 2016). An ESP is built up of several different components. If properly designed, it should achieve an efficiency of 55% in most configurations operating with rates between 100 and 300 m^3/h. Baker Hughes researches the lifetime of the ESP's in Dutch geothermal projects, and they estimate a lifetime of 5 years, after which it needs to be replaced. As it was difficult to obtain reliable numbers for Dutch geothermal projects, the investment costs of an ESP are based on purchases in the Paris Basin of France and are estimated to be between €180.000 and €300.000 for a pump with a capacity between 250 and 500 kW. The costs increase with increasing power. Due to the limited availability of the ESP costs data, an estimation is given in the table below (3.3).

Table 3.3: Estimated costs ESP (Van Dongen 2019)

ESP capacity (MWhr)	Estimated costs (M€)
0.250-0.500	0.300
0.500-0.800	0.800
0.800-1.000	1.000
0.1000-1.200	1.000
$\geq$ 1.200	1.200

The model used for this study incorporates €800.000 for the ESP costs (Daniilidis et al. 2017, Van Dongen 2019). Surface facilities include a water circulation pump, injection pump, screens and filters and the heat exchanger with a total cost ranging from €500.000 - €1.500.000 (van den Bosch et al. 2013). The most conservative amount is used in the model in order to conclude to a deterministic output of drilling and not a probabilistic (Low estimate, Mid estimate and High estimate case). After installation of all equipment, the operator needs an exploitation permit and an approved exploitation plan, after which she/he can start the production of geothermal energy. In the model, the project is estimated to go on for 30 years.

The capital expenditures abbreviated as CapEx, are the total investment costs of the project. The CapEx consists of the exploration, construction and unforeseen construction costs. Construction costs consist of all expenses associated with preparation, drilling and installation of the equipment and drill site. This includes the well drilling, the pumps, the heat exchanger and the screens and filters.

3.4.2 Operational Expenditures

Operational Expenditures, abbreviated as OpEx, are all costs made during production. The total OpEx comprise variable and the fixed operational costs. The variable OpEx are the costs that fluctuate over time, depending on the power required for production and the electricity prices. Fixed OpEx are the costs that remain unchanged during the entire production process. In this section, both fixed and variable OpEx are analysed, as they will be included in the economic model.

Fixed OpEx are the annual costs that do not fluctuate over time. In general, fixed OpEx include the maintenance and workover costs, rent of facilities, salaries and insurance costs. **Work-over and maintenance costs** are implemented throughout the whole production process. During workovers and maintenance operations, the facilities are controlled and cleaned every year. The total annual costs for workovers and maintenance are estimated to be 5% of the project's CapEx, built up by two elements. Yearly costs for inspection, workovers, maintenance, and staffing costs are determined as 4% of the project's CapEx. This percentage is derived from Energieonderzoek Centrum Nederland (ECN) and is based on data of Dutch geothermal projects (De Boer & et.al. 2016). From existing projects in the Netherlands, it is found that the maintenance costs of heat network are 1% of the project's CapEx (Van Dongen 2019), which makes a total of about 5% for the calculation of the fixed OpEx. The income not generated during maintenance and workovers is added to the fixed OpEx to consider the effects of the downtime (Daniilidis et al. 2017).

3.4.3 Abandonment Expenditures

The abandonment costs consist of plugging and closing the wells and returning the production site to its original state. Abandonment costs of geothermal wells in the Netherlands are based on values found in earlier European geothermal projects (Osundare et al. 2018). The author mentions a minimum abandonment and plugging cost of 1.275.500 dollar per well. This is introduced into the model with a USD/EUR conversion factor of 0.85, which leads to the value of 1.084.175 €.

3.5 Project Revenues

3.5.1 Revenues from production

In the Netherlands, the heating price is determined as 90% of the Dutch market price of gas (TTF) (Ministerie van Economische Zaken en Klimaat 2019). The TTF is calculated based on the High Heating Value (HHV) of gas. The ratio between the HHV and Low Heating Value (LHV) of gas is 90%, making the heating price around the same as LHV gas costs. The 2020 revised reference price is set equal to the predicted gas reference price in 2020 (Zaken 2020). The current market price of gas is 0.080 euro/KWh accessed in May 2021. (Global Petrol Prices 2021). The Rijksoverheid (2019*b*) forecasted for the future gas prices up to 2030. Similar to the electricity prices, the gas prices are subject to high volatility. Due to the volatility, the forecast gas prices are also incorporated with a range of values, indicating the price variance. This bandwidth (Figure 3.3) is based on the scenarios made by Schoots & Hammingh (2019).

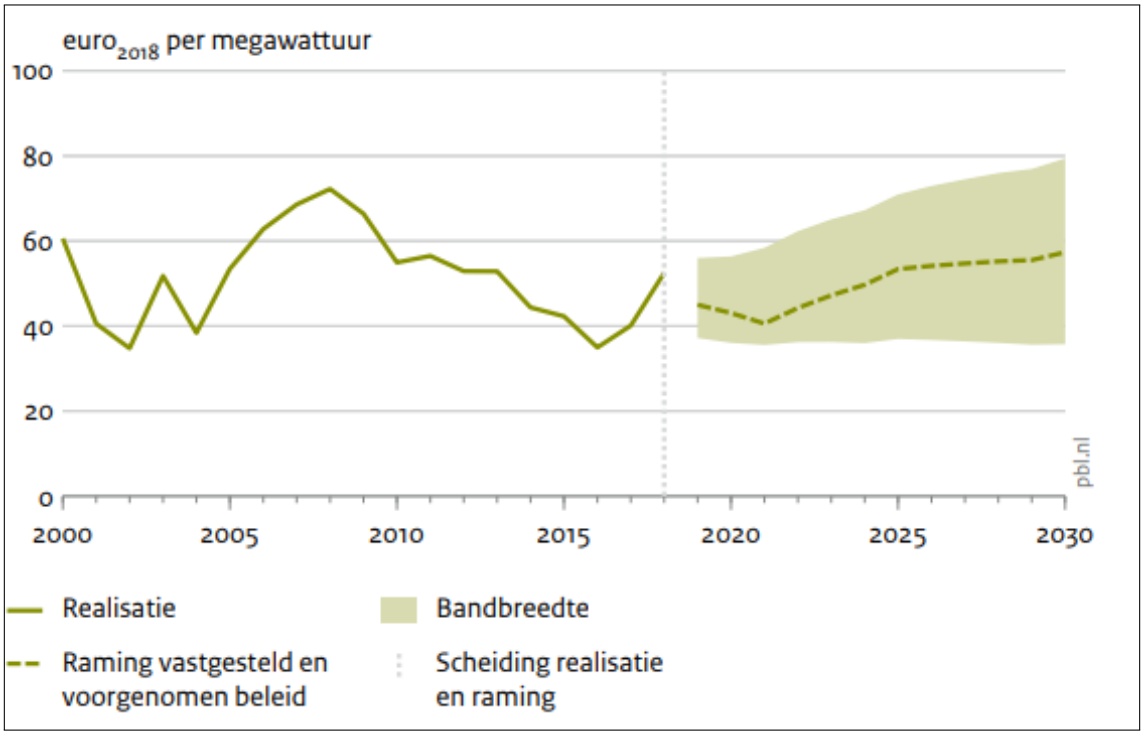

Figure 3.3: Forecast Electricity price Schoots & Hammingh (2019).

3.5.2 Revenues from SDE^{++} subsidy

The SDE^{++} is an extension of the former Stimulation Scheme for Sustainable Energy Production (SDE^{+}). In addition to sustainable energy production, this new scheme also stimulates CO_2 reduction. This way, the government wants to ensure that the energy transition in the Netherlands remains feasible and affordable (Rijksdienst voor Ondernemend Nederland 2019).

The production of sustainable energy is not always profitable because the production costs are generally higher compared to producing energy from oil. As a solution, producers of geothermal energy can request a SDE^{++} subsidy. This subsidy provides financial compensation for the extra costs of the production of sustainable energy (Rijksdienst voor Ondernemend Nederland 2019). The maximum subsidy period is 15 years, and the amount of compensation depends on the project itself. The subsidy is the buildup of the base amount of the energy and the correction amount. The base amount is the thermal energy production cost and is fixed over the entire duration of the subsidy. The correction amount is the thermal energy market price and is revised every year based on the market price development (Ministry of Economic Affairs and Climate Policy 2020). This correction amount is determined the same way as the market price, which is 90% of the TTF price.

$$SDE^{++} = Base_{amount} - Correction_{amount} = 0.052 - 0.019 = 0.033 M.Euros \tag{3.9}$$

3.6 Economic Model

Combining the project revenues and costs gives the cash-flows generated in the project. However, the cashflow gives only few details on the financial performance of the project.

One of the purposes of applying the proposed concept of well patterns in geothermal fields is to maximise an assigned objective function, either the net present value or total energy recovered. Going for the option of total energy recovered, a term of stability is established due to the static character of the reservoir (aquifer), amount of saturated brine in the reservoir, and fixed temperature variation present in the subsurface. This way, the total energy recovery is qualified as a robust and non-volatile term of optimisation. In contrast to energy recovery, the Net Present Value or Expected Monetary Value are regarded as quite sensitive to market volatility.

To make a robust analysis of cash-flows generated in the future, it is required to make a discount to their present value (PV). The PV is today's value of the amount of money paid or received in the future. The value of money fluctuates; hence it is most relevant to know the present values of cash flows to get a clear perspective related to, for example, other projects. This current value is determined by discounting the future cash flows with a discount rate and the time since the start of production. This is also called the discounted cash flow (DCF) and is given by equation 3.9.

$$DCF = \frac{CF_t}{(1+r)^t} \tag{3.10}$$

where C_t is the cash flow generated at time t (Euro), r is the annual discount rate [-], and t is elapsed time since project start (30 years assumed in this project). From the DCF, the net present value (NPV) can be determined, which is regarded as the sum of the discounted cash flows minus the investment costs.

The NPV is formulated as Daniilidis et al. (2020):

$$NPV = \sum_{n}^{t=0} \frac{CF_t}{(1+r)^t} \tag{3.11}$$

CF is the cash flow, r the discount rate, n is the project years and t the time. CF can be estimated as (Zhang et al. 2015):

$$CF_t = R - Capex - Opex - Abex \tag{3.12}$$

where R is the revenues, originating from profits of energy produced and subsidy. Capex, Opex and Abex are analytically above.

Chapter 4

Optimisation strategy of the objective function

4.1 Introduction to optimisation

The objective function used for this project was analysed in different aspects. As discussed in the subsection of the objective function definition, the optimisation algorithm needs to:

- Be derivative-free given that information (derivative or/and hessian) about the objective function is either unavailable or not practical to obtain. For example, the function might be non-smooth, or time-consuming to evaluate, or in some way noisy, so that methods that work based on derivatives or approximate them with finite differences are not helpful.
- Be fed with more than one input variables. The nature of the input variables is continuous. The output of the objective function is one: The Net Present Value of a development project. Another option could have been to target both NPV and drilling strategy.
- Be flexible in constraints settings for the arguments. This implies that there are no limits in the dimensions of the developed field when optimising well spacing.
- Be deterministic given that optimal control of the objective function can give in a single result. For example, if we impose a strategy with an well spacing of value A it is going to deliver a value B of NPV and not a probability distribution of B.
- Detect multiple minima present when projecting an objective function. In many nonlinear optimisation problems, the objective function has many local minima, and a global minimum needs to be identified that results in the optimal response.

In general, the optimisation problems are of the form:

$$min_x f(x), x \in R^n$$

$$s.t. g_i(x) \geq 0 \forall_i = 1, ..., m$$

$$h_j(x) = 0 \forall_j = 1, ..., p$$

where:

- x s a vector of one or more variables.$f(x)$ is the objective function: $f : R^n \rightarrow R$
- $g_i(x)$ the inequality constraints : $R^n \rightarrow R^m$
- $h_j(x)$ the equality constraints $\simeq$: $R^n \rightarrow R^p$
- f can be either smooth or non-smooth depending on the local minimisation method used.
- The variables x are assumed to be bounded

4.2 Choosing the most suitable optimiser

For this project, an objective function was defined. For the optimisation process, the character of the controls are discussed in the following aspects:

1. The total number of independent variables, arguments, controls or input variables that control the output or dependent variable. The number(s) of input variables correspond to a univariate (1-dimensional) or multivariate (multidimensional) function. In this problem, pattern size is considered the input of the problem. The pattern size can be directly fed in a regular pattern or indirectly with parameters controlling the flexible well density function.

2. The nature of the input variable. This can be a rational number or a range of values (probability distribution). The pattern size can receive continuous values in the case of regular patterns.

3. The constraints of the input variables. These constraints can be rational numbers in their simplest form and linear or non-linear functions, increasing the complexity of the objective function. These constraints can be imposed on equality or inequality conditions to the input variable. This holds for the actual constraints of pattern size in order not to exceed the actual field dimensions.

4. The permissible value of the decision variables. This also plays an essential role in the function. These are continuous or discrete variables. For example, a continuous input variable can be well spacing and a discrete variable the number of wells.

5. The deterministic or stochastic nature of the decision variables. An investigation is needed on whether the same set of parameter values and initial conditions will lead to an ensemble of different outputs (stochastic) to a unique result (deterministic). In this project, a series of pattern size would produce a unique series of net present values. Therefore the nature of the problem is deterministic.

6. The type of function that is going to be computed. The function can be either linear or non-linear. Generally, functions with reservoir simulations can result in non-linear and even discontinuous response. In our case the objective function includes a simulation therefore, a rather non-linear behaviour is expected. The large scale character of the development requires the investigation of the response of well spacing values much larger than the already applied. The wide range of investigation of pattern sizes, suggests a response function with multiple local minima and maxima. This behaviour is due to the number and type of wells that sweep the aquifer at each experiment.

The stochastic nature of the optimisation process implies evaluating a range of different pattern size configurations during the optimisation iterations. Thus, many pattern sizes were assessed,and compared by a sensitivity analysis. The response curve of the objective function to the pattern size can be observed in Figure 4.1. In the same figure, the positive part is magnified; that way, it can be seen that the variations of the objective function value as a function of pattern size is non-monotonic in different ranges of pattern sizes. This implies that the heat revenues of the project combined with and well costs present multiple local optima depending on the number of wells added in the aquifer when the pattern size becomes smaller.Within these local minima, the global minimum (optimum) pattern that delivers the highest possible NPV is found. Moreover, NPV curves of different development strategies preserve some upper and lower plateaus. These are related to the number of injectors and producers participating in the field development. When the pattern size becomes smaller, rows and columns of either producers or injector wells are introduced. When a row or column of producers is introduced, the energy recovered is subsequently higher by inserting only injectors. The large scale character of the development is a aspect to be discussed because it is the key that introduces this non linear nature in the objective function. If the development was not extensive the objective response would have been limited in a small range of pattern size like Figure 4.2. This figure proves that if the development was done in fields of several kms scale that could fit smaller patterns, the optimisation would need a more local approach like other authors have already worked on (Willems, Nick, Goense & Bruhn 2017, Willems, Nick, Weltje & Bruhn 2017, Kahrobaei et al. 2019). Therefore, the large scale character of the geothermal development suggests a different approach in the optimisation process that will be adopted.

It is inferred that the highest possible NPV can be obtained when the number of injectors is equal to the number of producers. This refers to the higher "plateau" of the objective function. The lower "plateau" represents patterns with one less row or column of producers, in other words, a complete 5-spot pattern (4 injectors and 1 producer). Therefore, it can be concluded that the pattern size is optimisable in large scale geothermal heat production systems for different development strategies, even for a simple 2D homogeneous case.

Endres et al. (2018) presented numerical experiments for open-source black-box algorithms, comparing the SHGO (Simplicial Homology Global Optimization) and TGO (Topographical Global Optimization) (Henderson et al. 2015) algorithms with the SciPy implementations (Jones et al. 2016) of basin-hopping (BH) (Li & Scheraga 1987, Wales & Doye 1997, Wales & Scheraga 1999) and differential evolution (DE) (Storn & Price 1997). BH is commonly used in energy surface optimisations (Wales 2015). DE has also been applied in optimising Gibbs free energy surfaces for phase equilibria calculations (Zhang et al. 2010). The choice of the algorithm was based on their open-source character from SciPy. A number of 180 multimodal test cases were adopted to evaluate the performance of the algorithms in terms

of processing time and the number of function evaluations. For every test, the algorithm was terminated if the global minimum was not found after 10 minutes of processing time, and the test was flagged as a fail. SHGO-Sobol (Sobol sampling method) demonstrated the best performance in function evaluations and process timing (Figure 4.3). SHGO briefly demonstrated efficiency in tracking global optimum in every iteration without further refinement sub-spaces.

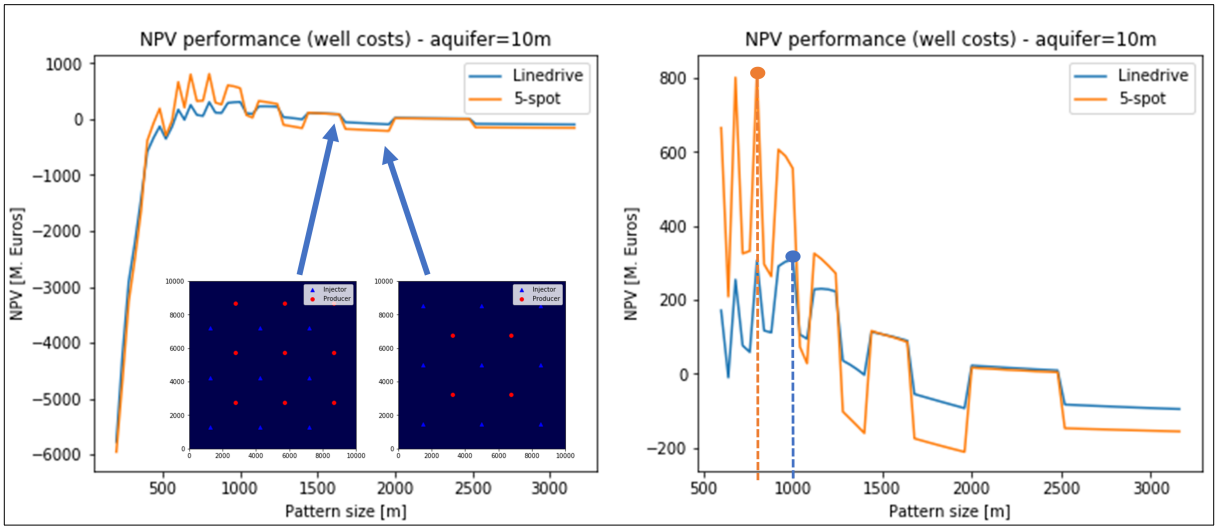

Figure 4.1: Response of the objective function on NPV. This curve represents full information about the objective function with one control. It is verified that the optimisation algorithm has found the optimal solution in both 5-spot and line-drive development strategies.

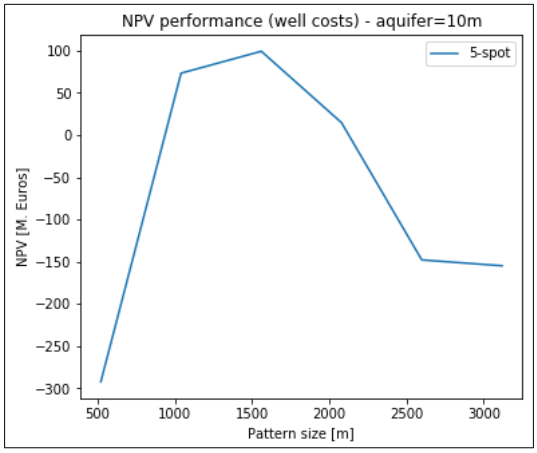

Figure 4.2: Response curve of a small scale 5-spot development. This plot clearly shows the presence of one optimum development (pattern size) unlike Figure 4.1.

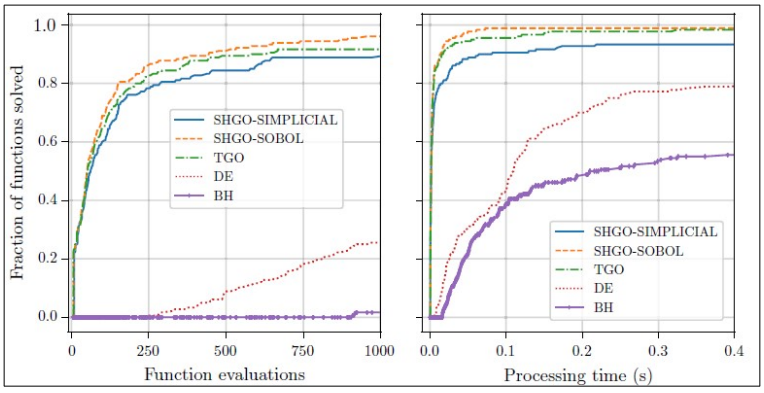

Figure 4.3: Performance profiles of Global Optimization methods on SciPy bench-marking test suite. SHGO stands for simplicial homology global optimization, TGO for topographical global optimisation, DE for differential evolution and BH for basin hopping. SHGO with Sobol sampling methodology presents the best performance in number of function evaluations and processing time (Endres 2019)

4.3 Simplicial Homology Global optimisation (SHGO)

The Simplicial Homology Global optimisation (SHGO) algorithm is a promising, recently published global optimisation (GO) algorithm (Endres et al. 2018, Endres 2019, Endres & Sandrock 2021). It is regarded as the most appropriate for solving a global and derivative-free, black-box optimisation problem. This optimisation type is especially suitable for engineering problems with embedded simulations (like in this case) or has a highly complex model structure. The SHGO algorithm is unique among global optimisation algorithms because it returns all local minima by novel, rigorously proven methods that detect the homological properties of the objective function surface. Within these local minima, the global minimum is identified. Therefore, SHGO is highly appropriate for problems where the local minima are desired. In this specific project, a non-smooth objective function surface is expected. When more wells are introduced to the objective function, the result of subtracting costs out of energy revenues is non-linear. So it is vital to address less optimal solutions but still hold a positive NPV response as alternative strategies in field development.

Some background theory is necessary to understand the properties of shgo. For better understanding, the process the optimiser undergoes will be divided into two major steps. The first step includes the approximation of locally convex areas in the response of the function that the local minima are located. Simply, the locally convex areas are function evaluations that the global optimum possibly could be found. The next step is to further refine and search in those promising areas the global optimum among the local optima identified.

4.3.1 Approximating locally convex areas

The algorithm utilises concepts from combinatorial integral homology theory to find sub-domains that are approximately locally convex and provide the characterisations of the objective function. The SHGO method constructs a simplicial complex (network of sampling points that create a line if the function has 1 control, a surface for 2 function controls ect.) using the sampling points in an objective function f(x) as vertices. These sampling points are used to detect the geometry of the response surface of the function. This way, their cost of calculating jacobians is by far reduced. In algebraic and combinatorial topology (Henle 1994, Hatcher 2002), a branch of mathematics that uses abstract algebra tools to study topological spaces, a $k-simplex$ is a set of $n+1$ vertices in a convex polyhedron of dimension n. This is explained in Figure 4.4. This part has direct application in the sampling part of the optimiser. For optimising an objective function with one control, if n number of sampling points (vertices) are set, $n-1$ edges will be created that connect these vertices (v_i). This group of connected vertices create $1-simplex$. When the function has two controls, a $2-simplex$ is created (triangles) and so on. A simplicial complex H is a set H^0 of vertices together with sets $.H^n$ of n-simplices, which are (n + 1)-element subsets of H^0. The only requirement is that each (k + 1)-elements subset of the vertices of an n-simplex in H^n is a k-simplex in H^k.

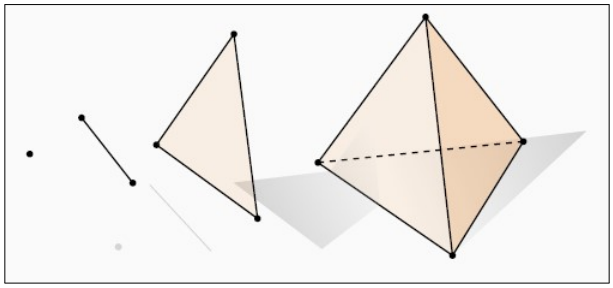

Figure 4.4: A 0-simplex (point-vertex), 1-simplex (edge-face), 2-simplex (triangle-) and a 3-simplex (tetrahedron) (Figure adapted from Crane (2013).

After that, the sampling needs to be introduced to the function, with a specific method that would reassure the uniformity and filling the space of possibilities more evenly (Figure 4.7). There is no way to know if the number and distribution of sampling points are adequate for black-box functions without more information (for example, if the number of local minima is known in the problem). Having created a set of vertices (H^0), a simplicial complex (H) is constructed by a triangulation (2-simplex) or connecting (1-simplex) every vertex in H^0. The connection supplies a set of undirected edges E. This is shown in Figure 4.5 where from the function with the sampling points, and the vertices are connected with edges (Figure 4.6). The last figure is created as a chain (union) of edges is called 1- chain. A k-chain is a union of simplices. A directed simplicial complex allows us to build an integral homology. Giving the directional characteristic to the edges allows the algorithm to estimate the direction in which an edge ($\overline{v_i, v_j}$) follows.

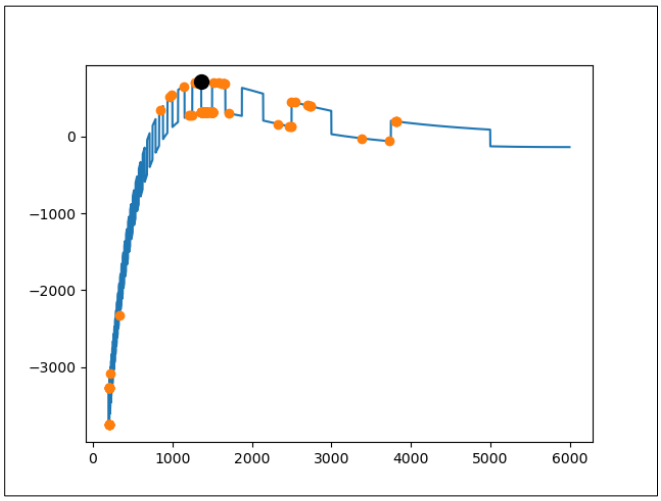

Figure 4.5: Sampling points on the 1D objective function surface $f : R^n \to R$.

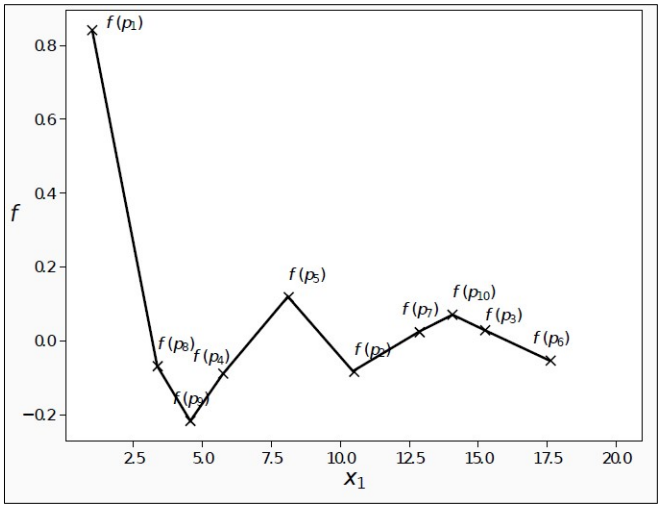

Figure 4.6: (Incomplete) geometric information available to an algorithm (Endres & Sandrock 2021).

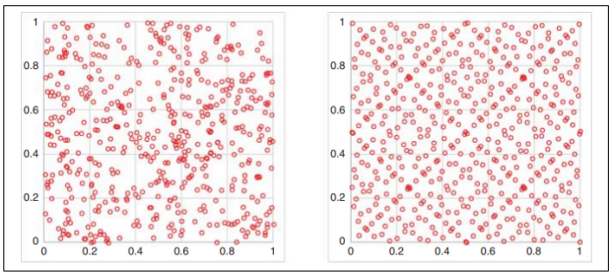

Figure 4.7: Random (left) and Sobol (right) sampling (Savine 2018). The x,y axes of both figures represent a 2D surface like the objective function with 2 controls used in this project.

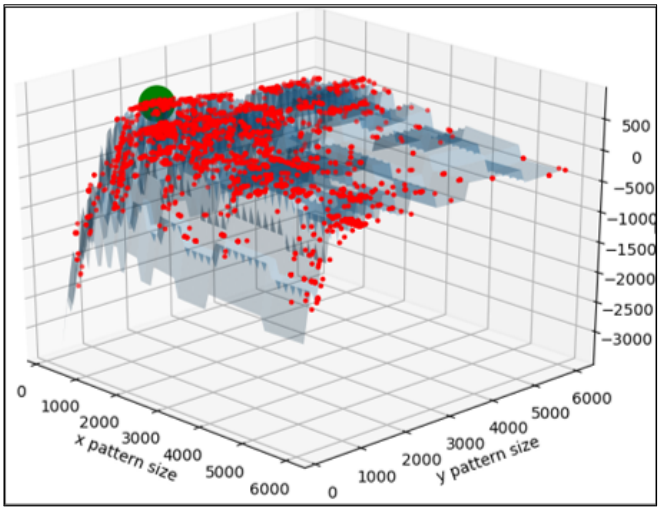

Figure 4.8: 2D Surrogate function sampling with sobol sequence (red points) and optimum (green point). The y axis represents the NPV on M.Euros.

So, from incomplete geometric information, directed integral homology introduces additional information about the path. The set of edges (H^1) is constructed by directing every edge in E. A vertex $v_i \in H^0$ is the connection to another vertex v_j by an edge contained in E. The edge is directed as $\overline{\mathrm{v_i v_j}}$ from v_i to v_j if $f(v_i) < f(v_j)$ so that $\partial(\overline{\mathrm{v_i v_j}}) = v_j - v_i$. H is used to find the minimiser pool for the local minimisation starting points used by the algorithm: A vertex v_i is a minimiser if every edge connected to v_i is directed away from v_i. The minimiser pool M is the set of all minimisers. Out of multiple minimisers found, only one will be the one corresponding to the global minimum. That is the simplex with vertices on the edges in the required direction, as shown in Figure 4.9. Further discussion regarding the topological transformation of this minimiser point to result in hyper-surfaces (tori construction), and thus, the minimiser pool M, is out of the scope of this study.

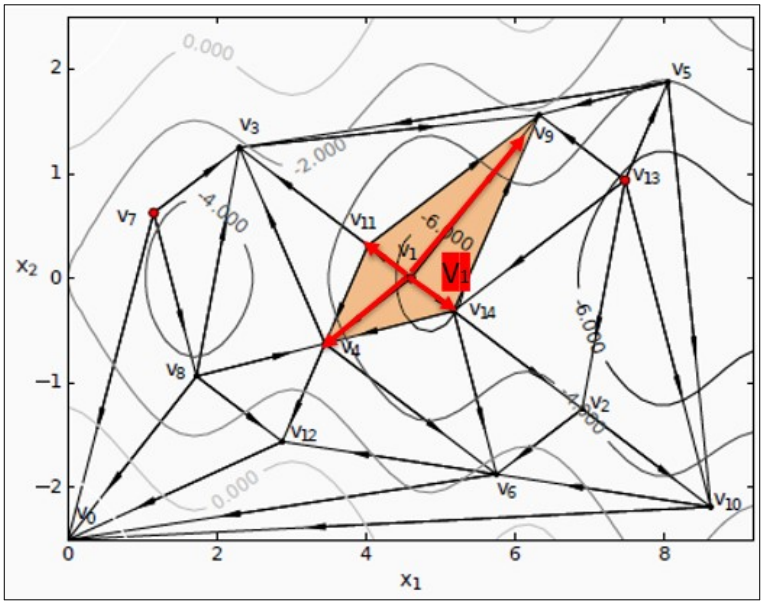

Figure 4.9: Minimizer point, in a directed 2-simplex. The red area indicates the locally convex area where the promising points are located (Endres 2019). A directed complex H forming a simplicial approximation off, three minimiser vertices M= f(v1 v7 v13) and the shaded domain (v1). Modified after Endres & Sandrock (2021)

4.3.2 Local minimisation in locally convex sub-domains

Since the locally convex sub-domains are processed, SHGO can concentrate on the global search. This circumvents the need to specify the usual trade-off between a local and global search. This is accomplished in several steps using a local minimization routine to identify the local minima in the locally convex areas. The further refinement of the promising domains is processed following the concept of Sperner's lemma (Sperner 1928) and Brouwer's fixed point theorem (Henle 1994). The minimiser pool found in the previous step is used in this process. Each minimiser point (vertex) found is used as an initial guess for a local minimisation algorithm. Each minimisation routine searches in the locally convex areas and identifies the local minimum. The default minimisation algorithm used is Sequential Least-Squares Programming (SLSQP), provided as an open-source package of SciPy. Method SLSQP uses Sequential Least-Squares Programming to minimize a function of several variables with any combination of bounds, equality and inequality constraints. The method wraps the SLSQP Optimization subroutine originally implemented (Kraft 1994). A detailed explanation of local minima identification with Sperner's lemma is out of the scope of this project. After all local minima are identified (figure 4.10), the function responses of all local minima are calculated, and the global minimum is approximated. Subsequently, the approximate global minimum and a list of all the minima found in the local minimisation step is returned. The full outline of the algorithm can be downloaded here (Endres 2019).

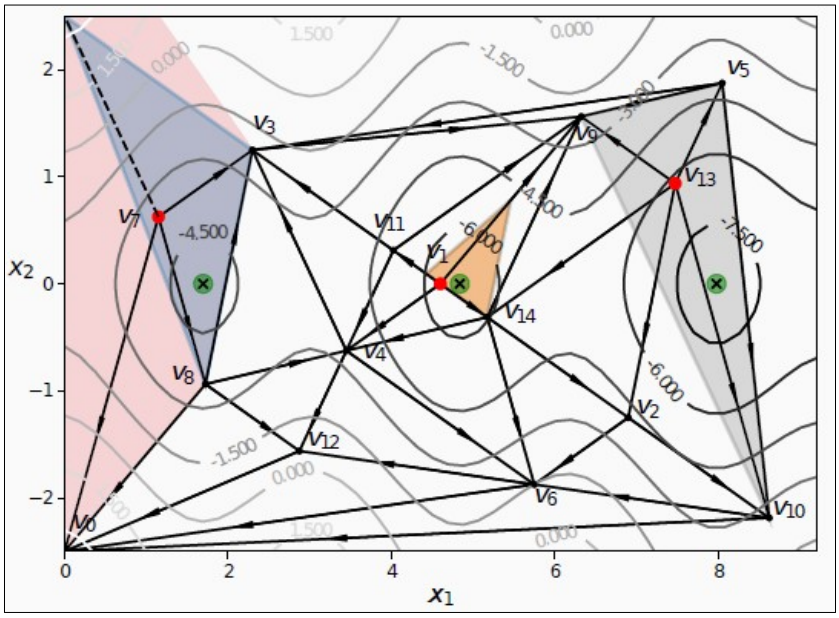

Figure 4.10: Three circled crosses are the (approximate) minima of the objective function within the given bounds (Endres 2019).

Chapter 5

Geothermal aquifer models

This chapter describes the different synthetic geological models created to serve and test and optimise the generated flexible well density function. The models need to contain properties described as homogeneous, heterogeneous, isotropic and anisotropic. Homogeneity describes the property that evenly holds the same value in space, and isotropy refers to the directional component, thus holding the same value in all directions. The synthetic models need to contain built up complexity from homogeneous-isotropic to heterogeneous-anisotropic. The space we are dealing with in these models is 2D, and thus 2 directions(x,y) are included. The 3rd dimension (z) is also included but does not play a role in flow patterns, only contributing to numerical volume . Porosity (ϕ) will characterise the model as homogeneous or heterogeneous. The permeability will express the isotropy or anisotropy of the flow patterns (K_z, K_x, K_y). The synthetic realisations generated are in Table 5.1.

Table 5.1: Synthetic geological models created, described in terms of homogeneity and isotropy.

Model	**Porosity (ϕ)**	**Permeability (K)**
Case 1	Homogeneous	Isotropic
Case 2	Homogeneous	Anisotropic
Case 3	Heterogeneous	Isotropic
Case 4	Heterogeneous	Isotropic

As mentioned in the Introduction chapter, for the proof of concept, in the following synthetic models, some formations do not show permeability values that follow the porosity-permeability correlation. Therefore permeability is not realistically correlated with the facies. The 2D variation of both porosity and permeability would require to impose injection and production pressure strategies that vary spatially and would create the development too complex. Subsequently, the selected modelling strategy is chosen in order to focus only in the effect of water volume present in the aquifer and production profiles. The injection is conducted under a fixed water rate so, there is no spatial variation of injected water mass. The production is done under fixed pressure meaning that no spatial variation of production pressure is expected (given the homogeneous permeability). Moreover, there is no explicit modelling of heat capacity and heat conductivity based on the spatial distribution of porosity (facies). Given that the thermal properties of the Mesozoic geothermal targets preserve a lot of uncertainty within a single facies, but also different values per facies (Willems et al. 2020), it going have an impact on the thermal recharge of the aquifer. Furthermore, the aquifer is assumed not to be confined by layers. In reality, confining layers would offer additional heat for the thermal recharge of the aquifer (de Bruijn et al. 2021). In general, further modifications are required to explicitly bring the testing geological models as much closer as possible to reality.

5.1 Case 1: 2D Homogeneous sandstone aquifer

A simple 2D homogeneous model with a dimension of 10000 m * 10000 m * 10 m has been used. The model is discretized in 250 * 250 * 1 grid blocks of size 40 m * 40 m * 10 m. The aquifer properties such as porosity, permeability, aquifer and fluid properties are based on Delft Sandstone Member, retrieved from Willems et al. (2020). Core plug measurements from the 1500–2500 m depth range of the Nieuwerkerk formation show a linear compaction-related porosity reduction trend of c.5% per 500 m. However, within the aquifer thickness of 10 m, no change in porosity is assumed. Given an average current depth of the sandstone of 2000–2500 m., a porosity range of 8–25% of the Delft Sandstone Member is assumed. The associated permeability ranges from several tens of mD up to 3000 mD. Since the depth of the reservoir was chosen at 2200 m, the corresponding porosity is 0.20. The following equation describes the porosity (ϕ measured from 0-1) correlation with permeability (measured in mD). For all the created models, the permeability is constant for all different porosity values and calculated based on the maximum porosity of the synthetic model (equation 5.1). The correlation is based on Willems et al. (2020). This is assumed to make the optimisation interpretation less complex when it comes to optimising the well density concept.

$$K_D = -3.523 * 10^{-7} * \phi^5 + 4.278 * 10^{-5} * \phi^4 - 1.723 * 10^{-3} * \phi^3 + 1.896 * 10^{-2} * \phi^2 \quad + 0.333 * \phi - 3.222 \tag{5.1}$$

The initial reservoir temperature and pressure are assumed to be 349.15 K and 237 bar, respectively. The rock and water thermal conductivity are 345.6 and 51.84 $kJ/m/day/K$, respectively. The heat capacities for the rock and water are 2.7 and 4.2 $\frac{kJ}{kg*K}$, respectively. The water has a density of 1000 $\frac{Kg}{m^3}$ and a viscosity of 0.001 Pa.s. These are the pure water properties at room temperature. Heat capacity and density for brine water composition would be different; however, it will not significantly affect the result in terms of the proof of concept of this study. The system (well) inputs are the (constant) injection water rate and water temperature and the (constant) bottom hole pressure (BHP) at the producer, which are all assumed to be known. Injectors operate at a constant rate of 1500 $\frac{m^3}{day}$. Production pressure is dependent on the depth of the reservoir. A pressure gradient of 0.11 $\frac{bar}{m}$ is assumed, and thus the pressure of the producers at 2200 m depth is assigned as 237 bars and calculated based on Equation 5.2:

$$BHP = 0.11 * depth_{res} - 5 \tag{5.2}$$

The pressure of injectors and rates of producers are free to be adjusted by the simulator itself. The injection temperature is set to 35 C (308.15 K). The simulation lifetime is 30 years. The table 5.2 illustrates aquifer data and used in this model.

Table 5.2: Aquifer properties of homogeneous sandstone model.

Property		**Value**	**Unit**
Porosity	ϕ	20	%
Horizontal permeability	K_x	902	mD
Horizontal permeability	K_y	902	mD
Vertical permeability	K_z	10	mD

5.2 Case 2: 2D Homogeneous and anisotropic sandstone aquifer

A reservoir model with different permeability in two horizontal directions has been used to study the impact of heterogeneity on pattern size optimisation in geothermal heat production systems. The average permeability of the x-direction (K_x) is calculated based on equation 5.1. The average permeability of y-direction is assigned as $K_y = \frac{K_x}{2}$. The aquifer porosity and other reservoir and fluid properties are the same as those used for the homogeneous model. For this study case, permeability in two horizontal directions implies the necessity to adjust pattern size directionally to avoid early cold breakthrough and sweep the aquifer efficiently in the given lifetime. The ta 5.3 illustrates the aquifer properties used in this model.

Table 5.3: Aquifer properties of heterogeneous sandstone model.

Property		**Value**	**Unit**
Porosity	ϕ	20	%
Horizontal permeability	K_x	902	mD
Horizontal permeability	K_y	$K_x/2$	mD
Vertical permeability	K_z	10	mD

5.3 Case 3: 2D Aquifer with linear porosity trend

An aquifer model with a linear trend on porosity and thus permeability has been used to study the effect of heterogeneity on flexible pattern size optimisation in geothermal heat production systems. The higher porosity is 20 %, while the background shale facies has an average porosity of 12%. A linear trend of the porosity from the offset is imposed. The following equation describes the offset and the gradient of the porosity distribution in the x-direction.

$$\phi = -a * x + b \tag{5.3}$$

Where:

- $a = \frac{\phi_{max} - \phi_{min}}{nx}$ where nx is the x-dimension of the field in grid blocks.
- b is minimum porosity (ϕ_{min}) of the field

The permeability is calculated with equation 5.1 with a given porosity of 0.20. The concept of keeping the permeability constant is adopted. This is assumed to study the effect of warm water volume produced concerning the number of wells needed. This concept, in reality, would hold high porosity and permeable channels and low porosity

and permeability shales leading to a different well placement strategy. However, it is adopted to prove the concept of flexibility in well placement. The more realistic concept can be incorporated in the flexible well density function by allowing wells to be placed far away from each other instead of closer than it is assigned now. Other reservoirs and fluid properties are the same as those used for the homogeneous model. For this study case, porosity variation implies adjusting pattern size to sweep the higher volume present in the channel. The effect of permeability is not studied, and it would fall in the more realistic case. Figure 5.2 illustrates the porosity of the linear porosity model used.

Table 5.4: Aquifer properties of linear porosity model. Permeability values of both formations are not realistic and are chosen for the proof of the thesis concept.

Property		**Value**	**Unit**
Formation 1 (channel) porosity	ϕ_1	20	%
Formation 2 porosity	ϕ_2	12	%
Formation 1 horizontal permeability	K_x, K_y	902	mD
Formation 2 horizontal permeability	K_x, K_y	902	mD
Vertical permeability	K_z	10	mD

Figure 5.1 represents the output of the porosity function with a = 12, b = 20. The figure 5.2 is a 2D representation of the porosity field.

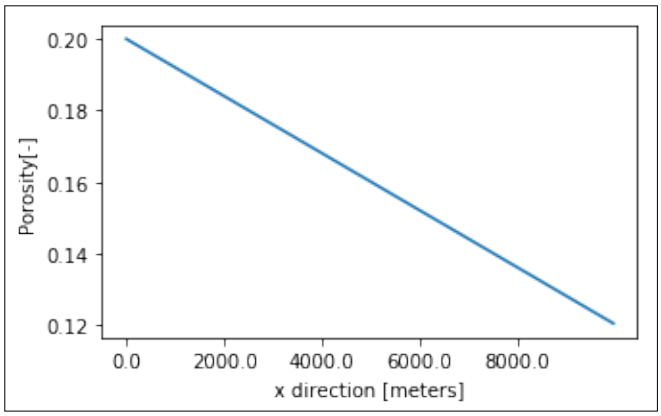

Figure 5.1: Porosity distribution of a field in x-direction, modeled with a linear function.

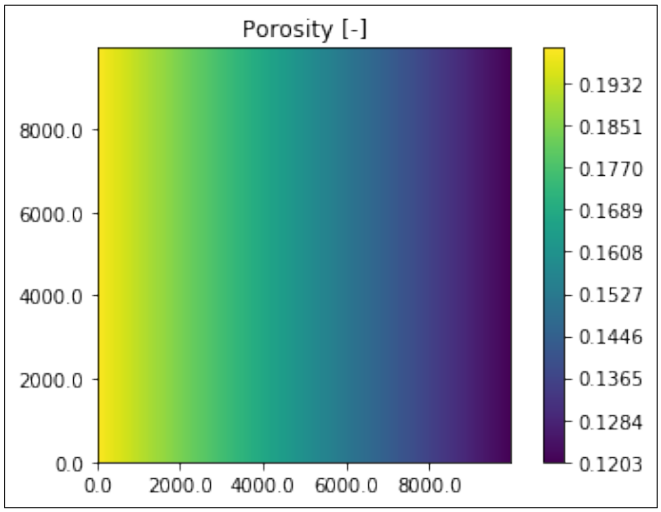

Figure 5.2: 2D Porosity distribution of the field with a linear trend in porosity.

A realistic representation of this synthetic field could be the Rotliegend Formation (figure 5.3) in the subsurface of The Netherlands. Mijnlieff (2020) presented permeability maps of this formation that show a large scale linear trend. Since the permeability is positively correlated with porosity, this map qualitatively represents also porosity. Therefore the Rotliegend Formation, given that it is a possible geothermal target, it could be developed with the discussed methodology. Moreover another clear realistic representation of the synthetic field is from USA, Florida (figure 5.4).

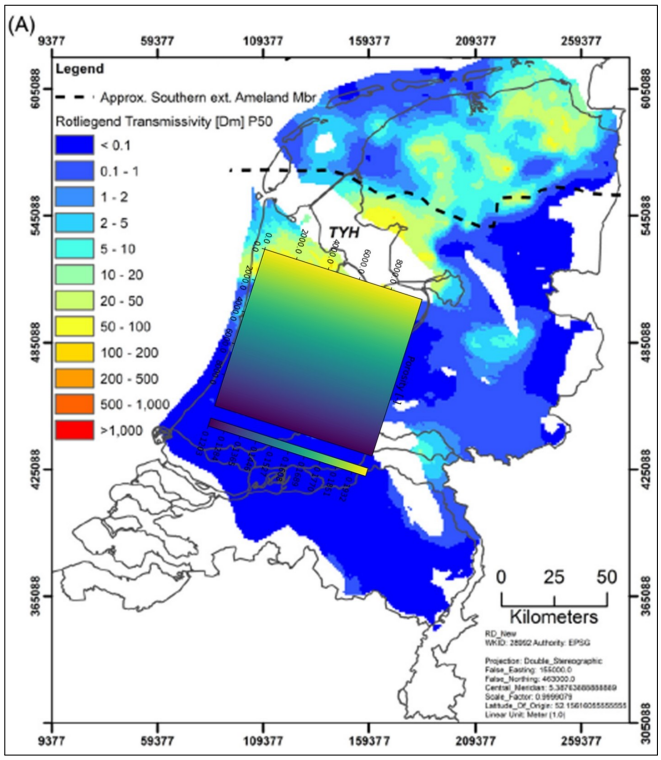

Figure 5.3: Realistic field where a large scale linear porosity trend is encountered in the Netherlands (Mijnlieff 2020).

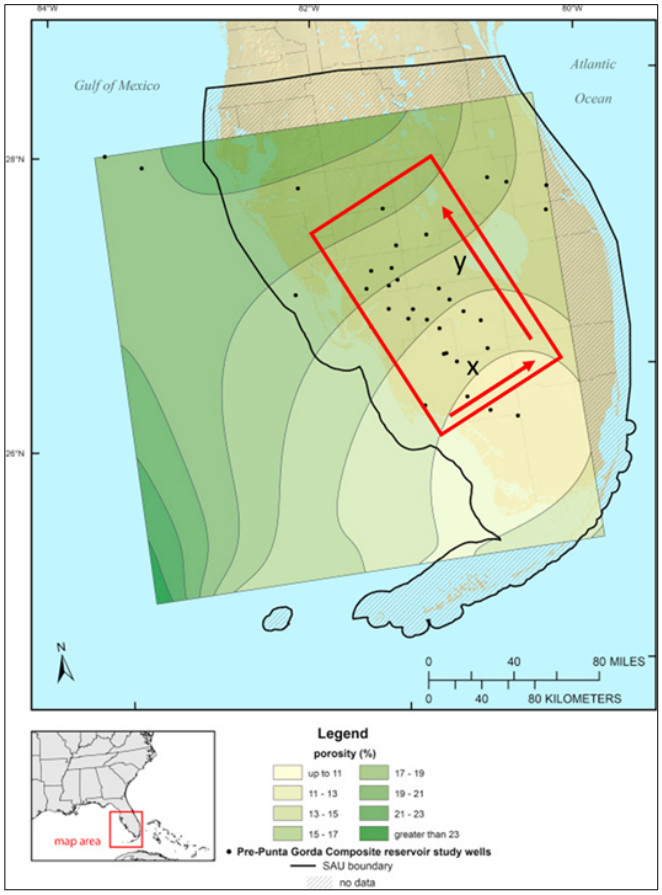

Figure 5.4: Realistic field where large a scale linear porosity trend is encountered. This example is from a oil and gas development field in Florida, USA. Modified after Roberts-Ashby & Ashby (2016).

5.4 Case 4: 2D Aquifer with channel belt

An aquifer model with a channel belt has been used to study heterogeneity on flexible pattern size optimisation in geothermal heat production systems. The average porosity of the channel is 20 %, while the background shale facies has an average porosity of 5%. A Gaussian trend of the porosity from the offset is imposed. The following equation describes the porosity distribution in the x-direction.

$$\phi = a + b * e^{\left(-\frac{(x-c)^2}{d^2}\right)} \tag{5.4}$$

Where:

- a is the minimum porosity in the x-direction.
- b is the fractional addition (0-1) to the minimum porosity in the x-direction.
- c is the location in x-direction where the Gaussian distribution peak is encountered (i.e., the location of the channel).
- d represents the variance of the Gaussian curve.

The permeability of both formations is the same and calculated with Equation 5.1 based on the values of 0.20. This is assumed to study the effect of warm water volume produced concerning the number of wells needed. This concept, in reality, would hold high porosity and permeable channels and low porosity and permeability shales leading to a different well placement strategy. However, it is adopted to prove the concept of flexibility in well placement. The more realistic concept can be incorporated in the flexible well density function by allowing wells to be placed far away from each other instead of closer than it is assigned now. Other reservoir and fluid properties are the same as those used for the homogeneous model. For this study case, porosity variation implies adjusting pattern size to sweep the higher volume present in the channel. The effect of permeability is not studied, and it would fall in the more realistic case.

Table 5.5: Aquifer properties of the channel belt model.

Property		Value	Unit
Formation 1 porosity	ϕ_1	20	%
Formation 2 porosity	ϕ_2	12	%
Formation 1 horizontal permeability	K_x, K_y	902	mD
Formation 2 horizontal permeability	K_x, K_y	902	mD
Vertical permeability	K_z	10	mD

Figure 5.5 represents the output of the porosity function with a = 5, b = 20, c = 125, d = 40. Figure 5.6 is a 2D representation of the porosity field.

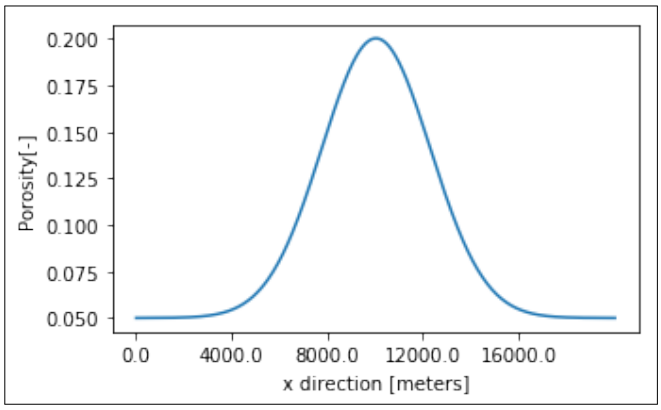

Figure 5.5: Porosity distribution of a field in x-direction, modeled with a Gaussian function.

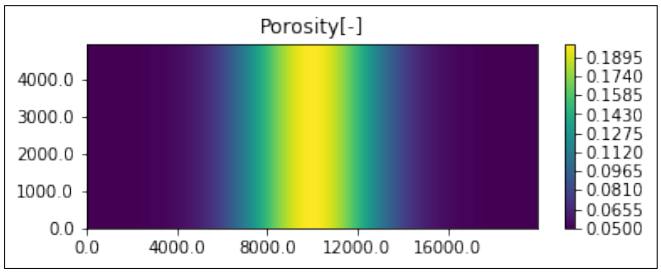

Figure 5.6: 2D Porosity distribution of a field

A realistic representation of this synthetic field could be the West Netherlands Basin (WNB) (Willems et al. 2020). This Mesozoic formation is typical for the large scale channel belt extended axially to the SE - NW paleoflow direction. The perpendicular extension of the channel belt covers several 10s of kilometers. Subsequently is falls within the description of the synthetic field. It is not necessary to capture the individual channel formations since all channels are developed with higher porosity than the adjacent shales.

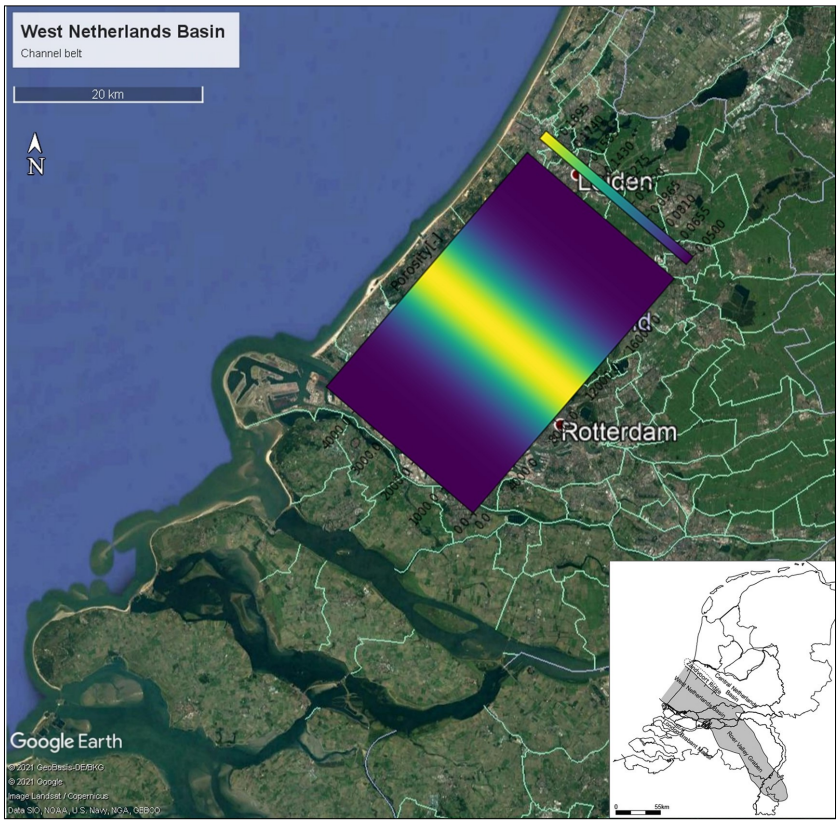

Figure 5.7: Aerial view of the location of the synthetic channel formation presented could represent the West Netherlands Basin. Modified after Willems et al. (2020).

Chapter 6

Results

This section will present the results of the simulations with the optimal controls of the objective function.

6.1 Case 1: 2D homogeneous and isotropic sandstone aquifer

The optimisation workflow is set up for the 2D homogeneous system, with a pattern size in the range of $5 - 80$ grid blocks that correspond to $120 - 3200$ m of pattern size (injector-injector, producer-producer distance). So, The function evaluates the development strategies with the defined pattern sizes. These bounds of search area were set such that the simulation would converge with the minimum pattern size, and a complete pattern would fit in the aquifer with the preset maximum pattern size. The highest bound (3200 m) when inserted in the objective function, suggests a development strategy with only one 5-spot of line-drive (doublet) pattern sweeping the reservoir. The lowest bound of 120 m, introduces a field development with repeated 5-spot or line drive pattern of a injector-injector or producer-producer well spacing of 120 m. The sampling method of optimisation is Sobol, which evenly distributes sampling points to gain the geometrical information of the objective function. The number of points is set to 100. The maximum number of iterations was set to 5, and the optimisation process performed converged successfully to the global minimum. Experiments were carried out with different number of sampling points or number of iterations. They are going to be discussed as a sensitivity analysis in the performance of the optimiser.

6.1.1 Line drive pattern

After the successful termination of the optimisation process , the **global optimum** is reported as 25 grid blocks or 2000 m (Figure 6.1) for both the x, y-direction. The evaluated optimal NPV is 361 M.€.

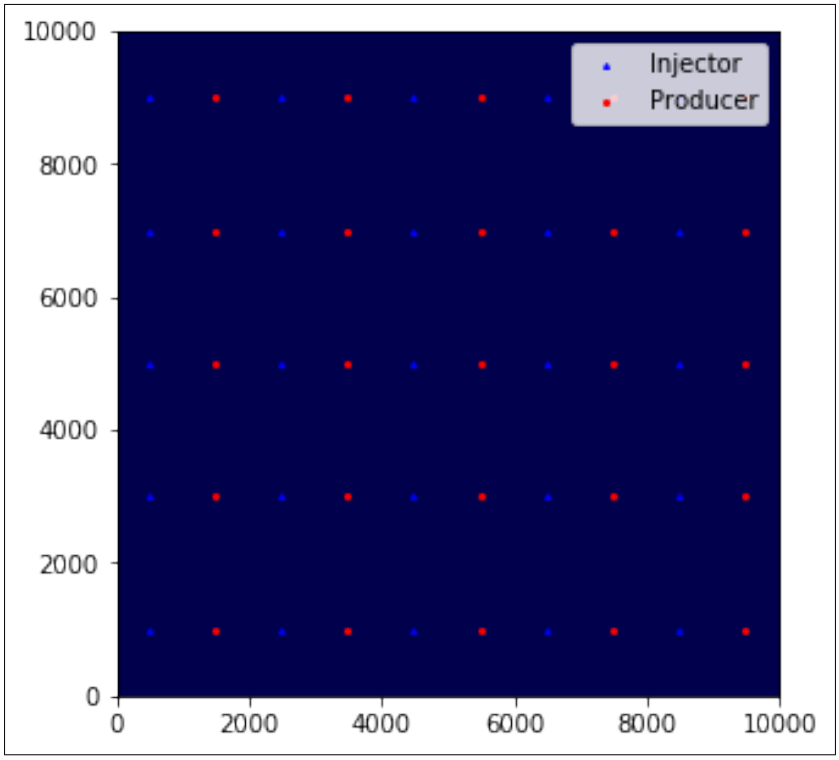

Figure 6.1: Optimal line drive pattern for the homogeneous and isotropic aquifer.

The optimal pattern sizes were fed to an experiment to show the aquifer status during the simulated time. This was done for all experiments conducted in all synthetic models and for both development strategies (5 spot and line-drive). Figure 6.2 presents the temperature field in time-steps of 10 years of production until 30 years of lifetime. It is apparent that with this pattern type, the optimum pattern size is not fully sweeping the aquifer under the current reservoir and production conditions due to the placement of the producers. The same geometry is observed in all following line drive developments of all synthetic models. Thus, there are "stripes" in the aquifer left un-swept in between rows of injectors and producers. Figure 6.3 shows the pressure field in time-steps of 10 years of production until reaching 30 years of lifetime. After ten years of production, there is a minor pressure build-up in the centre of the aquifer, which is increased totally by 20 bars until the end of production. Generally, the imposed production fixed pressure combined with the isotropic permeability does not result in extreme pressure values in the reservoir.

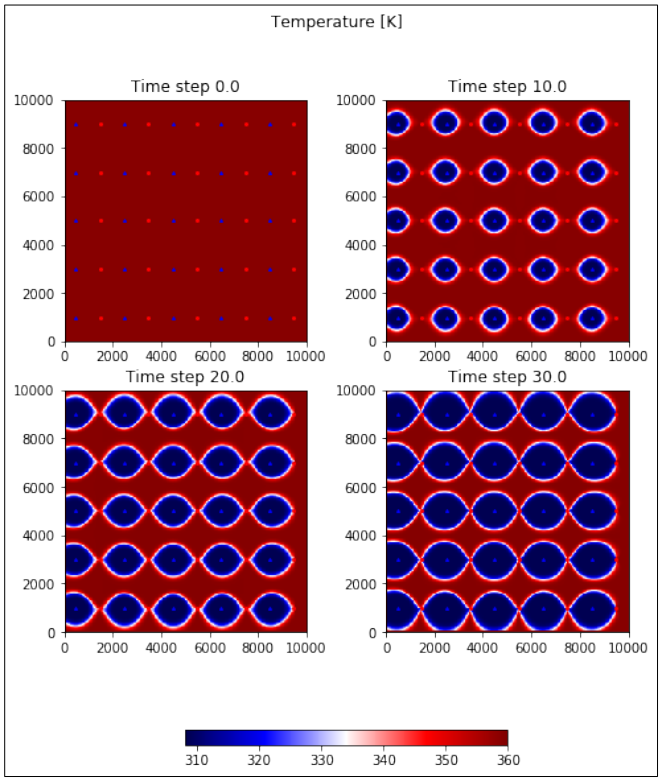

Figure 6.2: Temperature (K) every 10 years of production in the produced aquifer.

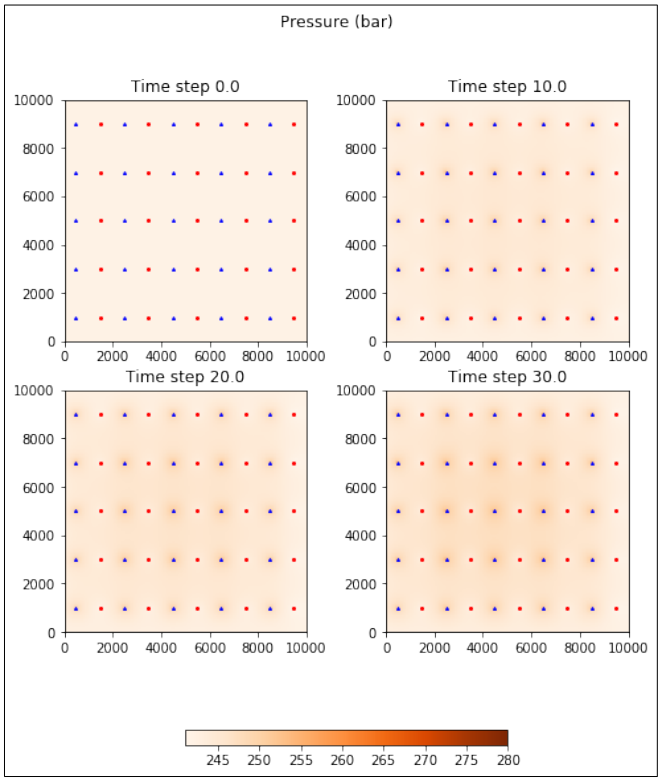

Figure 6.3: Pressure (bar) every 10 years of production in the produced aquifer.

Figure 6.4 presents the result of developing the reservoir with the optimal pattern size per injector and producer well, bottom hole pressure, temperature, flow rates and energy rates. Early breakthrough (25 years) is observed in few producers, but generally the breakthrough temperature is only 35 K lower than reservoir temperature meaning that the line drive is not that efficient. Injectors are constrained in constant water rate, visible by the flat line in flow rate plots, temperature and energy rate. Producers have prescribed a fixed pressure.

Energy rates (Figure 6.5) are presented as a sum per well type (injectors, producers) and net energy rates, a time series of total energy rate injected and produced. Having a basis of the energy time-series curve, the heat revenues are calculated with 0.066€ millions /GWh without any annual discount. This curve indicates the yearly cash flow rate. After introducing subsidy revenues for the first 15 years of production, the cashflow curve is modified 6.5). For the current project, drilling costs are introduced in the year-0 of production, creating the final value of NPV thus, the cash flow curve is modified. After the year 0 of production the project becomes profitable with revenues from energy extracted (Figure 6.6).

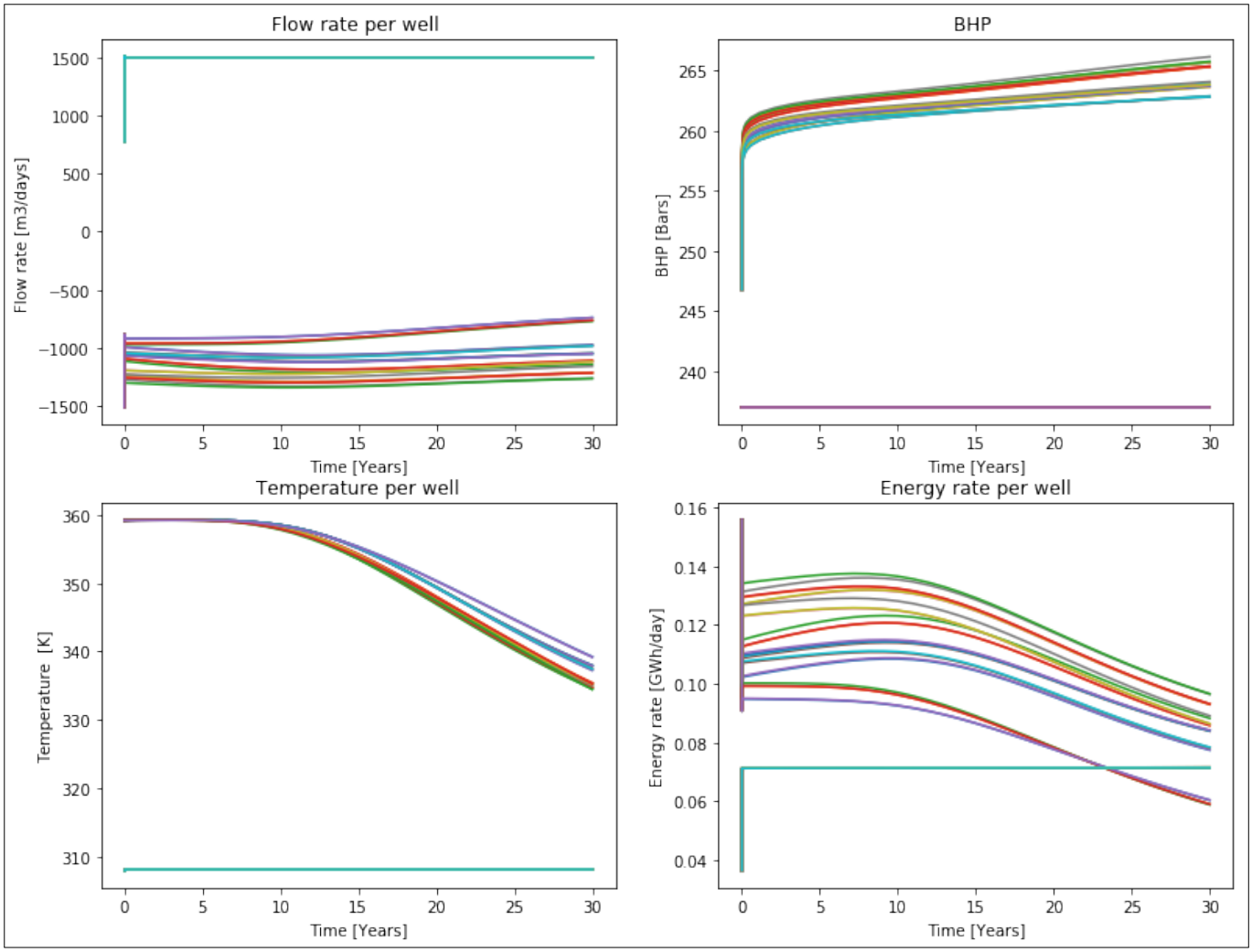

Figure 6.4: Simulator output data of temperature, pressure, flow rates and energy rates. Injectors are constrained in constant water rate which is visible by the flat line in plots of flow rate, temperature and energy rate. Flow rates of producer wells are assigned with a minus (-). Producers are prescribed a fixed pressure.

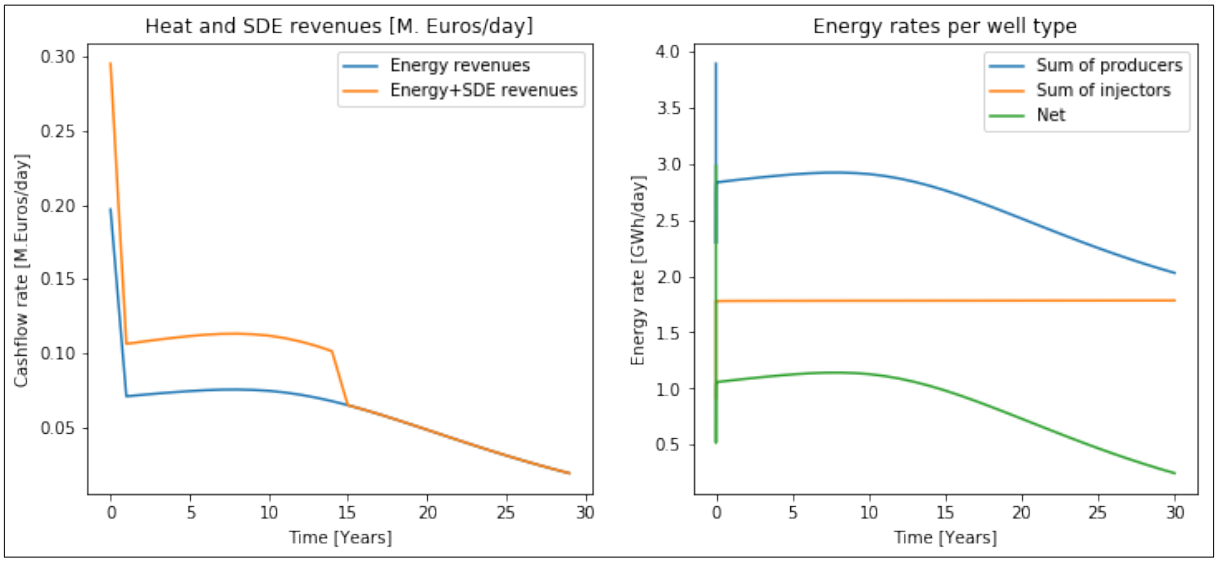

Figure 6.5: Revenues cashflow rate of the optimal development strategy and energy rates summed over well type and net energy recovered.

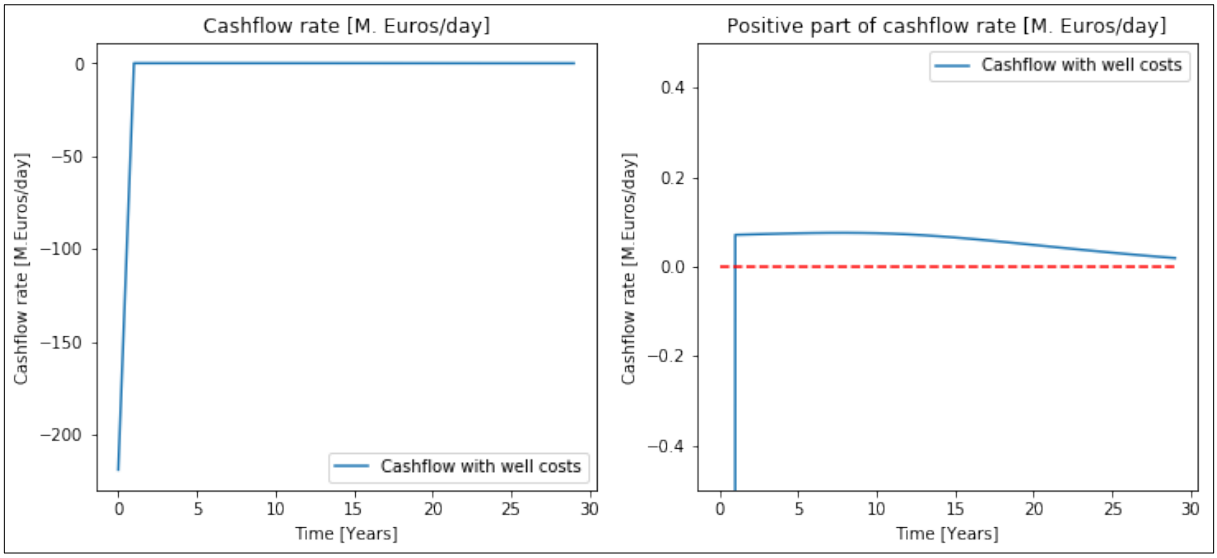

Figure 6.6: Cash flow rates with well costs included in year 0 of production, also focused in the positive part of the project.

6.1.2 5 spot pattern performance

After the successful termination of the optimisation process, the **global optimum** is reported at 20 grid blocks or 800 m for both the x and y-direction. The evaluated optimal NPV is 810 M.€.

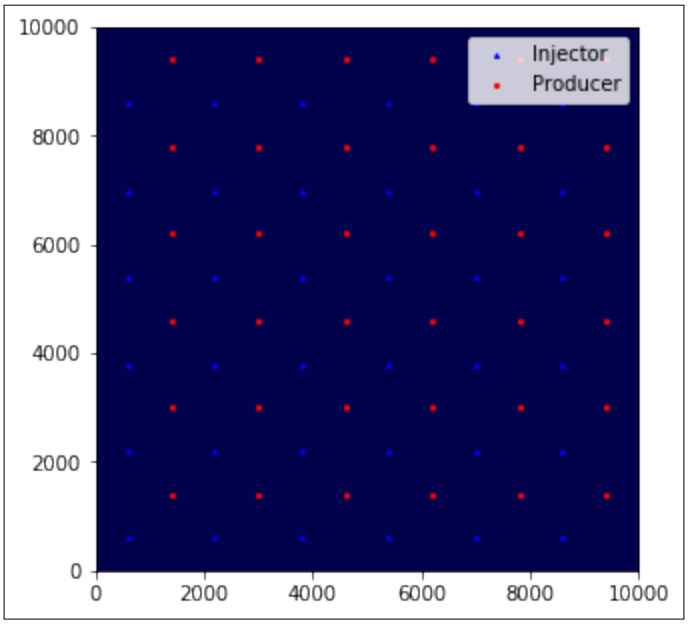

Figure 6.7: Optimal 5 spot pattern for the homogeneous and isotropic aquifer.

The optimal pattern sizes were fed to an experiment to show the aquifer status during the simulated time. Figure 6.8 presents the temperature field in time-steps of 10 years of production until 30 years of lifetime. This pattern type, sweeps more efficiently the aquifer than the line drive. Figure 6.9 shows the pressure field in time-steps of 10 years of production until 30 years of lifetime. After ten years of production, there is a minor pressure build-up in the centre of the aquifer, which is increased totally by 20 bars until the end of production. The 5 spot creates minor pressure discrepancies in the field compared like line drive pattern.

Figure 6.10 presents the results of the development with the optimal pattern size per injector and producer well, bottom hole pressure, temperature, flow rates and energy rates. Injectors are constrained in constant water rate, visible by the flat line in flow rate plots, producer flow rates are assigned with minus(-), temperature and energy rate. Producers have prescribed a fixed pressure. The breakthrough of the five spot is at 30 years in most of the producers, but generally the breakthrough temperature is only 35 lower (50 degrees of reservoir-injection temperature) than the reservoir temperature meaning that the five spot is more efficient that the line drive in terms of delaying the breakthrough time for 5 years. Although, both patterns end up with the same temperature difference.

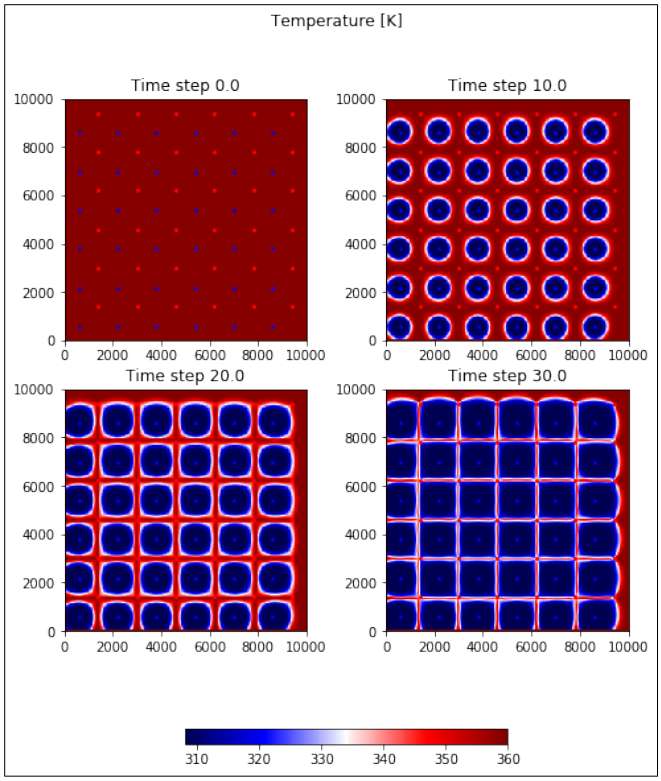

Figure 6.8: Temperature (K) every 10 years of production in the produced aquifer.

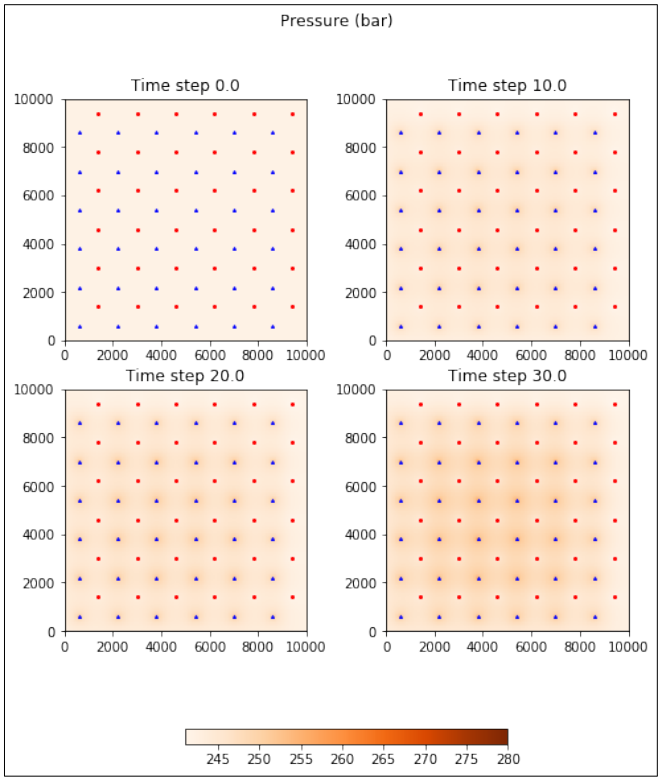

Figure 6.9: Pressure (bar) every 10 years of production in the produced aquifer.

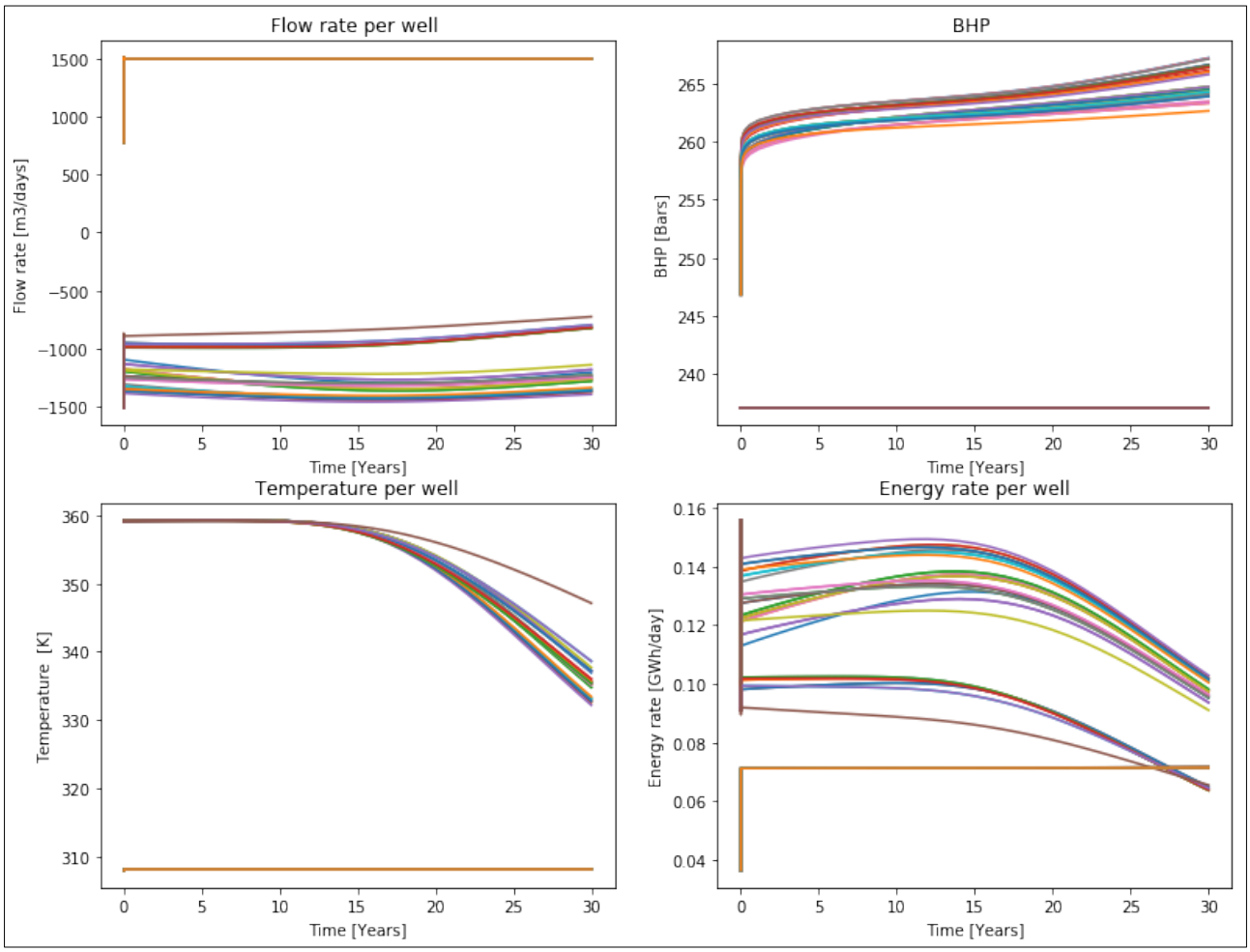

Figure 6.10: Simulator output data of temperature, pressure, flow rates and energy rates. Injectors are constrained in constant water rate which is visible by the flat line in plots of flow rate, temperature and energy rate. Producers are prescribed a fixed pressure.

Energy rates (Figure 6.11) are presented as a sum per well type (injectors, producers) and net energy rates, a time series of total energy rate injected and produced. Having a basis of the energy time-series curve, the heat revenues are calculated with a 0.066€ millions /GWh without any annual discount. This curve indicates the yearly cash flow rate. After introducing subsidy revenues at the first 15 years of production, the cashflow curve is modified 6.11). For the current project, drilling costs are introduced in the year-0 of production, creating the final value of NPV. Thus, the cash flow curve is modified, and when zooming in the positive part, the profit of the project only with revenues from energy is extracted (Figure 6.12). The cashflow curve for the 5-spot indicates the boosting of the revenues over the last 5 years of the project compared to the line drive. Therefore, the more energy the 5-spot sweeps the last 5 years, is boosting the cashflow at the end of the project.

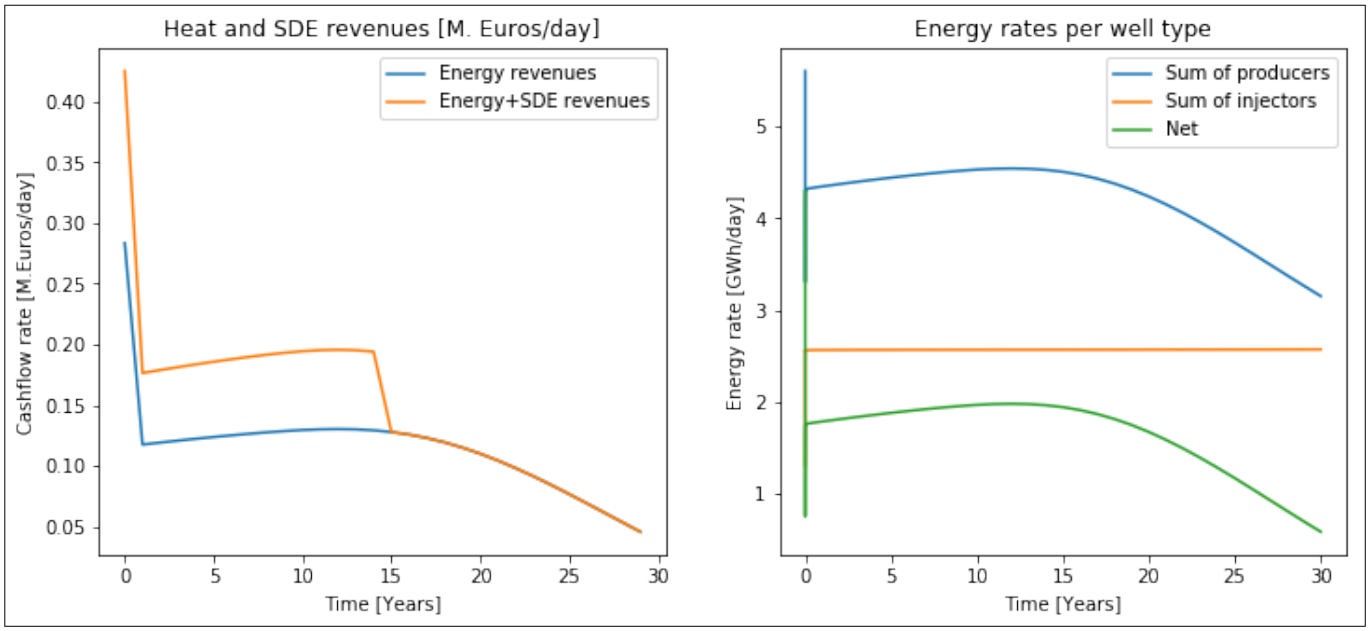

Figure 6.11: Revenues cashflow rate of the optimal development strategy and energy rates summed over well-type and net energy recovered.

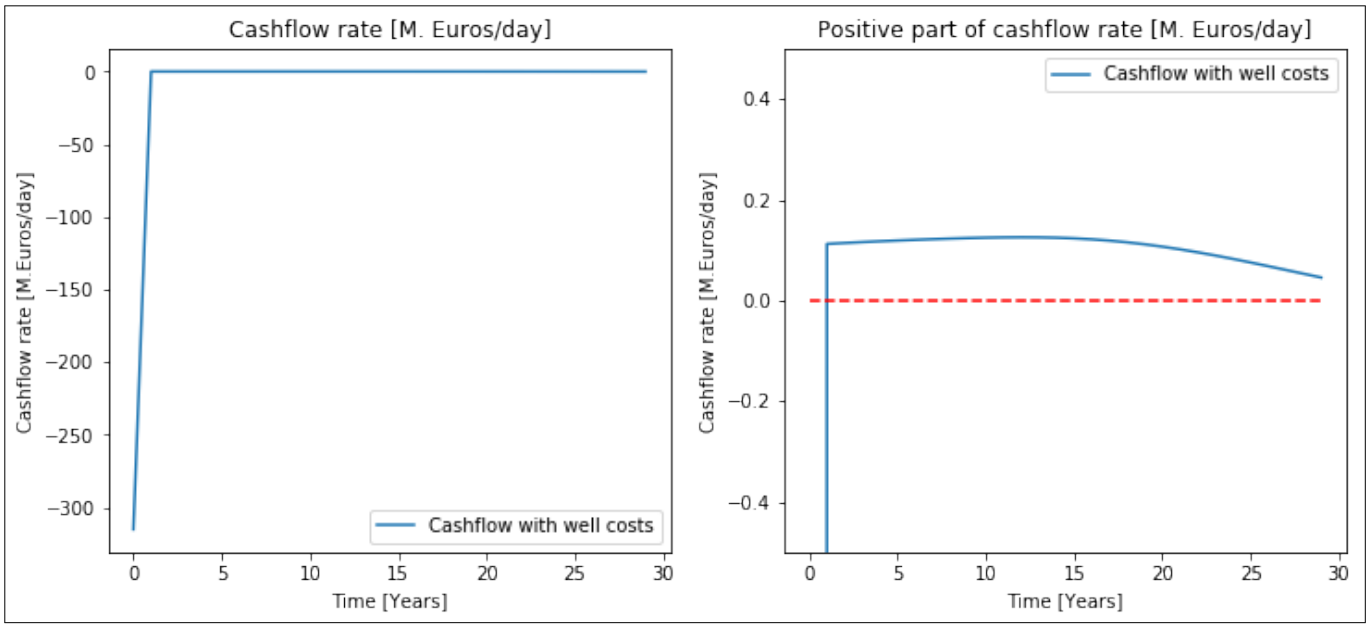

Figure 6.12: Cash flow rates with well costs included in year 0 of production, also focused in the positive part of the project. The cashflow curve of the 5-spot outperforms the cashflow curve of the line drive for the last 5 years of the project.

6.2 Case 2: 2D homogeneous and anisotropic sandstone aquifer

The optimisation workflow is set up for the 2D homogeneous system, with a pattern size in the range of $5 - 80$ grid blocks that correspond to $120 - 3200$ m of pattern size (injector-injector, producer-producer distance). These bounds of search area were set such that the simulation would converge with the minimum pattern size, and a complete pattern would fit in the aquifer with the preset maximum pattern size. The sampling method of optimisation is Sobol, which evenly distributes sampling points to gain the geometrical information of the objective function. The number of points is set to 50. The maximum number of iterations was set to 5, and the optimisation process performed converged successfully to the global minimum.

6.2.1 Line drive pattern

After the successful termination of the optimisation process, the **global optimum** is reported as 39, 10 grid blocks or $3020, 400$ m for the x, y-direction. The evaluated optimal NPV is 429 M.€.

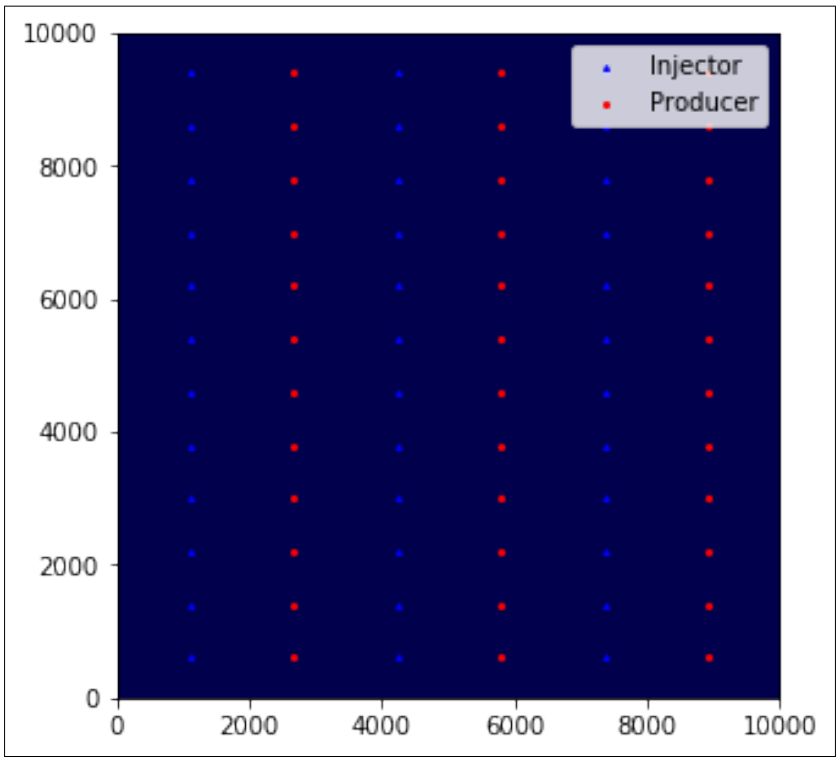

Figure 6.13: Optimal line drive pattern for the homogeneous and anisotropic aquifer.

The optimal pattern sizes were fed to an experiment to show the aquifer status during the simulated time. Figure 6.14 presents the temperature field in time-steps of 10 years of production until 30 years of lifetime. It is apparent that with this pattern type, the optimum pattern size is not fully sweeping the right part of the aquifer under the current reservoir and production conditions due to limitations on placing extra wells close to the boundaries. Figure 6.15 shows the pressure field in time-steps of 10 years of production until 30 years of lifetime. After ten years of production, there is a pressure build-up in the centre of the aquifer , which is increased totally by 40 bars until the end of production. Figure 6.16 presents the optimal pattern size per injector and producer well, bottom hole pressure, temperature, flow rates and energy rates. Energy rates (Figure 6.17) are presented as a sum per well type (injectors, producers) and net energy rates, a time series of total energy rate injected and produced. Having a basis of the energy time-series curve, the heat revenues are calculated with a 0.066 € millions/GWh without any annual discount. This curve indicates the yearly cash flow rate. After introducing subsidy revenues at the first 15 years of production, the cashflow curve is modified 6.17).

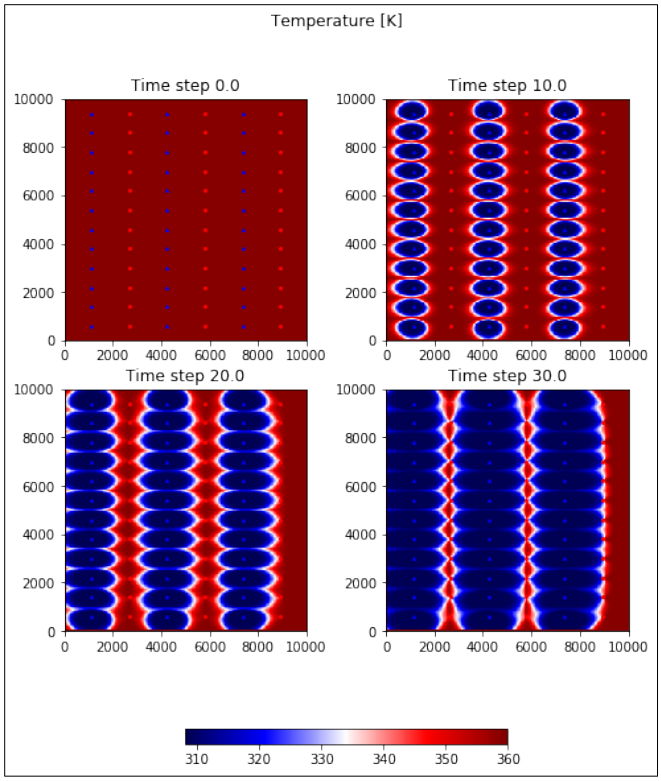

Figure 6.14: Temperature (K) every 10 years of production in the produced aquifer.

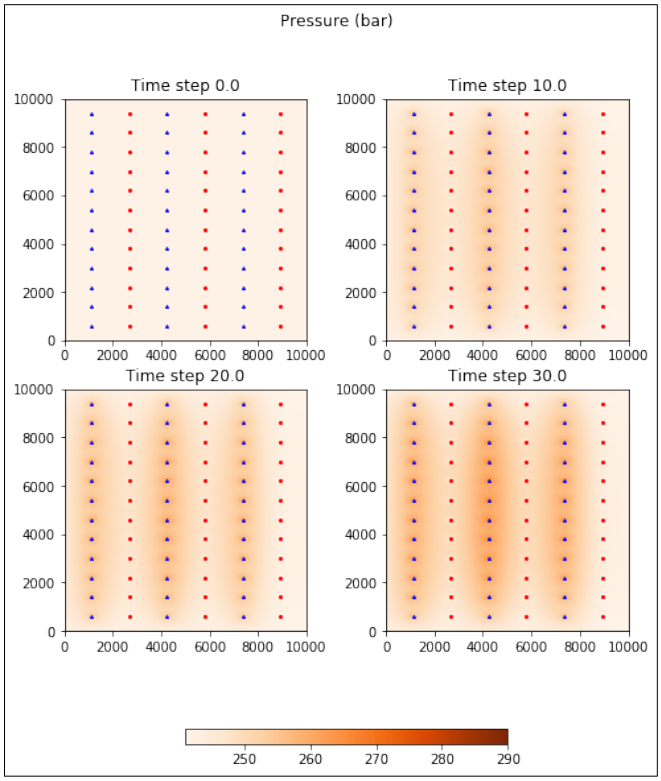

Figure 6.15: Pressure (bar) every 10 years of production in the produced aquifer.

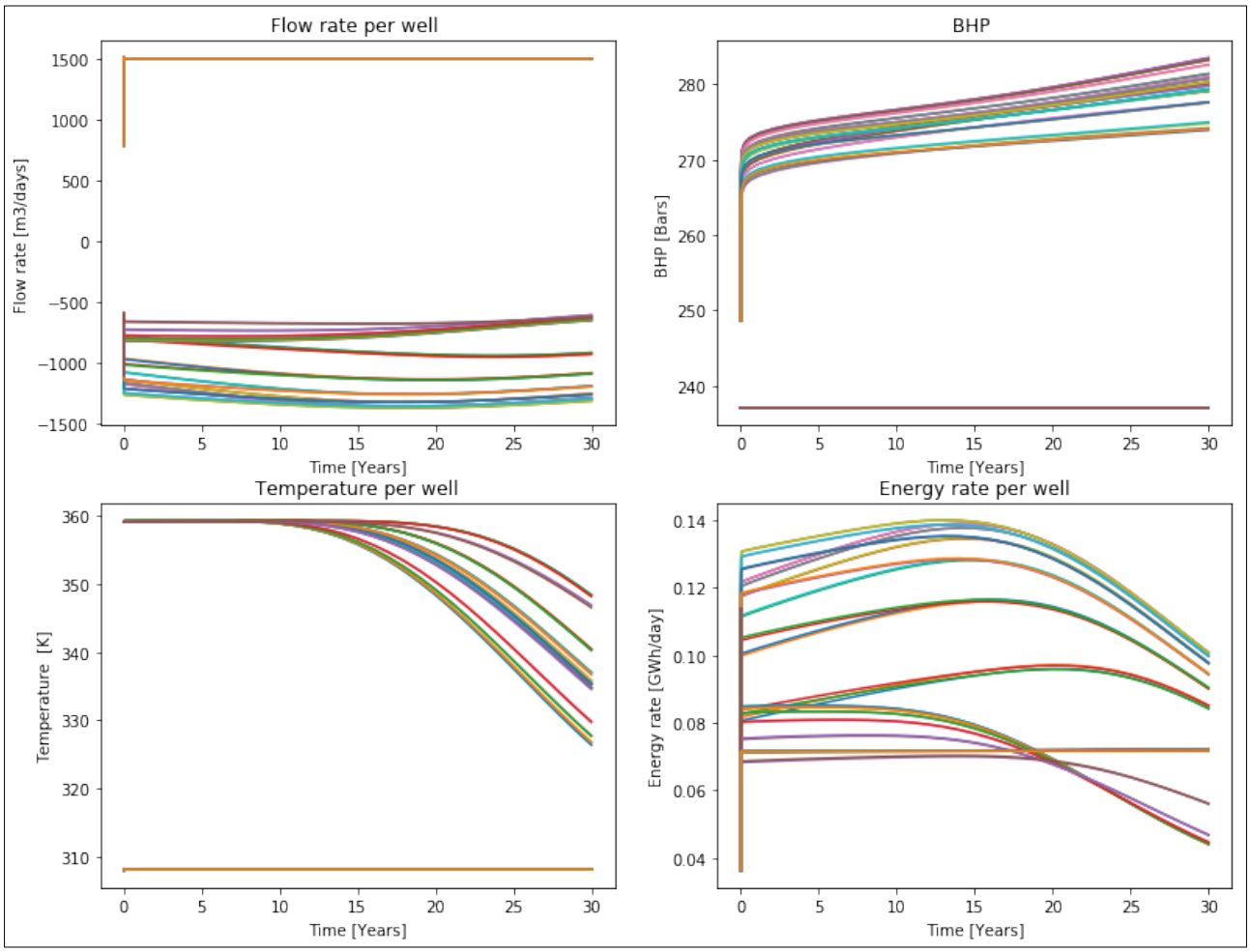

Figure 6.16: Simulator output data of temperature, pressure, flow rates and energy rates. Injectors are constrained with constant water flow rate which is visible by the flat line in plots of flow rate, producers are assigned with a minus (-) on flow rates, temperature and energy rate. Producers are prescribed a fixed pressure.

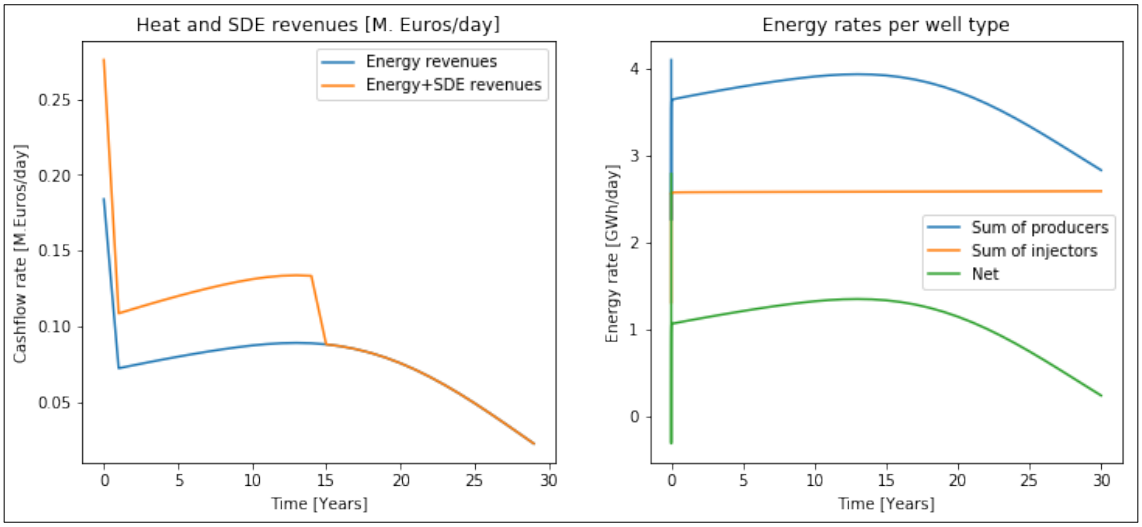

Figure 6.17: Revenues cashflow rate of the optimal development strategy and energy rates summed over well-type and net energy recovered.

For the current project, again the drilling costs are introduced in the year-0 of production. Thus, the cash flow curve is modified, and when zooming in the positive part, the profit of the project only with revenues from energy extracted (Figure 6.18). After 20 years of production the cashflow starts to drop down due to the cold front arrival in most of the producer wells.

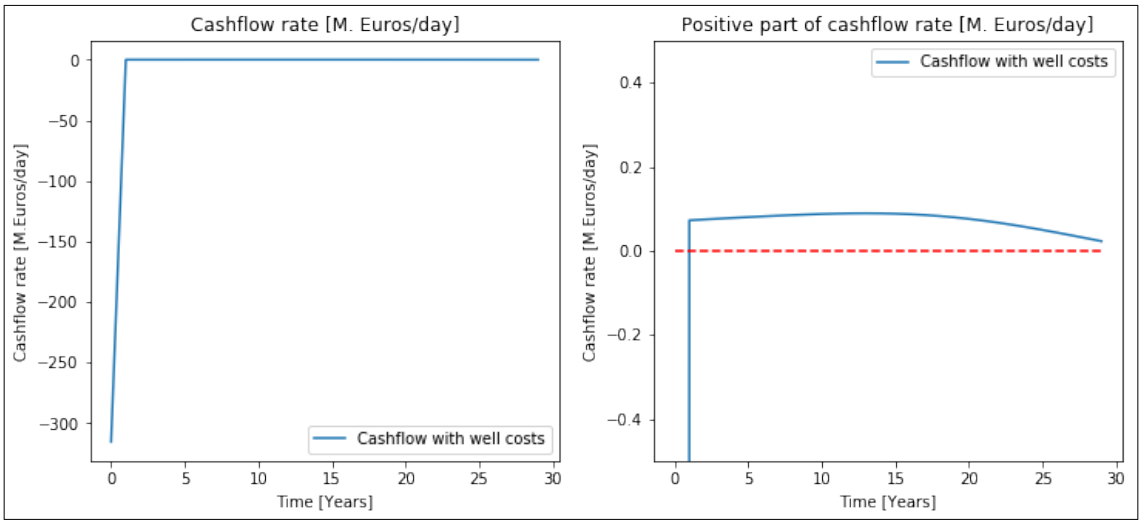

Figure 6.18: Cash flow rates with well costs included in year 0 of production, also focused in the positive part of the project.

6.2.2 5 spot pattern performance

After the successful termination of the optimisation process, the **global optimum** is reported at 23, 15 grid blocks or 1840, 1200 m for the x, y-direction. The evaluated optimal NPV is 548 M.€. Comparing this output with the line-drive, the 5-spot is again more efficient in terms of profitability.

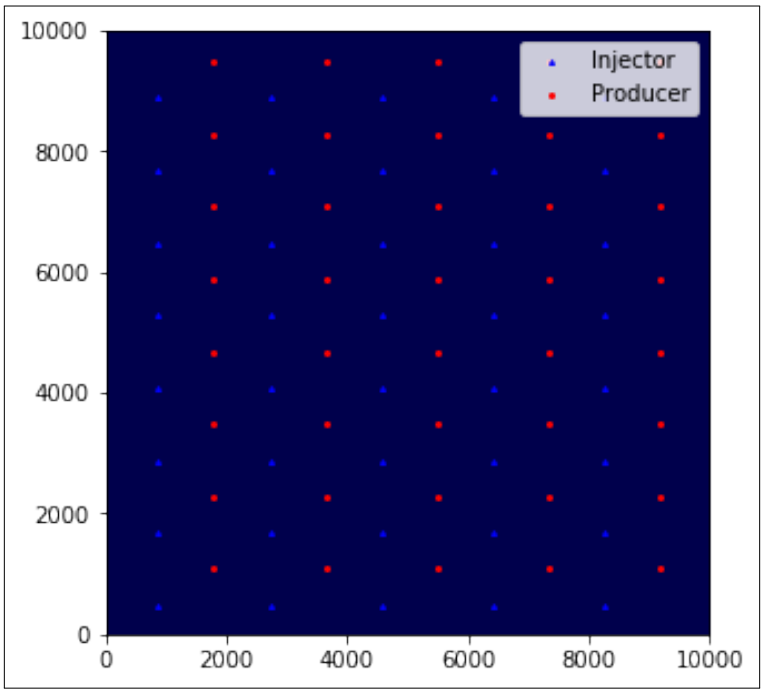

Figure 6.19: Optimal 5 spot pattern for the heterogeneous aquifer.

The optimal pattern sizes were fed to an experiment to show the aquifer status during the simulated time. Figure 6.20 presents the temperature field in time-steps of 10 years of production until 30 years of lifetime. The 5-spot pattern is more efficiently sweeping the aquifer in the centre compared to the line-drive. Figure 6.21 shows the pressure buildup of the 5-spot is much higher that the line-drive. After 30 years of production, there is a pressure build-up in centre of the aquifer, which is increased totally by 30 bars for both 5-spot and line-drive. Figure 6.22 presents the results of the optimal pattern size per injector and producer well, bottom hole pressure, temperature, flow rates and energy rates. Temperature time-series reveals that many more producers of the 5-spot see the cold front arrival at 30 years compared to the line-drive. The temperature difference though is for both 35 degrees. Energy rates (Figure 6.23) are presented as a sum per well type (injectors, producers) and net energy rates, a time series of total energy rate injected and produced. Having a basis of the energy time-series curve, the heat revenues are calculated with a 0.066 € millions /GWh without any annual discount. This curve indicates the yearly cash flow rate. After introducing subsidy revenues at the first 15 years of production, the cashflow curve is modified (Figure 6.23). When comparing line-drive and 5-spot cashflow curves (Figure 6.24), 5-spot is rendering the development the development more profitable since it is exceeding the 0.1 M.Euros/day especially in the first 15 years of the project compared to the line-drive .

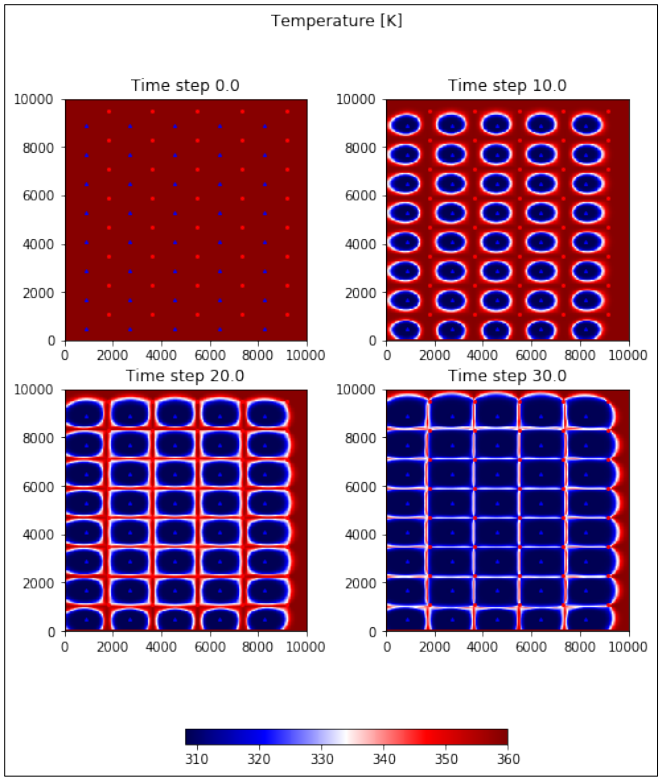

Figure 6.20: Temperature (K) every 10 years of production in the produced aquifer.

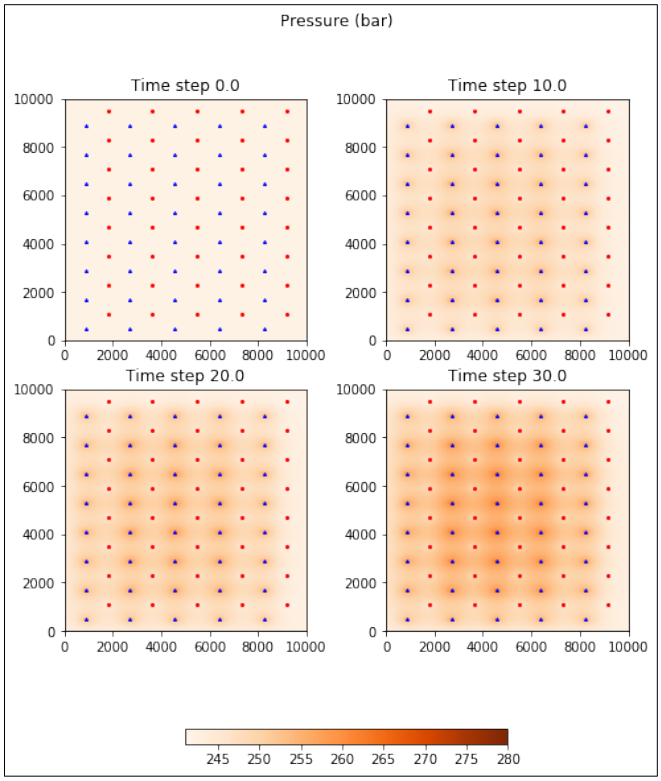

Figure 6.21: Pressure (bar) every 10 years of production in the produced aquifer.

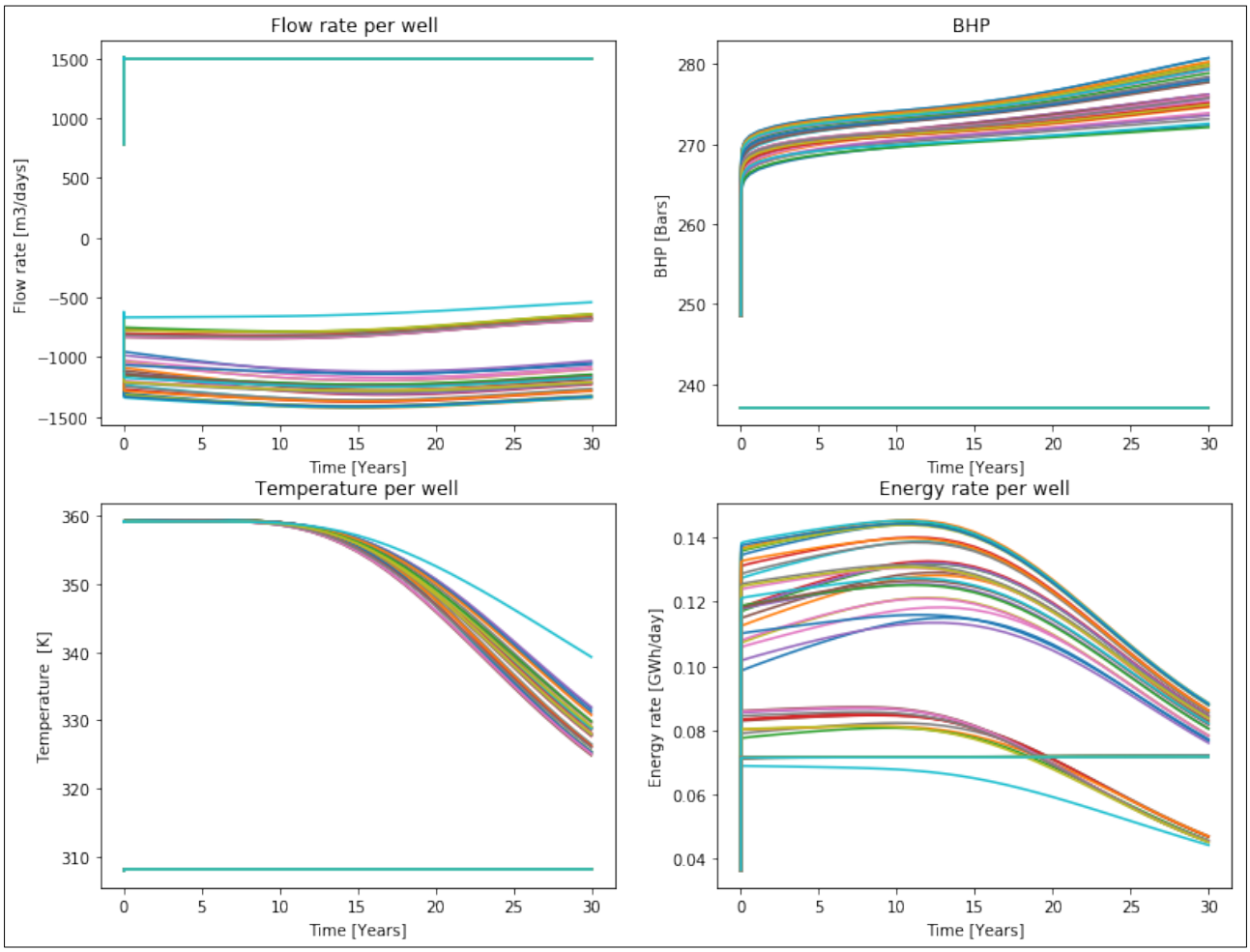

Figure 6.22: Simulator output data of temperature, pressure, flow rates and energy rates. Injectors are con-strained in constant water rate which is visible by the flat line in plots of flow rate, temperature and energy rate. Producers are prescribed a fixed pressure. Producers are assigned with a minus (-) in the flow rate curve.

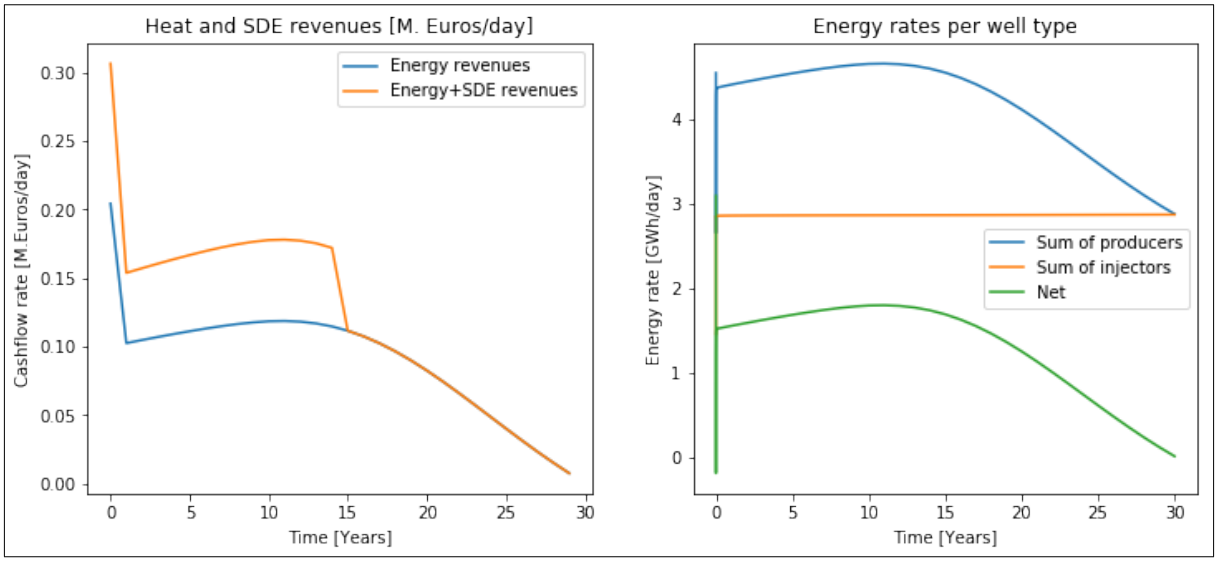

Figure 6.23: Revenues cashflow rate of the optimal development strategy and energy rates summed over well-type and net energy recovered.

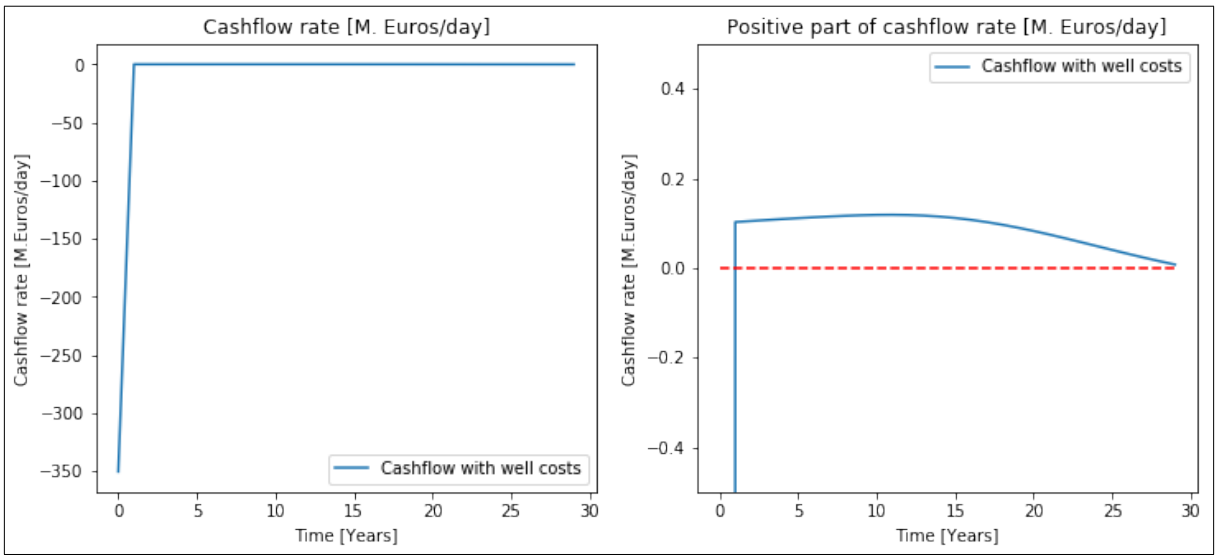

Figure 6.24: Cash flow rates with well costs included in year 0 of production, also focused in the positive part of the project.

6.3 Case 3: 2D aquifer with linear porosity trend

The optimisation workflow is set up for the 2D homogeneous system, with a pattern size in the range of $5 - 80$ grid blocks that correspond to $120 - 3200$ m of pattern size (injector-injector, producer-producer distance). These bounds of search area were set so as the simulation would converge with the minimum pattern size, and a complete pattern would fit in the aquifer with the preset maximum pattern size.

6.3.1 Line drive pattern performance

Table 6.1 shows the output of the optimiser with the optimal output and tuning controls, for the homogeneous reservoir with the linear trend in porosity.

Table 6.1: Input parameters for the optimisation algorithm.

Optimiser tuning parameters	**Value**
Sampling points	100
Sampling sequence	Sobol
Maximum number of iterations	5
Flexible pattern size boundaries	[5,80]

After the successful termination of the optimisation process, the **global optimum** is reported for a well density function in x-direction in **grid blocks**:

$$D_x = \frac{25.0390625}{250} * x + 25.0390625 \tag{6.1}$$

This corresponds to a well density function in **meters**:

$$D_x = \frac{1000}{10000} * x + 1000 \tag{6.2}$$

The optimal pattern size at the y-direction is at 15 grid or 600 m. The evaluated optimal NPV is 263 M.€.

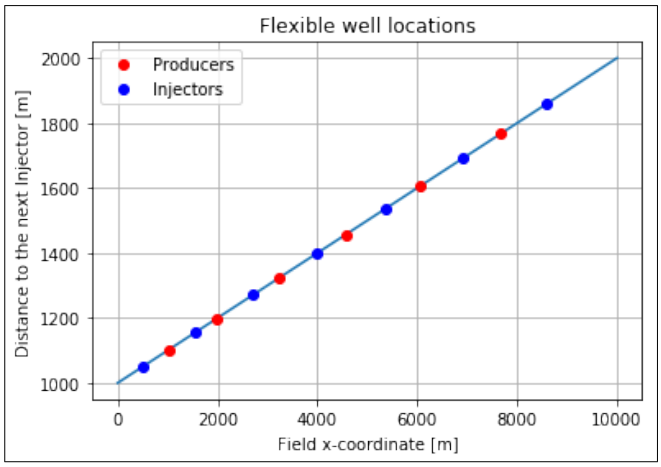

Figure 6.25: Optimal suggested well density function for the line drive pattern

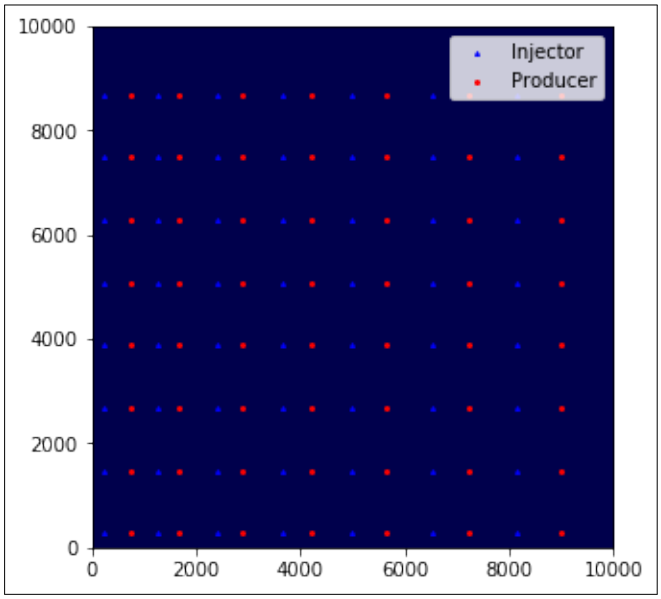

Figure 6.26: Optimal 5 spot pattern for the aquifer with the linear porosity.

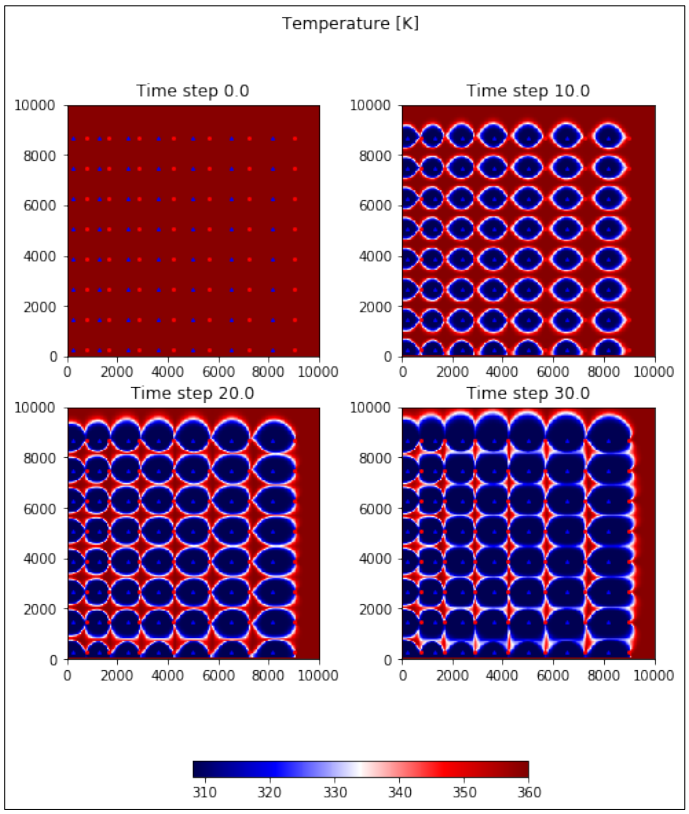

Figure 6.27: Temperature (K) every 10 years of production in the produced aquifer.

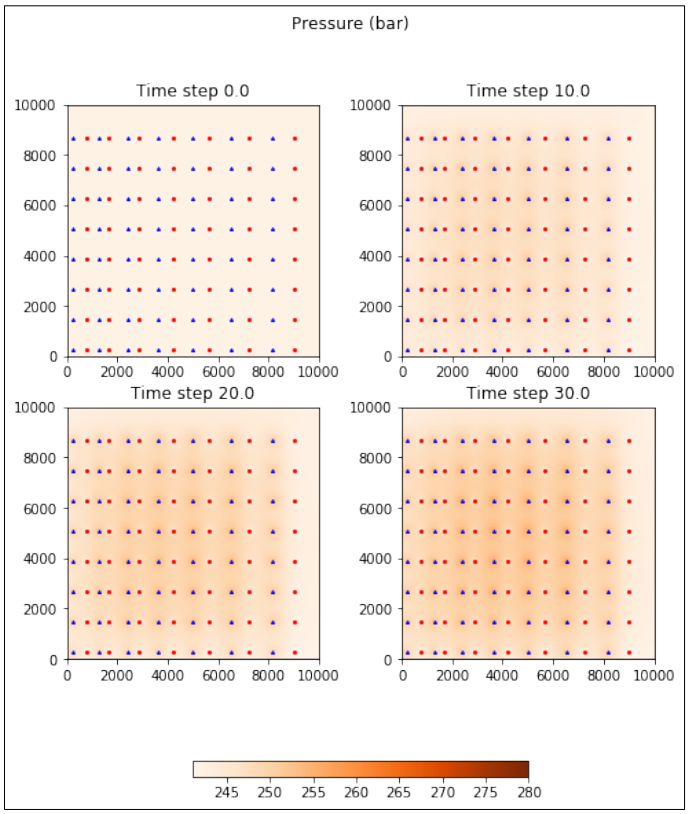

Figure 6.28: Pressure (bar) every 10 years of production in the produced aquifer.

After receiving the control that the algorithm indicated as optimal, an experiment is run to show the aquifer status during the simulated time. Figure 6.27 presents the temperature field in time-steps of 10 years of production until 30 years of lifetime. Figure 6.28 shows the pressure field in time-steps of 10 years of production until 30 years of lifetime. After 30 years of production, there is a pressure build-up in the centre of the aquifer, which is increased totally by 20 bars until the end of production. Figure 6.29 presents the results of the development of the optimal pattern size per injector and producer well, bottom hole pressure, temperature, flow rates and energy rates. The temperature time-series indicates that the production temperature starts to drop from the very beginning of the project. Finally at 30 years of production, most of the producers have seen a cold breakthrough and a temperature drop by 30-45 degrees of K. Energy rates (Figure 6.30) are presented as a sum per well type (injectors, producers) and net energy rates, a time series of total energy rate injected and produced. Having a basis of the energy time-series curve, the heat revenues are calculated with a 0.066€ millions /GWh without any annual discount. This curve indicates the yearly cash flow rate. After introducing subsidy revenues at the first 15 years of production, the cashflow curve is modified 6.30).

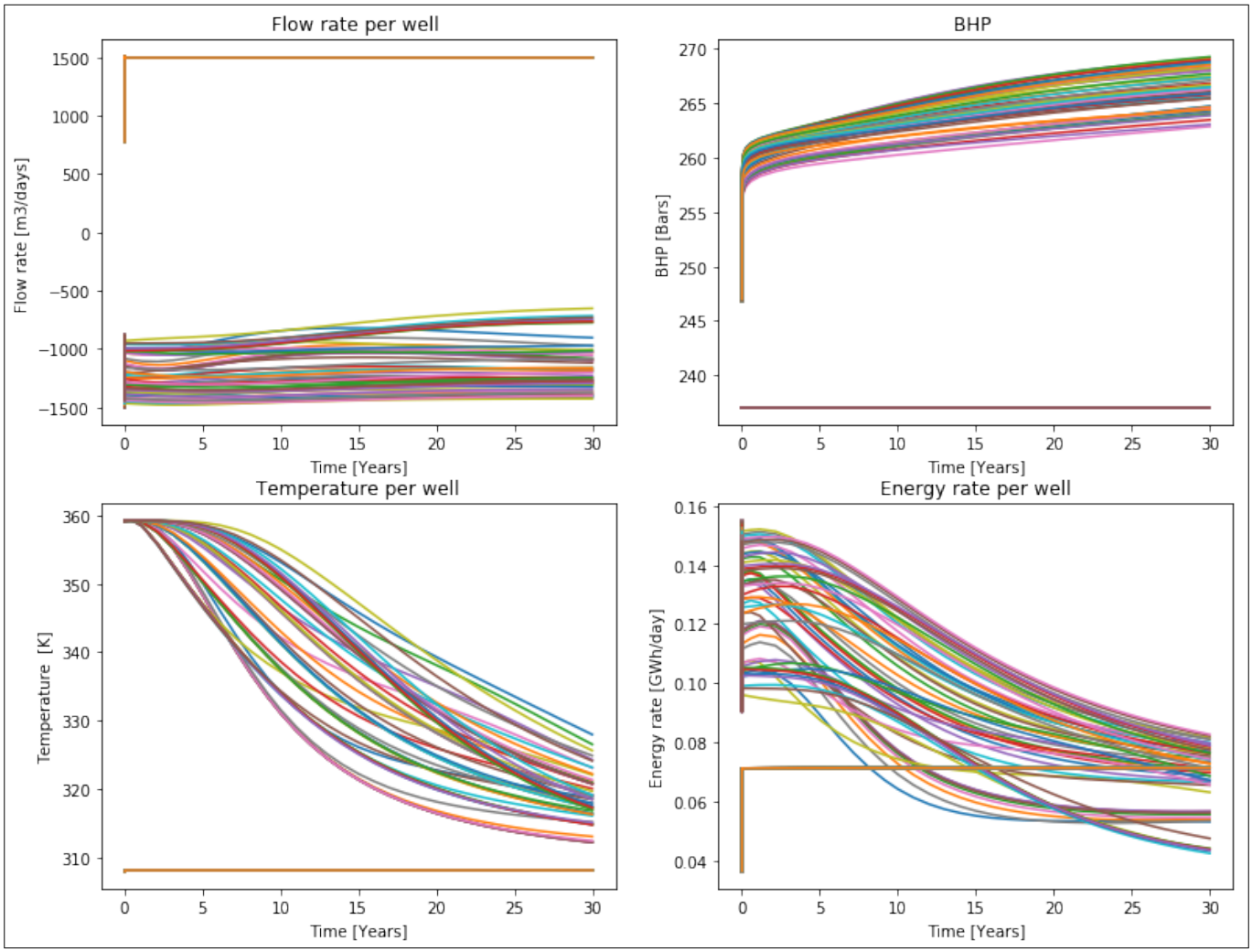

Figure 6.29: Simulator output data of temperature, pressure, flow rates and energy rates. Injectors are con-strained in constant water rate which is visible by the flat line in plots of flow rate, temperature and energy rate. Producers are prescribed to operate at a fixed pressure. Producers are assigned with a minus (-) in the flow rate plot.

For the current project, drilling costs are introduced in the year-0 of production, creating the final value of NPV. Thus, the cash flow curve is modified, and when zooming in the positive part, the profit of the project only with revenues from energy extracted (Figure 6.31). The project in the very beginning seems to be the highest revenues which immediately drop. After 25 years of operation, the development becomes uneconomical.

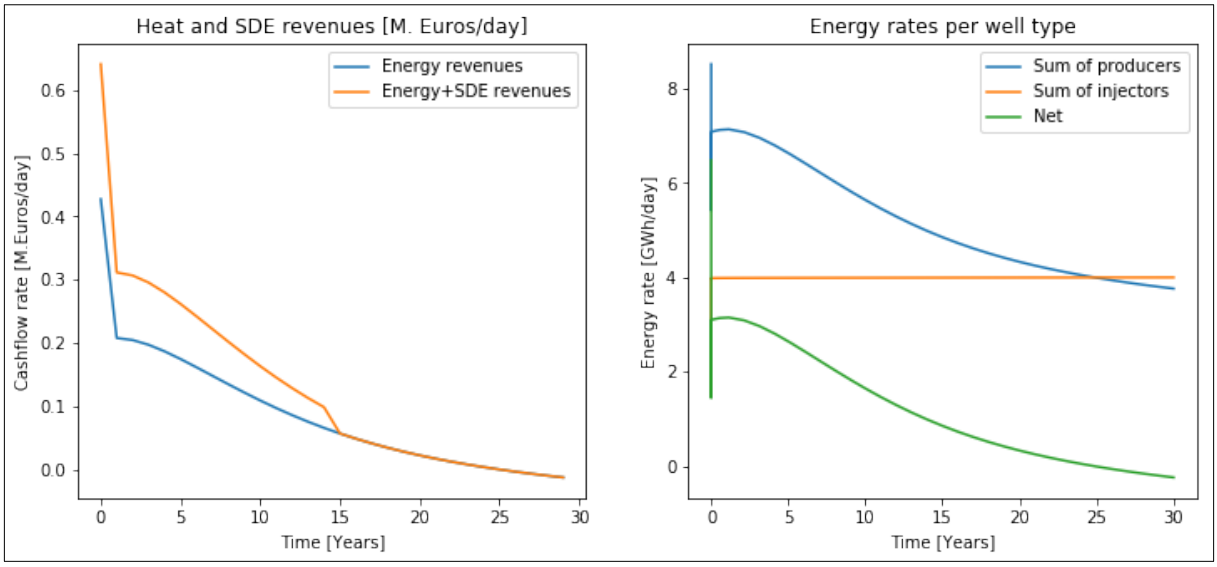

Figure 6.30: Revenues cashflow rate of the optimal development strategy and energy rates summed over well-type and net energy recovered.

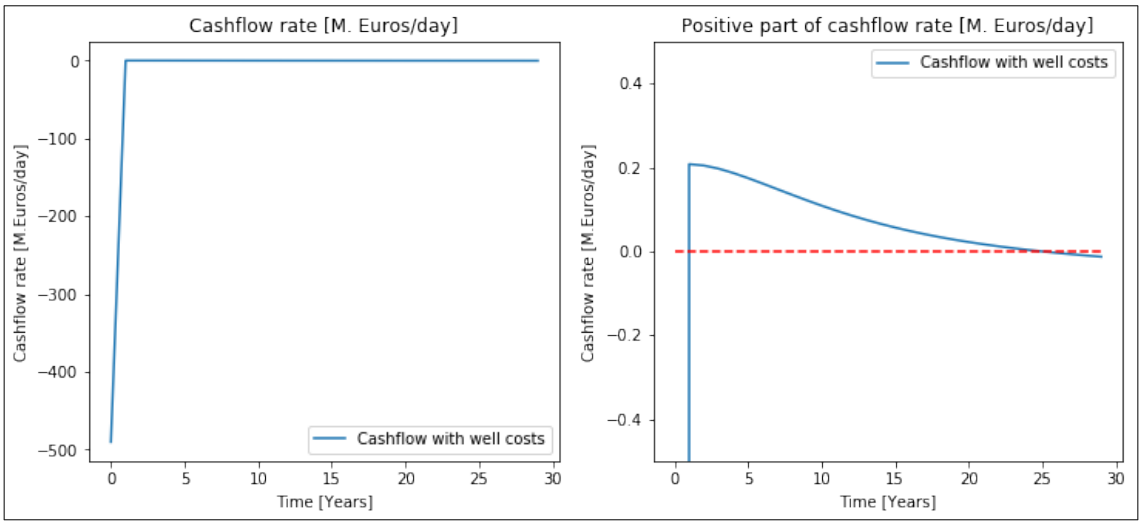

Figure 6.31: Cash flow rates with well costs included in year 0 of production. Focusing on the positive part, the project remains profitable in most of its lifetime.

6.3.2 5 spot pattern performance

Table 6.2 shows the output of the optimiser with the optimal output and tuning controls.

Table 6.2: Input parameters for the optimisation algorithm.

Optimiser tuning parameters	**Value**
Sampling points	200
Sampling sequence	Sobol
Maximum number of iterations	5
Flexible pattern size boundaries	[5,80]

After the successful termination of the optimisation process, the **global optimum** is reported for a well density function in x-direction in **grid blocks**:

$$D_x = \frac{5.40429688}{250} * x + 36.11523438 \tag{6.3}$$

This corresponds to a well density function in **meters**:

$$D_x = \frac{200}{10000} * x + 1440 \tag{6.4}$$

The optimal pattern size at the y-direction is at 20 grid blocks or 800 m. The evaluated optimal NPV is 735 M.€.

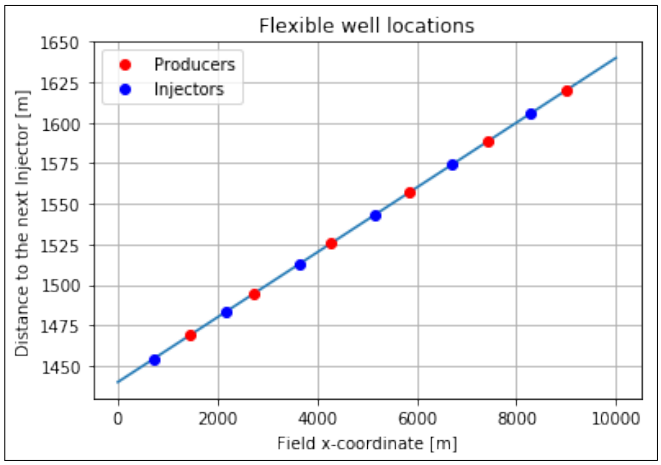

Figure 6.32: Optimal suggested well density function for the 5 spot pattern

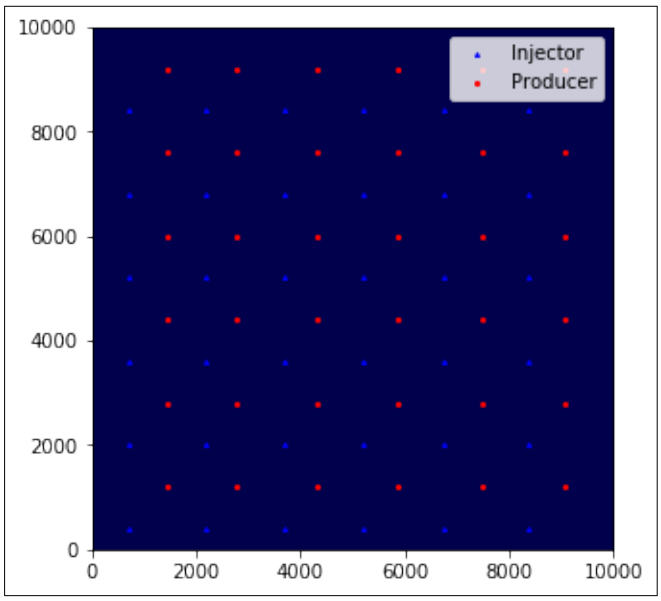

Figure 6.33: Optimal 5 spot pattern for the aquifer with the linear porosity.

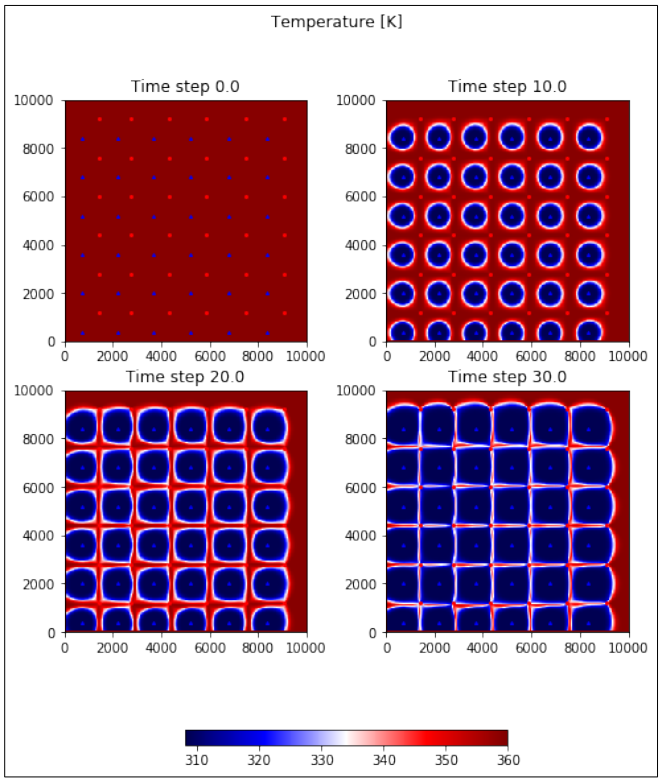

Figure 6.34: Temperature (K) every 10 years of production in the produced aquifer.

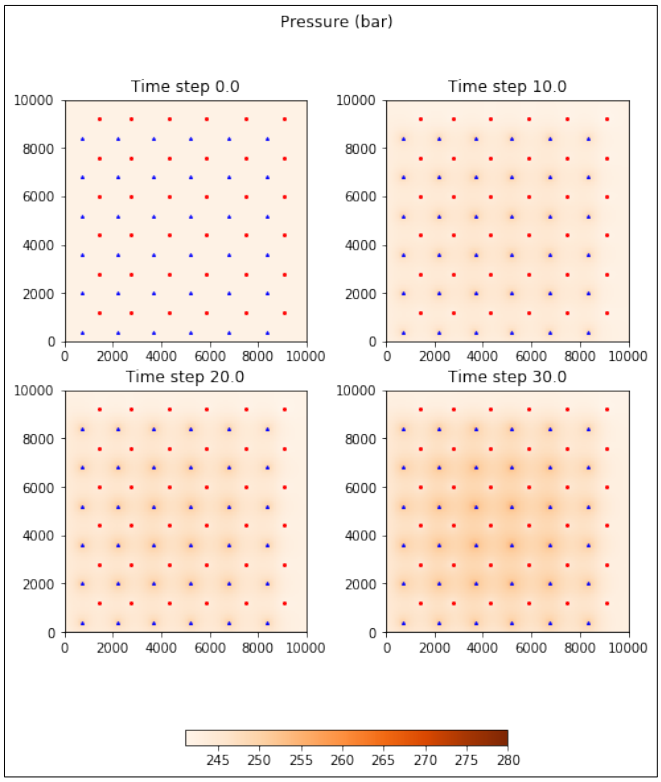

Figure 6.35: Pressure (bar) every 10 years of production in the produced aquifer.

After receiving the control that the algorithm indicated as optimal, an experiment is run to show the aquifer status during the simulated time. Figure 6.34 presents the temperature field in time-steps of 10 years of production until 30 years of lifetime. It is apparent that with this pattern type, the optimum pattern size is performing much better than the line-drive. The centre of the reservoir is swept more efficiently. Though, the right and top side of the aquifer again is not swept under the current reservoir and production conditions due to limitations on placing extra wells close to the boundaries. Figure 6.35 shows the pressure field in time-steps of 10 years of production until 30 years of lifetime. After 30 years of production, there is a pressure build-up in the centre of the aquifer, which is increased totally by 10 bars. Comparing 5-spot with line-drive, 5-spot is safer given that the reservoir pressure is not significantly changing. Figure 6.36 presents the development results of the optimal pattern size per injector and producer well, bottom hole pressure, temperature, flow rates and energy rates. Taking a look at the temperature time series, we observe that

the cold front arrives more or less at the same time at the producers. Generally, a temperature drop by 25-30 K is seen at the end of the lifetime of the project. This development strategy presents more consistent results in terms of temperature because more or less all producers follow the same trend and the temperature starts to drop after 10 years of production. Line-drive presented less efficient results since the temperature started dropping from the very beginning of the project.

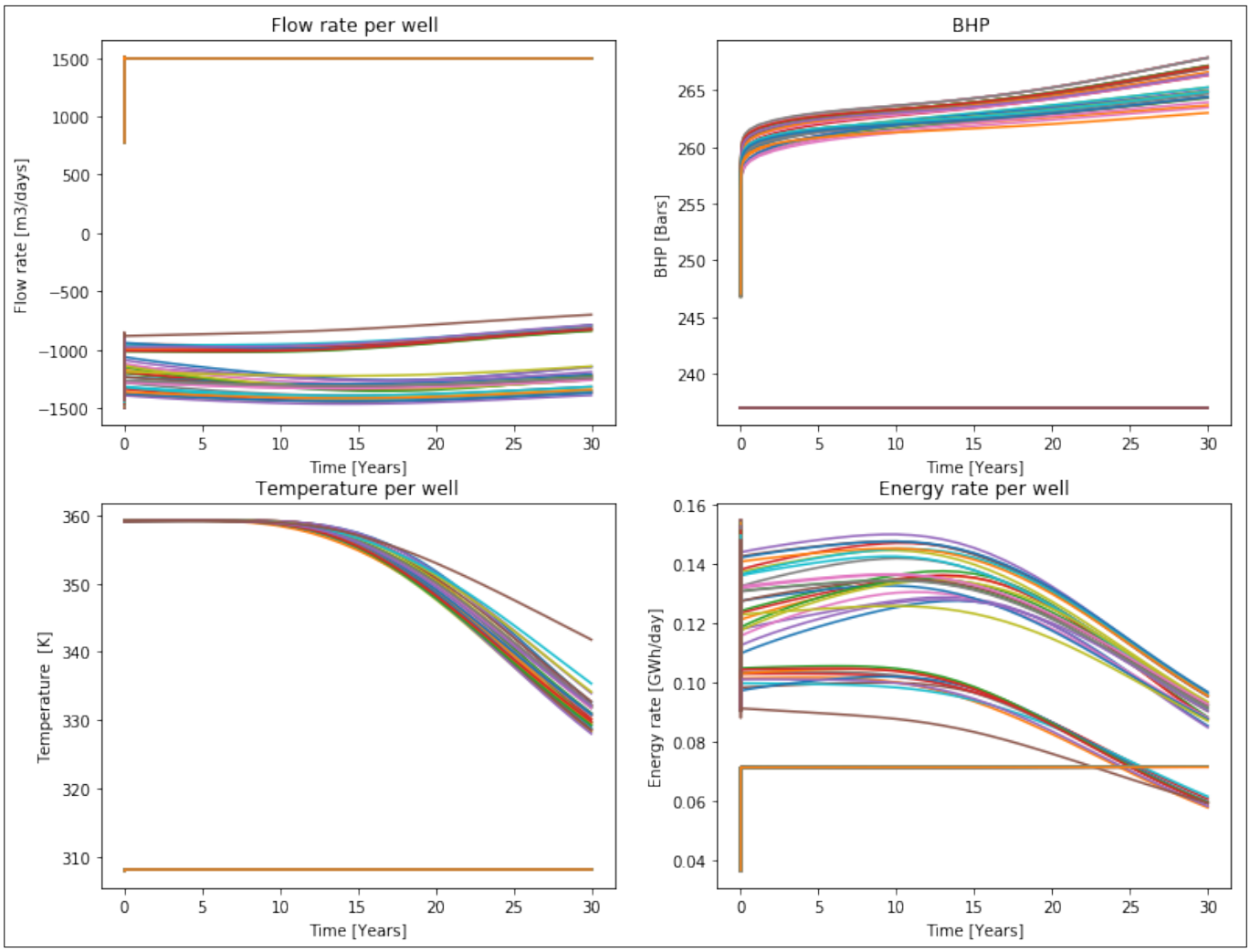

Figure 6.36: Simulator output data of temperature, pressure, flow rates and energy rates. Injectors are constrained in constant water rate which is visible by the flat line in plots of flow rate, temperature and energy rate. Producers are prescribed a fixed pressure. Producers are assigned with a minus (-) in the flow rate plot.

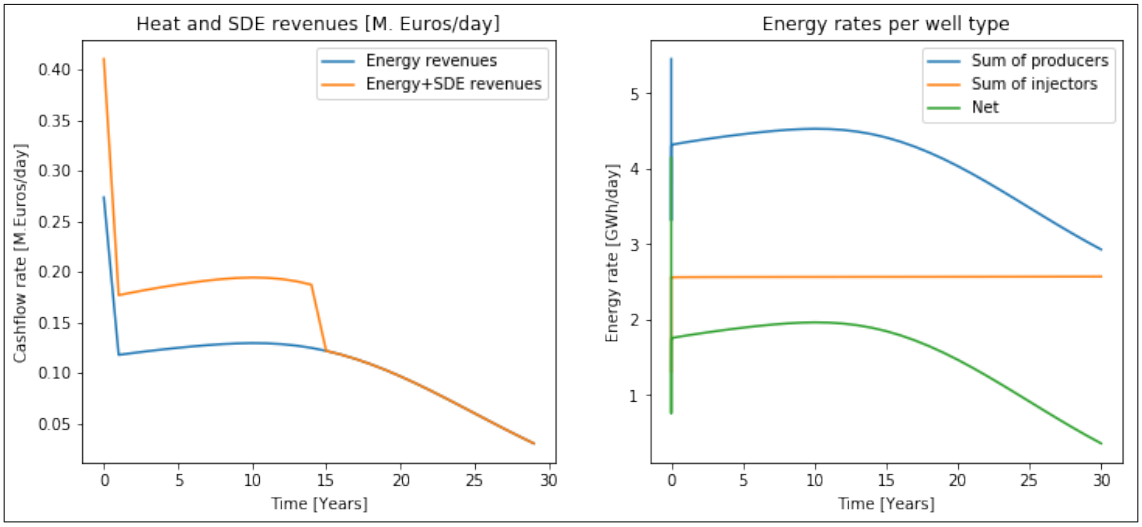

Figure 6.37: Revenues cashflow rate of the optimal development strategy and energy rates summed over well-type and net energy recovered.

Energy rates (Figure 6.37) are presented as a sum per well type (injectors, producers) and net energy rates, a time series of total energy rate injected and produced. Having a basis of the energy time-series curve, the heat revenues are calculated with 0.066 € millions/GWh without any annual discount. This curve indicates the yearly cash flow rate. After introducing subsidy revenues for the first 15 years of production, the cashflow curve is modified 6.37). Drilling costs are again introduced in the year-0 of production. Thus, the cash flow curve is modified, and when zooming in the positive part, the profit of the project only with revenues from energy is extracted (Figure 6.38). The 5-spot out-performance in energy is also depicted in the cashflow curve where it is profitable throughout the whole lifetime, compared to the line-drive development. Only after 20 years of production the income starts to fall but never becomes 0.

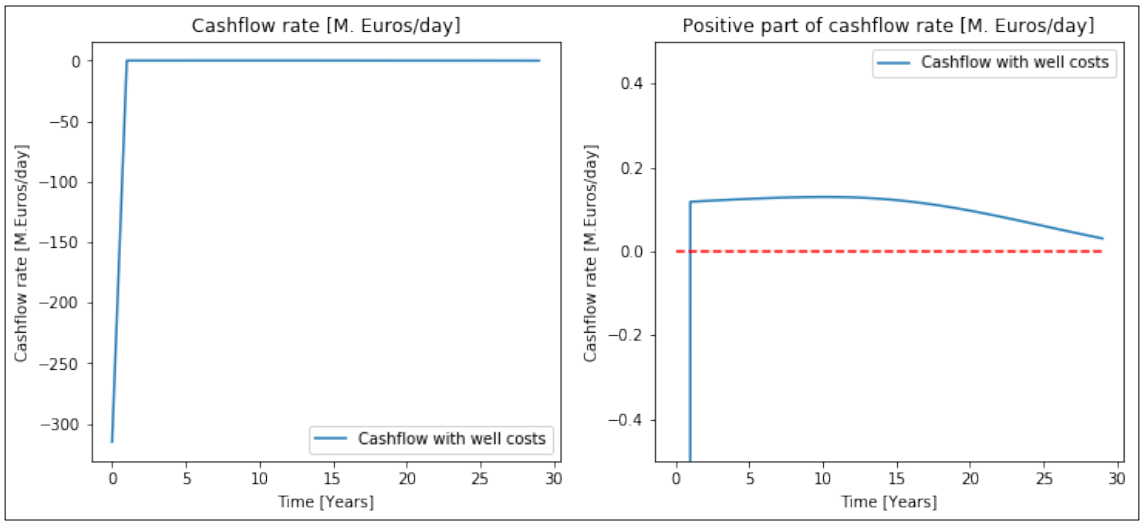

Figure 6.38: Cash flow rates with well costs included in year 0 of production. Focusing on the positive part, the project remains profitable in all of its lifetime.

6.4 Case 4: 2D aquifer with channel belt

6.4.1 Line drive pattern performance

Table 6.3 shows the output of the optimiser with the optimal output and tuning controls.

Table 6.3: Input parameters for the optimisation algorithm.

Optimiser tuning parameters	Value
Sampling points	200
Sampling sequence	Sobol
Maximum number of iterations	5
Flexible pattern size boundaries	[5,160]

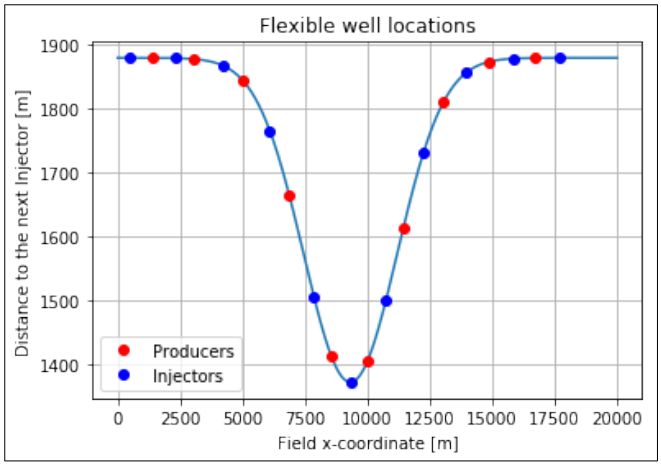

Figure 6.39: Optimal suggested well density function for the line drive pattern.

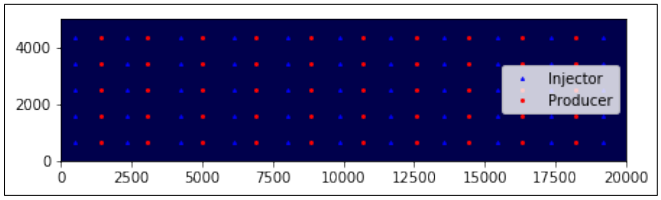

Figure 6.40: Optimal line drive pattern for the aquifer with the channel belt.

After the successful termination of the optimisation process, the **global optimum** is found for a well density function in x-direction in **grid blocks**:

$$D_x = 47 - 0.27 * e^{(-\frac{(x-233)^2}{66^2})} \tag{6.5}$$

This corresponds to a well density function in **meters**:

$$D_x = 1880 - 0.27 * e^{(-\frac{(x-9320)^2}{2640^2})} \tag{6.6}$$

The optimal pattern size in the y-direction is at 11 grid blocks or 2*440 m. The evaluated optimal NPV is 381 M.€. After receiving the control that the algorithm indicated as optimal, an experiment is run to show the aquifer status during the simulated time. Figure 6.41 presents the temperature field in time-steps of 10 years of production until 30 years of lifetime. Figure 6.42 shows the pressure field in time-steps of 10 years of production until 30 years of lifetime. After 30 years of production, there is a pressure build-up of around 20-25 bars. Figure 6.43 presents the results from developing optimal pattern size per injector and producer well, bottom hole pressure, temperature, flow rates and energy rates. The temperature time-series plot indicates that after 5-10 years of operation, the production temperatures starts to drop and at the end of the project the temperature difference between injection temperature and reservoir temperature is around 40-45 K.

Energy rates (Figure 6.44) are presented as a sum per well type (injectors, producers) and net energy rates, a time series of total energy rate injected and produced. Having a basis of the energy time-series curve, the heat revenues are calculated with a 0.066 € millions/GWh without any annual discount. This curve indicates the yearly cash flow rate. After introducing subsidy revenues for the first 15 years of production, the cashflow curve is modified 6.44).

For the current project, drilling costs are introduced in the year-0 of production, creating the final value of NPV. Thus, the cash flow curve is modified, and when zooming in the positive part, the profit of the project only with revenues from energy is extracted (Figure 6.45). The line-drive development indicates that after 20 years of operation the project becomes uneconomical since the cashflow drops below 0.

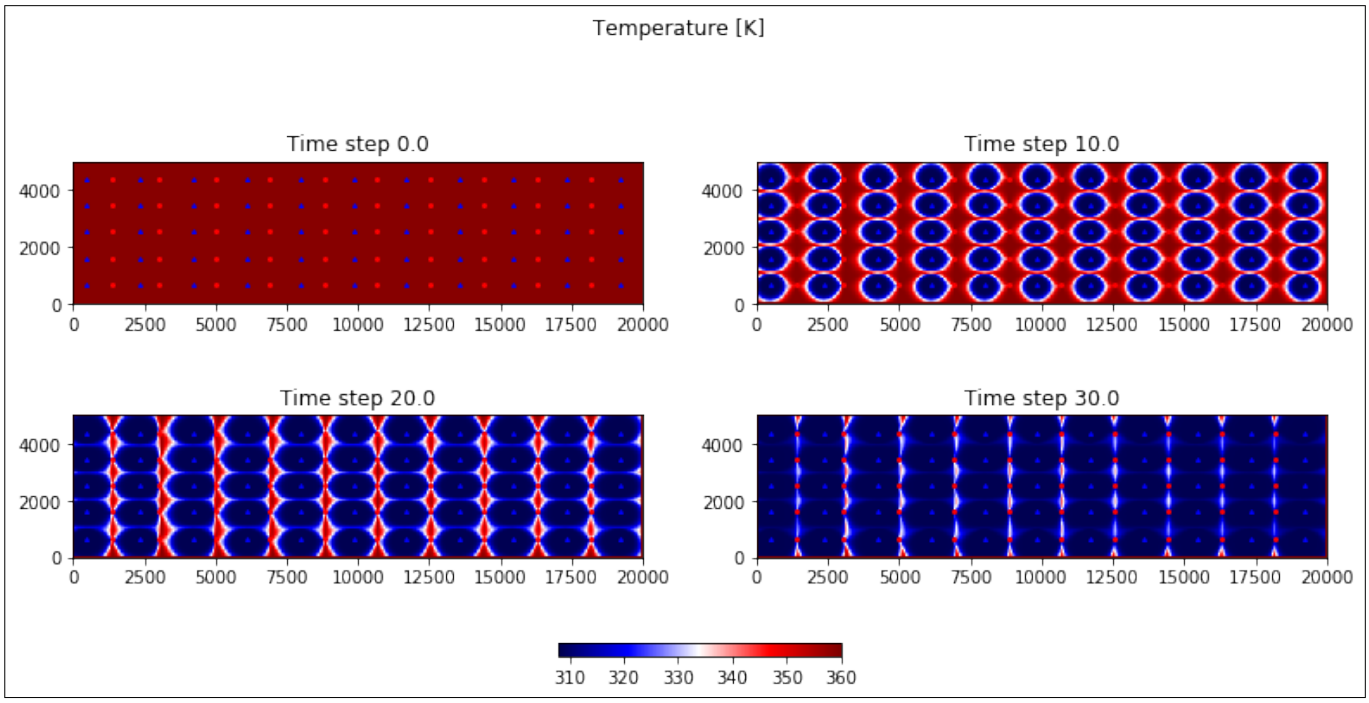

Figure 6.41: Temperature (K) every 10 years of production in the operating aquifer.

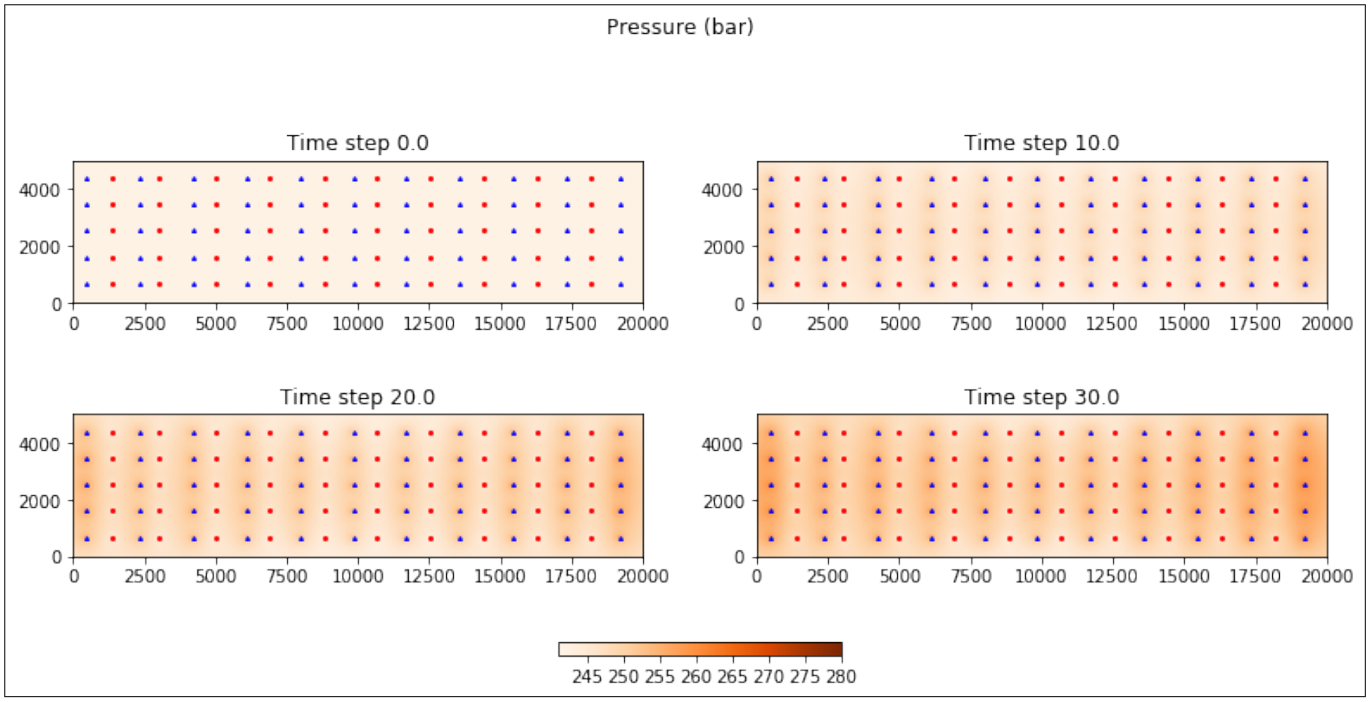

Figure 6.42: Pressure (bar) every 10 years of production in the operating aquifer.

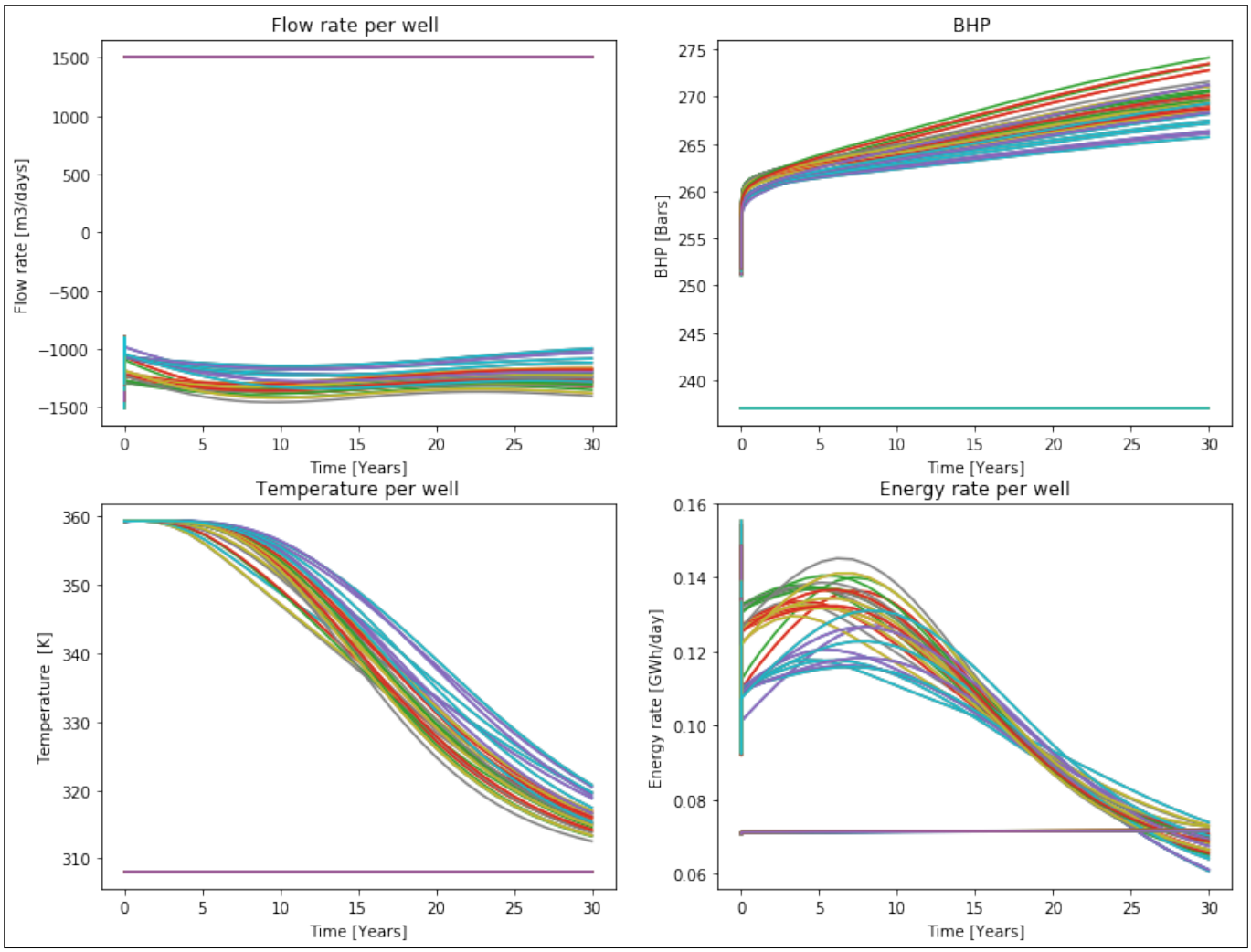

Figure 6.43: Simulator output data of temperature, pressure, flow rates and energy rates. Injectors are constrained in constant water rate which is visible by the flat line in plots of flow rate, temperature and energy rate. Producers are prescribed a fixed pressure. Producers are assigned with a minus (-) in the flow rate plot

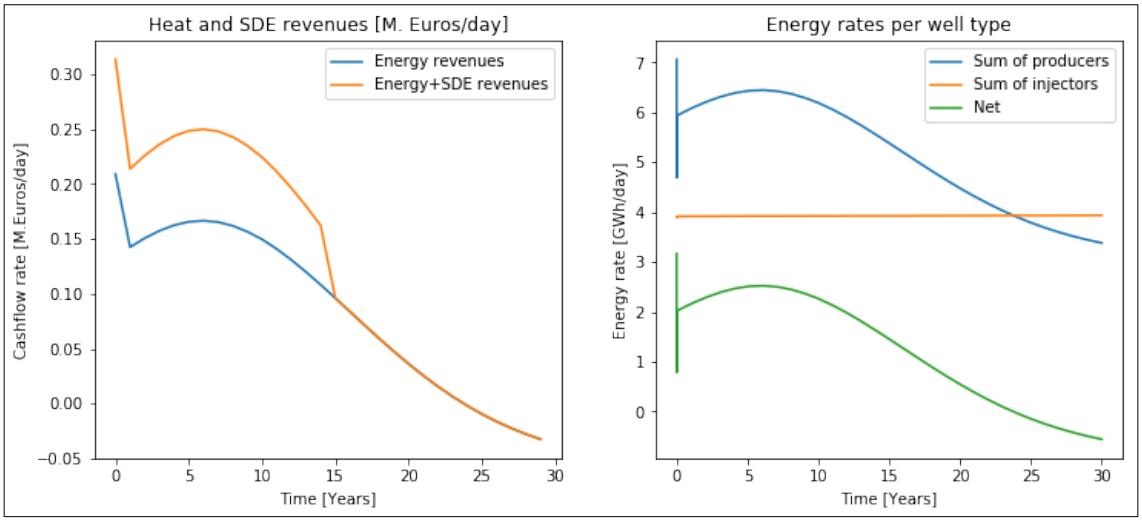

Figure 6.44: Revenues cashflow rate of the optimal development strategy and energy rates summed over well-type and net energy recovered.

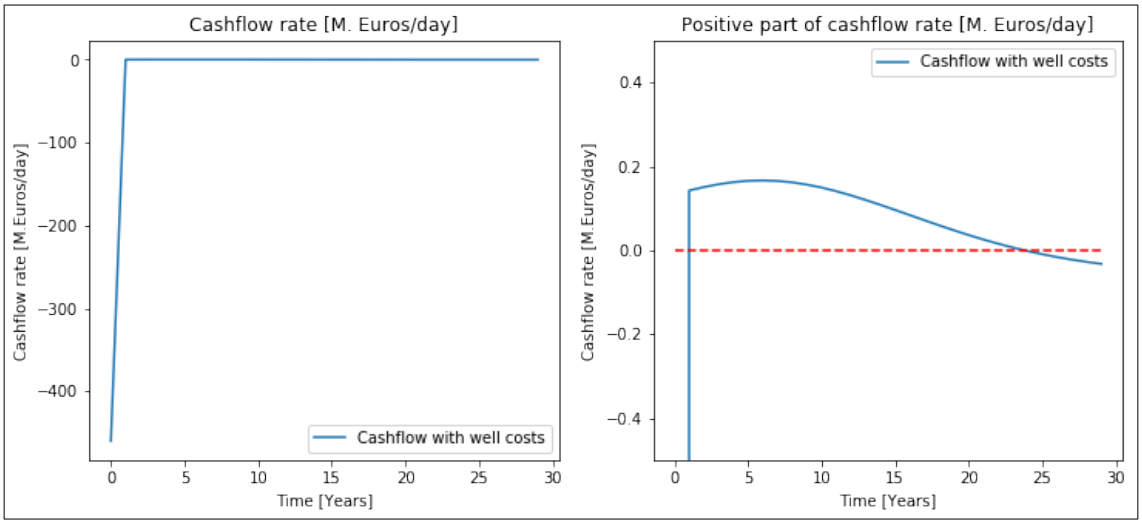

Figure 6.45: Cash flow rates with well costs included in year 0 of production. Focusing on the positive part,the project remains profitable through most of the lifetime.

6.4.2 5 spot pattern performance

Table 6.4 shows the output of the optimiser with the optimal output and tuning controls.

Table 6.4: Input parameters for the optimisation algorithm.

Optimiser tuning parameters	**Value**
Sampling points	200
Sampling sequence	Sobol
Maximum number of iterations	5
Flexible pattern size boundaries	[5,160]

After the successful termination of the optimisation process, the **global optimum** is reported for a well density function in x-direction in **grid blocks**:

$$D_x = 41 - 0.18 * e^{(-\frac{(x-269)^2}{72^2})} \tag{6.7}$$

This corresponds to a well density function in **meters**:

$$D_x = 1640 - 0.18 * e^{(-\frac{(x-10760)^2}{2880^2})} \tag{6.8}$$

The optimal pattern size at the y-direction is at 20 grid or 2*800 m. The evaluated optimal NPV is 589M.€.

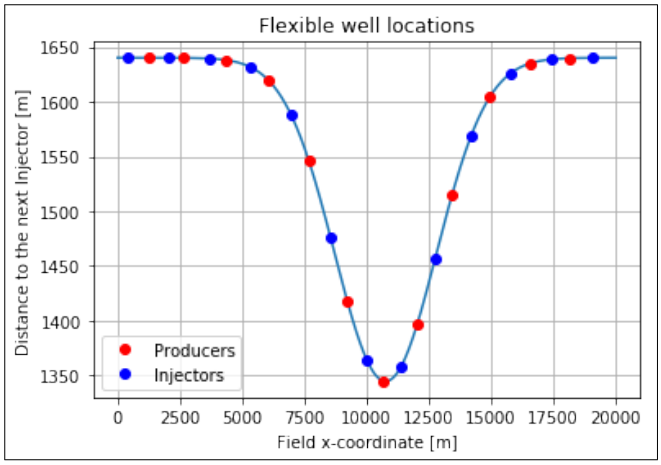

Figure 6.46: Optimal suggested well density function for the line drive pattern

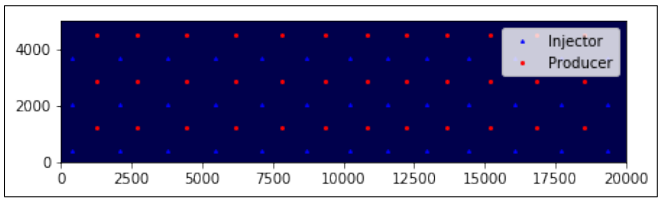

Figure 6.47: Optimal 5 spot pattern for the aquifer with the channel belt.

After receiving the control that the algorithm indicated as optimal, an experiment is run to show the aquifer status during the simulated time. Figure 6.48 presents the temperature field in time-steps of 10 years of production until 30 years of lifetime. It is apparent also here that the optimum 5-spot pattern size is not fully sweeping the top part of the aquifer under the current reservoir and production conditions due to limitations on placing extra wells close to the boundaries. Line-drive development was removing the warm water rim at the top boundary. Figure 6.49 shows the pressure field in time-steps of 10 years of production until reaching 30 years of lifetime. After 30 years of production, there is a pressure build-up of 30 bars. Line-drive development presented much higher pressure difference meaning that it is operationally less safe than the 5-spot. Figure 6.50 presents the development results of the optimal 5-spot pattern per injector and producer well, bottom hole pressure, temperature, flow rates and energy rates. The temperature time-series curve suggests that after 10 years of production the temperature will start to drop. Comparing this to the line-drive, the line-drive had a much earlier drop of the temperature. At the end of the lifetime of the project, the 5-spot produces at 20-30 degrees lower than the initial reservoir temperature. Line-drive though, at the end of the project produced at a much lower temperature.

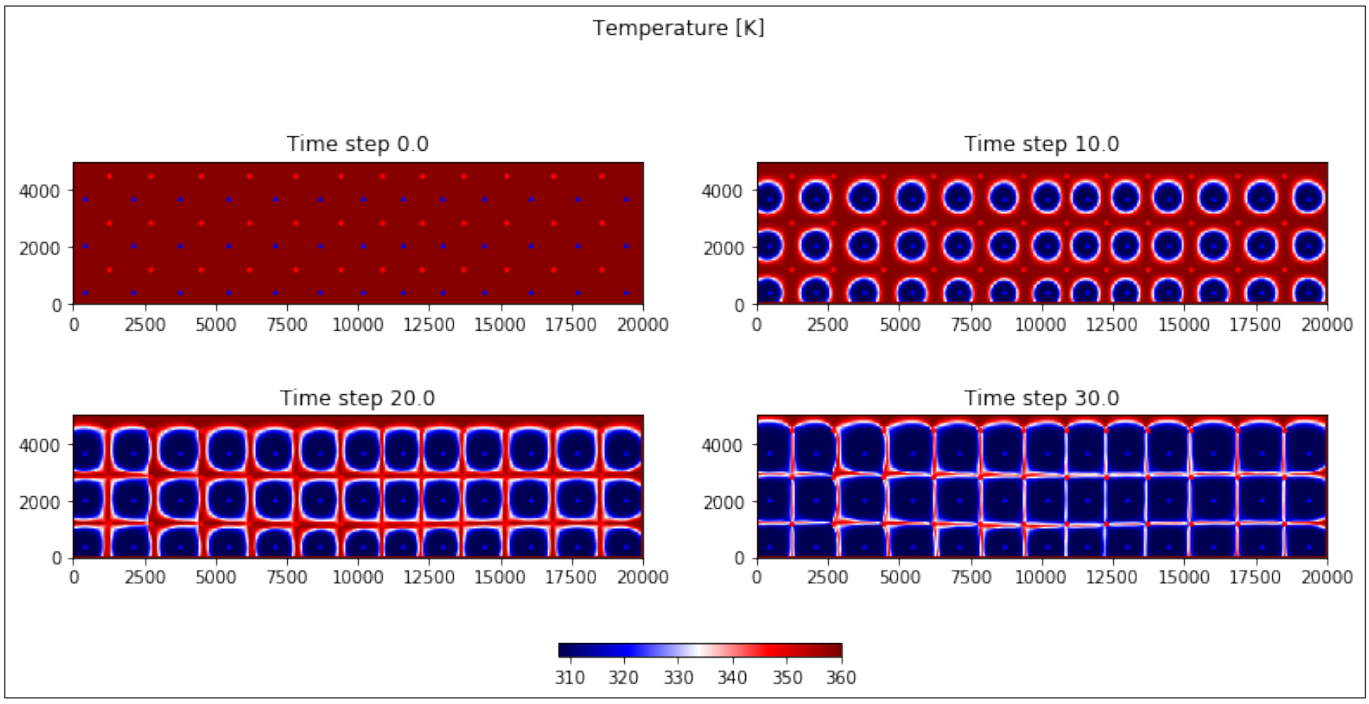

Figure 6.48: Temperature (K) every 10 years of production in the produced aquifer.

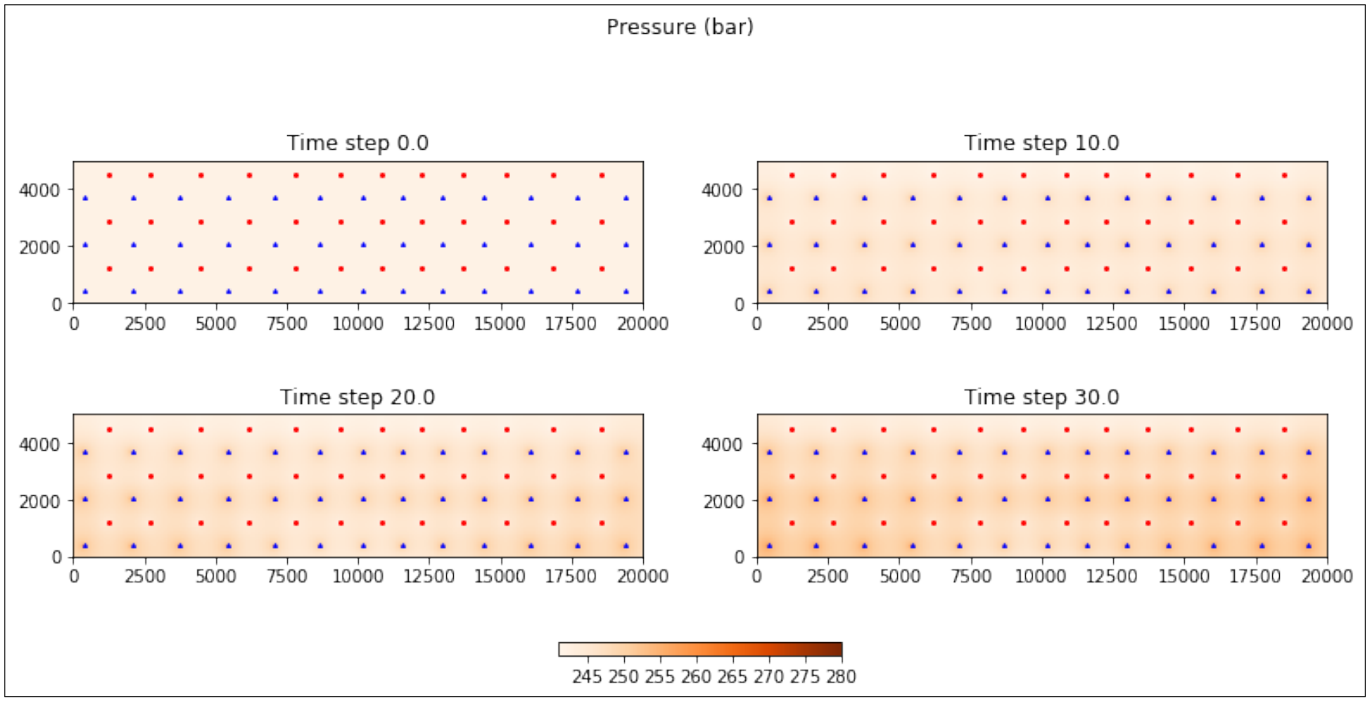

Figure 6.49: Pressure (bar) every 10 years of production in the produced aquifer.

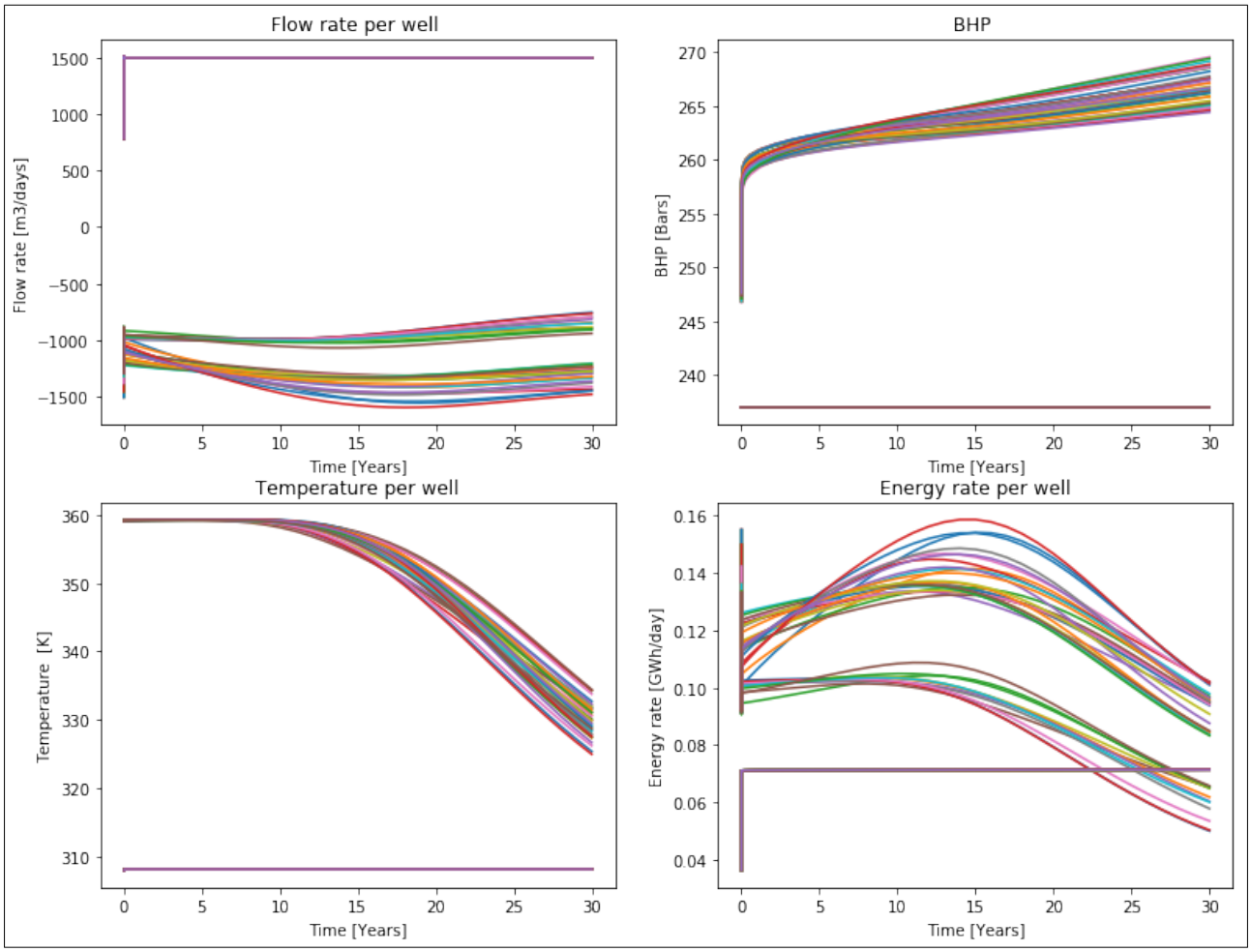

Figure 6.50: Simulator output data of temperature, pressure, flow rates and energy rates. Injectors are constrained in constant water rate which is visible by the flat line in plots of flow rate, temperature and energy rate. Producers are prescribed a fixed pressure..

Energy rates (Figure 6.51) are presented as a sum per well type (injectors, producers) and net energy rates, a time series of total energy rate injected and produced. Having a basis of the energy time-series curve, the heat revenues

are calculated with 0.066 € millions /GWh without any annual discount. This curve indicates the annual cash flow rate. After introducing subsidy revenues for the first 15 years of production, the cashflow curve is modified 6.51).

For the current project, drilling costs are introduced in the year-0 of production, creating the final value of NPV. Thus, the cash flow curve is modified, and when zooming in the positive part, the profit of the project, only with revenues from energy is extracted (Figure 6.52). The 5-spot pattern keeps more or less constant the profits of the project. Only after 20 years of production, the curve drops but never reaches 0, compared to the line-drive which became uneconomical.

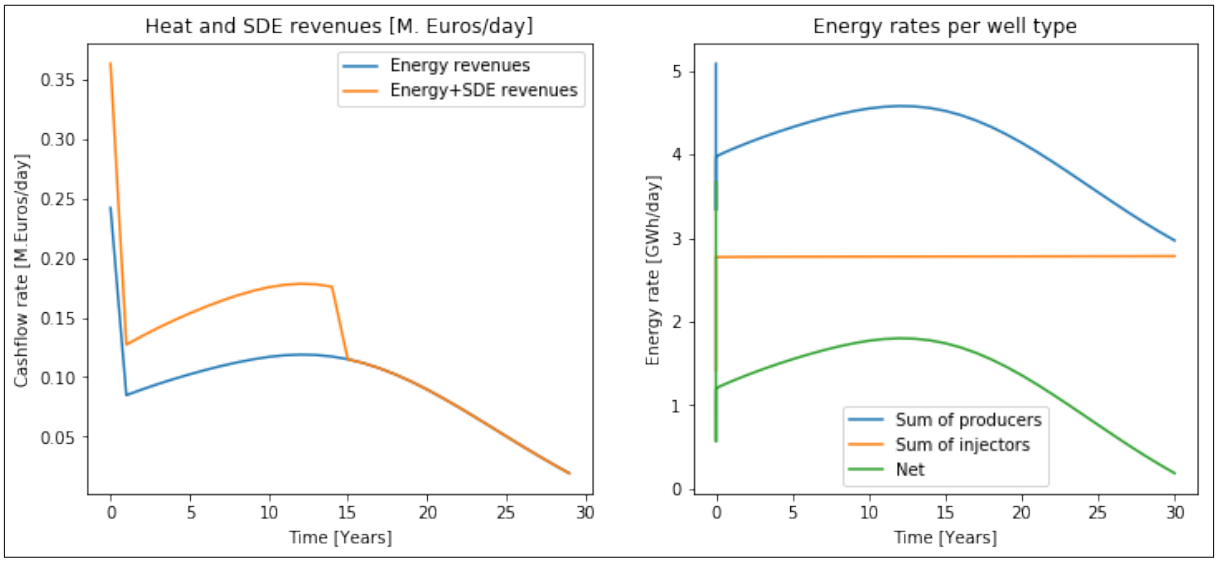

Figure 6.51: Cash flow rate from energy revenues and revenues with subsidy for the first 15 years of production.

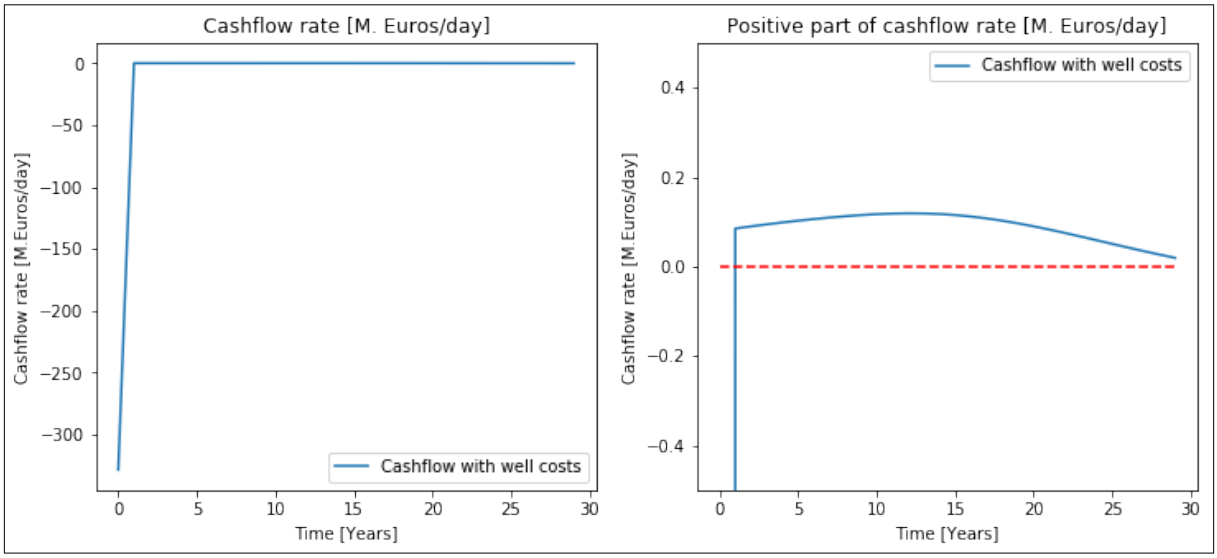

Figure 6.52: Cash flow rates with well costs included in year 0 of production. Focusing on the positive part,the project remains profitable in all of its lifetime.

Chapter 7

Discussion

This chapter will present several discussion points regarding the results of the different development strategies. The addressed optimal results will be compared to the sweep efficiency of each operation. The comparison of the optimal regular-isotropic pattern versus the flexible pattern will follow. Sensitivity analysis was conducted with the scope to search explicitly the response of the objective function under a full economic model where all costs (OPEX, CAPEX, ABEX, Subsidies) account on the geothermal development. Moreover the response of the objective function was investigated under uncertainty on the thermal conductivity properties of the aquifer rock. The concept is based on uncertainties identified in Willems et al. (2020). Furthermore, the thickness of the modelled aquifer is investigated and its impact on the objective function. Last, the performance of the optimisation algorithm is investigated and presented.

7.1 Discussion of the results

7.1.1 Homogeneous and isotropic aquifer

This test case proves that modelling an aquifer and simulating production with an isotropic well pattern is optimisable, and the optimal development strategy is addressed. The optimal strategy found still holds some room for improvement, especially the areas around the licensed field edges that are not fully swept.

The performance of the line-drive and 5-spot development strategy is also judged based on the sweep efficiency. The first step is to calculate the heat recovered from the reservoir and the fluid present in the aquifer. Equation 7.1 , 7.2 are used to derive the energy recovered analytically. The actual property values are presented in Table 7.1.

$$E_f = m_f * c_f * \Delta T = V_f * \rho_f * c_f * \Delta T = dx * nx * dy * ny * dz * nz * \phi * \rho_f * c_f * (T_{res} - T_{inj}) * KJ2GWh \quad (7.1)$$

$$E_s = m_s * c_s * \Delta T = V_s * \rho_s * c_s * \Delta T = dx * nx * dy * ny * dz * nz * (1 - \phi) * \rho_s * c_s * (T_{res} - T_{inj}) * KJ2GWh \quad (7.2)$$

Table 7.1: Constant parameters used as simulation inputs, in all models

Constant		Value	Unit
Aquifer x-discretization	nx	250	Grid blocks
Aquifer y-discretization	ny	250	Grid blocks
Aquifer z-discretization	nz	1	Grid blocks
Grid x-dimension	dx	40,80	m
Grid x-dimension	dy	40	m
Grid x-dimension	dz	10	m
Fluid density	ρ_f	1021	Kg/m^3
Fluid heat capacity	C_f	4	KJ/Kg*K
Rock density	ρ_r	2680	Kg/m^3
Rock heat capacity	C_r	2.2	KJ/Kg*K
Aquifer top depth	d	2200	m
Aquifer temperature	T_{res}	359.15	K
Injection temperature	T_{inj}	308.15	K
KJ to GWh	KJ2GWh	2.77777778e-10	

The sweep efficiency is calculated as the fraction of net energy recovered compared to the available energy from the present fluid and the rock itself thus:

$$E_t = E_s + E_f \quad (7.3)$$

$$S_{ef} = \frac{E_r}{E_t} * 100 \tag{7.4}$$

where:

- E_t is the total available heat in the subsurface
- E_s is the heat available in the solid rock
- E_f is the heat available in the fluid in the aquifer
- E_r is the net energy recovered with the proposed development strategy
- S_{ef} is the sweep efficiency of the development strategy in %

The available energy of the aquifer is calculated based on equation 7.1 and 7.2 for fluid and solid state. Based on Table 7.1, the calculations are presented below:

$$E_f = 250 * 40m * 250 * 40m * 1 * 10m * 0.20 * 1021\frac{Kg}{m3} * 4\frac{KJ}{Kg * K} * 40K * 2.77777778e - 10 = 11571GWh \tag{7.5}$$

$$E_s = 250 * 40m * 250 * 40m * 1 * 10m * (1 - 0.20) * 2680\frac{Kg}{m3} * 2.2\frac{KJ}{Kg * K} * 40K * 2.77777778e - 10 = 66821GWh \tag{7.6}$$

$$E_t = 11571 + 66821 = 78392GWh \tag{7.7}$$

The net energy recovered for the 5-spot is 17743 GWh and for line-drive is 9169 GWh. As far as the sweep efficiency is concerned, 5 spot results in 21.84 % and the line drive 11.69%. Thus, 5- spot is by 10.93% the most efficient development strategy for this aquifer.

7.1.2 Homogeneous and anisotropic aquifer

This test case shows some similarities and differences with the previous case. First of all both have the same volume of both bulk rock and warm water available given that they have the same homogeneous porosity. The difference lies in the imposed directional permeability discrepancies. The permeability in the x-direction is double the permeability of the y-direction meaning that the expected optimal sweep efficiency of this model is going to have minor discrepancies from the test case 1.

This test case proves that modelling an aquifer and simulating production with an anisotropic well pattern is optimisable, and the optimal development strategy is addressed. The optimal strategy found still holds some room for improvement, especially the areas around the licensed field edges that are not fully swept.

The available energy of the aquifer is calculated the same way with equations 7.5, 7.6, 7.7. The total energy available for the homogeneous and anisotropic aquifer is the same as the homogeneous and isotropic one. The net energy recovered for the 5-spot is 14040 GWh and for line-drive is 11664 GWh. As far as the sweeping efficiency is concerned, 5 spot results in 17.90 % and the line drive 14.87 %. Thus, 5- spot is by 3.03 % the most efficient development strategy for this aquifer.

7.1.3 Aquifer with linear porosity trend

The energy available from bulk rock and pore fluid for test case 3 is presented in Figure 7.1. The aquifer and fluid heat available is calculated explicitly per grid block for this test case and the channel belt model. Here the linear heterogeneity due to porosity is taken into consideration. Therefore, the pore fluid and the available energy from the rock are calculated based on the pore fluid energy based on linear porosity and rock energy based on a linear porosity trend.

The area containing totally the greater amount of energy is located where the high porosity is located. Though the smaller porosity implies that more rock is present there, thus more energy available to sweep.

The available energy of the aquifer for this aquifer is calculated to 79423 GWh. The net energy recovered for the 5-spot is 14882 and for line-drive is 12089 GWh. As far as the sweeping efficiency is concerned, 5 spot results in 18.73 % and the line drive 15.22 %. Thus, 5- spot is by 3.51 % the most efficient development strategy for this aquifer.

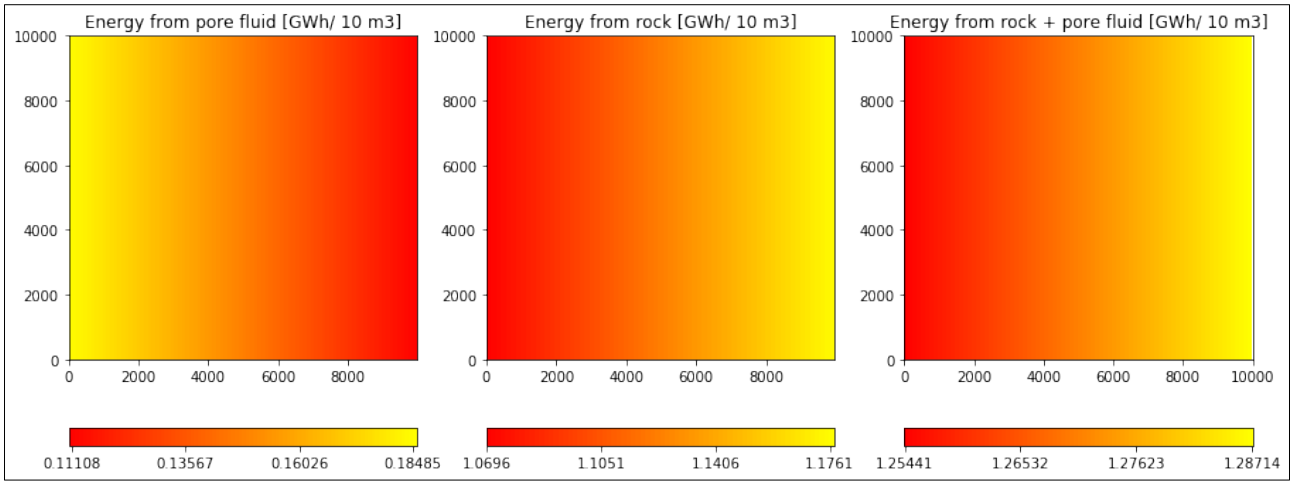

Figure 7.1: Energy present in the aquifer rock and pore fluid. The majority of the fluid energy is stored in the high porosity area (left). In total the low porosity area has more energy stored because of the volume of rock present can store more energy. The color bar represents the energy available in GWh per 10 m^3 of volume.

As far as the optimality of the optimal pattern is concerned, it is necessary to have a basis of comparison. To be more specific, the performance of the optimal flexible pattern should be compared with the performance of the optimal isotropic pattern in the heterogeneous channel belt aquifer and the performance of the isotropic pattern in the presumed homogeneous model. Therefore, the following steps will be compared:

- A synthetic geology is introduced with a naive and minimal case of assumed reservoir knowledge or information. The porosity is constant and everywhere $\phi = 16\%$. This is model A. For this geology, an optimisation experiment is run to find the optimal regular and isotropic well pattern that delivers the optimum NPV value. The optimal pattern size is called A (m). The suggested optimal NPV (A) performance is returned. This step aims to suggest the optimal regular and isotropic well pattern that delivers the optimum performance under lack of subsurface knowledge.
- Step B describes the optimisation process under full knowledge of the subsurface. It aims to find the optimal regular and isotropic well pattern that delivers the highest NPV. Thus the optimal well pattern (B) is found. The NPV (A) is compared with NPV (B). A comparison of optimal and isotropic well patterns, under full information of subsurface is shown: NPV (B) - NPV (A)
- The final step aims to address the optimal flexible well pattern (C) under complete subsurface knowledge. The performance of the optimal flexible pattern is NPV (C). The purpose of this experiment is to compare the NPV when applying a regular and isotropic pattern versus the NPV when adapting well configurations on local geological properties with a well density function.

The optimal NPV decreases from case A to B. The assumed porosity of 16% does not efficiently represent the realistic geology; therefore, a different optimal NPV is found with the same optimal pattern. Step A and B optimisation were conducted under a full search of the control of well spacing. This means that all possible well spacings were evaluated and the NPV of each development was established. So, analytical the calculations of the objective function ensured that the optimum well spacing on cases A and B are reliable. The next step (C), with the optimal well density function, delivers slightly lower NPV than case B. Case C was optimised by the algorithm, so there is no way to ensure that the delivered value is the optimal. Therefore comparing the last wo cases is not done under a fair basis. If the optimiser would perform better, it should have found at least an NPV of case C same with case B. It was expected that the case C, would show if not the same NPV value as case B, a much higher value. Moreover, a more flexible pattern than the one showed here, was expected. But why the results are different from what we expected?

The contrast of porosity of 0.12-0.20, suggests a contrast of 1:1.6 of warm brine volume present in the aquifer at the extreme porosity areas. The effect of volume directly would impact the well spacing. The higher the present volume, the smaller the required well distance, thus more wells need to inject and produce in order to sweep the high porosity area in the aquifer. Therefore a ratio of 1.6:1 was expected for the optimal well spacing where the extreme values of porosity are present. Though that was not the result. Taking a step back, it is necessary to reflect, on how the geothermal development was conducted. Two are the components that were investigated for this project, the geothermal synthetic aquifer models and the injection and production constraints. It was explained that the development was performed under the assigned constraints in order to simplify all interpretations. Although, the synthetic models generated, were explicitly modelled only in terms of porosity and permeability. The aspect of modelling heat capacity, that in reality would follow the different facies and therefore porosity-permeability distribution, was not taken into consideration. The motivation behind explicitly modelling also the property of heat capacity, lies on the basis of the aspect of thermal recharge of the reality. Both the reservoir rock and over-and-underlying layers, can act as heat (energy) providers and subsequently have a major impact on the optimal well spacing and production lifetime.

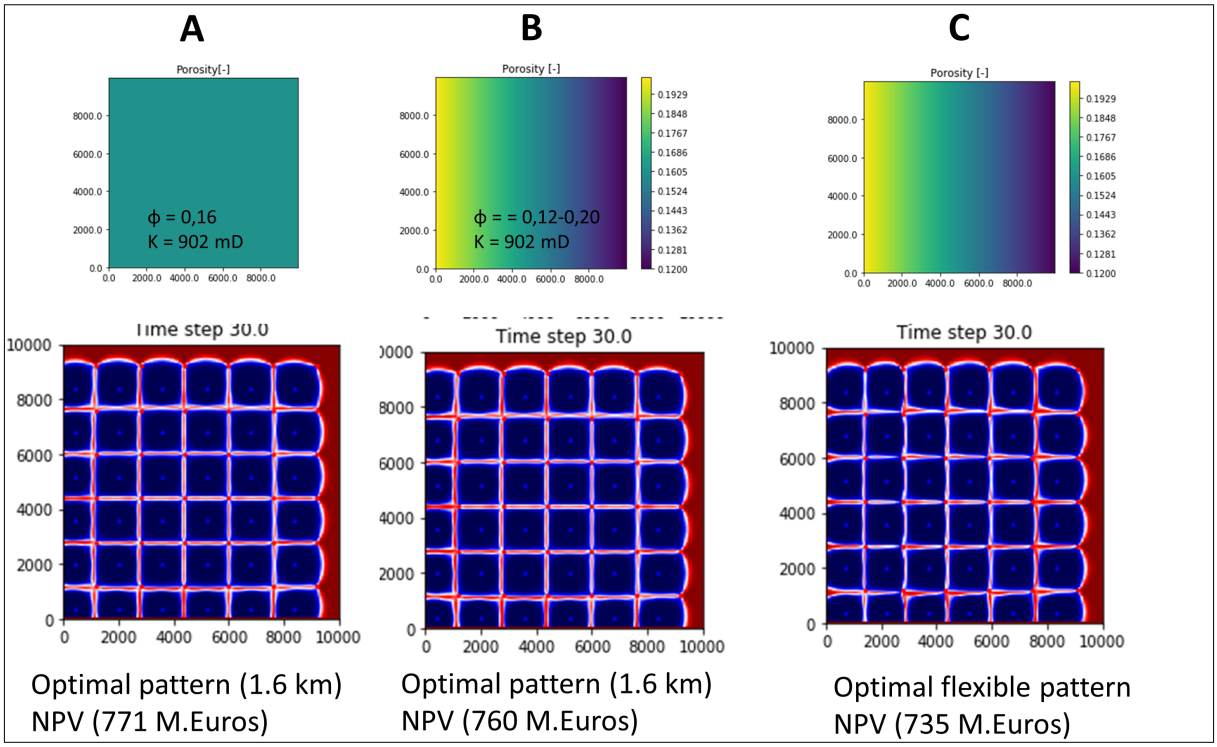

Figure 7.2: Methodology for comparing optimal isotropic and flexible well pattern performance on aquifer with linear porosity trend. In the top row I see the porosity trends, with the porosity indicated by the colour coding. A: uniform porosity, B and C: linear porosity increase from right to left. Bottom row Temperature in reservoir for the different well patterns in case A, B and C. The performance of each model in terms of optimal well spacing and NPV is presented on the bottom. Case C is under-performing case B because the search of the global optimum development strategy is done analytically on B and numerically in C.

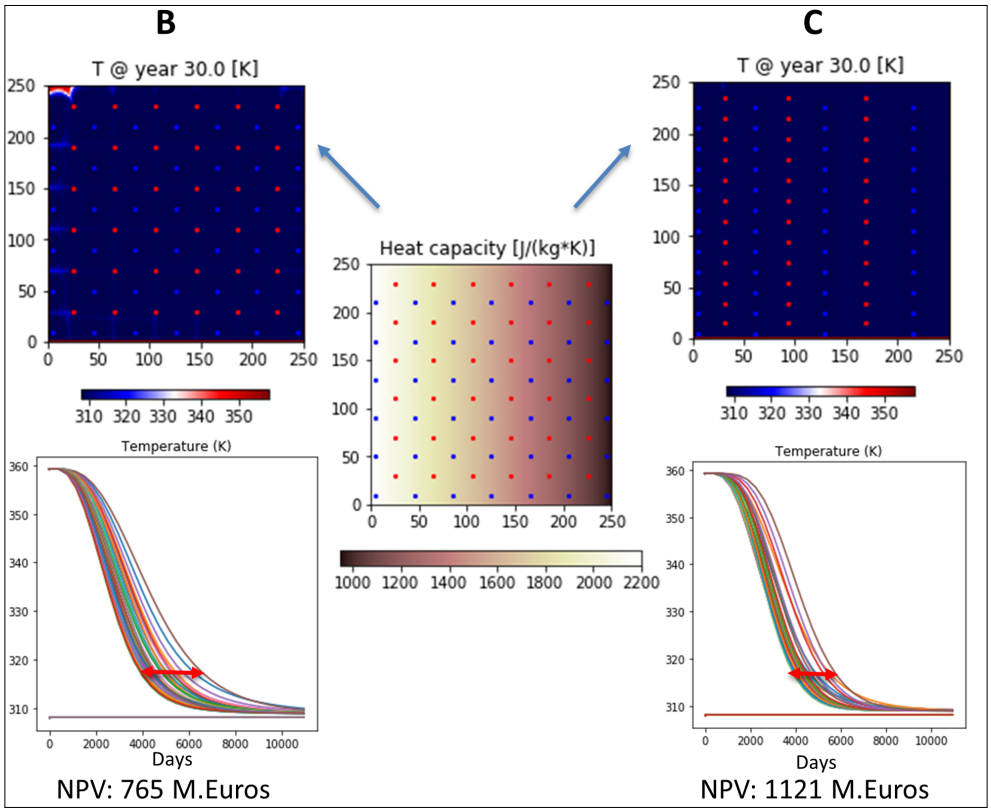

Figure 7.3: Heat capacity modelling of synthetic model with linear trend, based on values derived from Willems et al. (2020). Case B and C compare the performance of the optimal isotropic well pattern of figure 7.2 versus flexible well pattern. Both cases are not optimised but show that there is room for improvement. The response of the flexible well pattern outperforms the isotropic well pattern strategy.

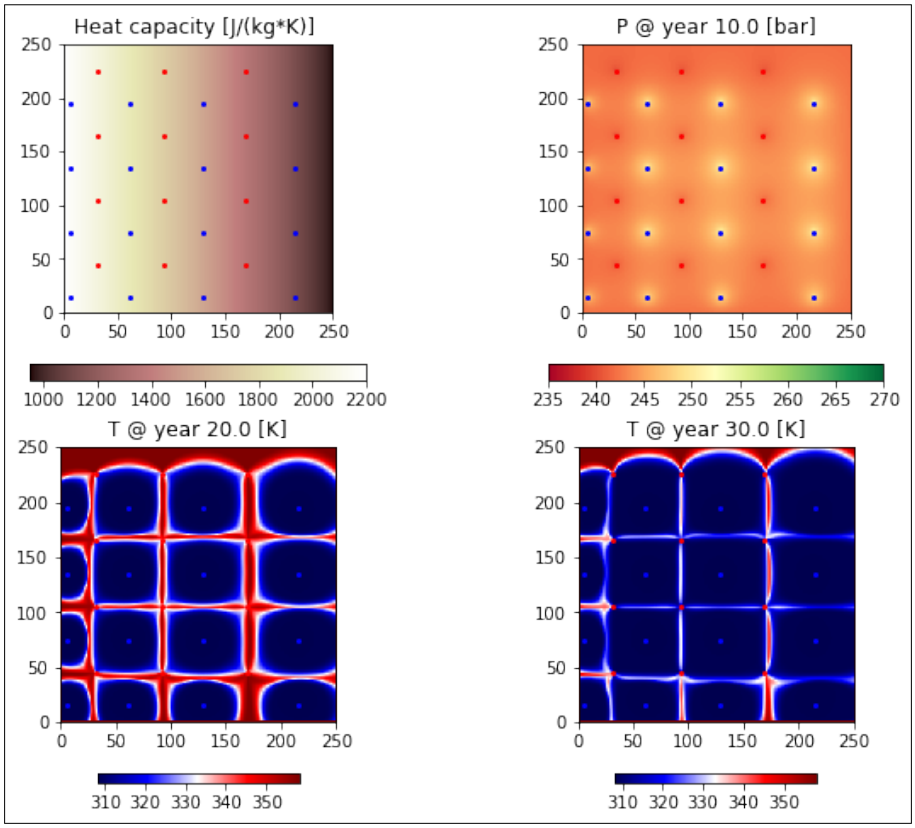

Figure 7.4: When modeling heat capacity explicitly, the thermal radius of the cold front changes being aligned with the porosity contrast and allows for the application of the flexible well pattern concept.

For this the spatial variation of heat capacity was taken into account. The spatial variation of heat capacity should align with the spatial variation of the lithological facies. Since facies are directly linked to porosity, so porosity can directly be linked with heat capacity and modelled with the same function. Heat capacity is highly dependent on the mineralogy of the rock but also on the porosity of the rock itself if the pore spaces are saturated with brine. Brine has a specific heat around 4 times higher that the rock so the higher the porosity, the more fluid the rock can accommodate, the higher the heat capacity. Based on Willems et al. (2020), a gap was identified regarding the thermal properties of the Delft Sandstone Member. As mentioned in the paper, there is an uncertainty when addressing heat capacity for different formations. These assumptions of heat capacity range from 730 J kg−1 K−1 for sandstone and 950 J kg−1 K−1 for claystone to 2700 J kg−1 K−1 for both sandstone and claystone. Apparently there is overlap of heat capacity values for both lithologies that needs further investigation. An experiment with spatially varying heat capacity was conducted (Figure 7.3). For this experiment, it was assumed that the shale (consolidated claystone) has the lowest heat capacity of 950 $J/KG*K$ and sandstone the lowest 2200 $J/KG*K$. These values are retrieved from Crooijmans et al. (2016), Willems et al. (2020). The value of 950 was inserted to represent the shale formation (lowest porosity) while 2200 represents the sandstone which is saturated with brine. If the the sandstone would have been dry then the heat capacity would approach the one of the shale. Moreover, these values would change with the different mineralogy but a simplistic approach is required for the proof of concept. It was inferred that, under the same injection and production constraints, the 2D variation of heat capacity based on different lithologies, induces discrepancies in the speed of the cold front. Low porosity (shale) allows more heat to be stored in the rock, so shales can transfer more heat to the injected water and mask reheat the injected water. Though, the minor volume of present water directly links to faster propagation of the cold front in shales compared to the sandstone. Case B and C in Figure 7.3 compare the performance of the isotropic and flexible well pattern on the same reservoir but with explicit modelling of heat capacity. It needs to be clarified that case B operates under the optimal pattern that was identified in figure 7.2 and has not been optimised. Also case C is not the optimal flexible well pattern but from this comparison it is shown that explicit modelling of heat capacity can better show the concept of flexible well patterns that perform better than isotropic well patterns for large scale geothermal developments.

When feeding the objective function with the new synthetic models that incorporate heat capacity variation, the optimal flexible well pattern is going to adapt, so that all producers more or less have thermal breakthrough at the same time (Figure 7.3). Thus, it is suggested that the application of a flexible well density function requires further investigation and explicit geological modelling of the geothermal aquifers. It is proposed here that heat capacity should be adapted to geological facies. Only then, more flexible patterns with fewer wells than case B are able to efficiently sweep the geothermal reservoir.

7.1.4 Aquifer with channel belt

The aquifer and fluid heat available for this test case, is again calculated explicitly per grid block. Here the heterogeneity of porosity introduced by the channel belt is taken into consideration. Therefore, the available energy from the rock the pore fluid are calculated based on pore fluid volume with a Gaussian porosity trend and rock energy with a Gaussian 1- porosity trend. The 2D representation of energy present is found in Figure 7.5. The area containing totally (rock + fluid) the greater amount of energy is located where the lower porosity is located. Though the high porosity are has the greatest amount of energy due to the water present there. The suggestion here is that shales (porosity = 0.05) can serve as great thermal storage formations.

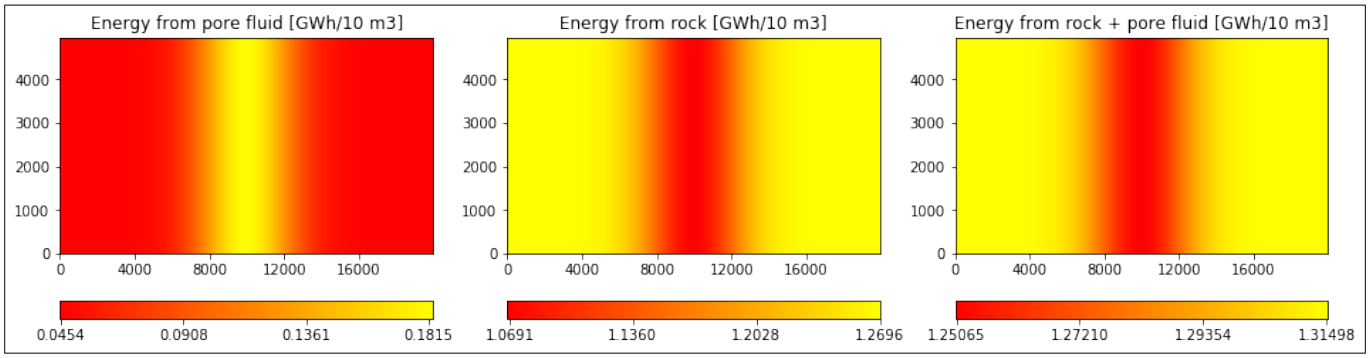

Figure 7.5: Energy present in the aquifer rock and pore fluid. The majority of the energy from the pore fluid is stored in the channel. Though the shale is a much higher contributor of energy in total.

The available energy this aquifer is calculated to 81188 GWh. The net energy recovered for the 5-spot is 38130 and for line-drive is 34661 GWh. As far as the sweep efficiency is concerned, 5 spot results in 46.96 % and the line drive 42.69 %. Thus, 5- spot is by 4.27 % the most efficient development strategy for this aquifer.

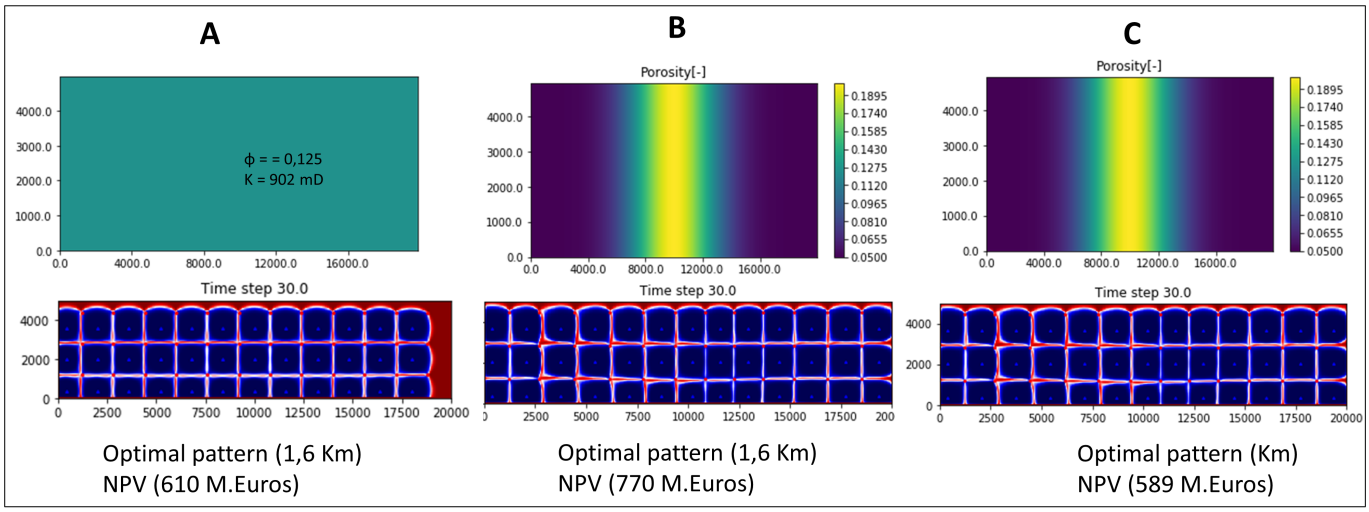

Figure 7.6: Methodology for comparing optimal isotropic and flexible well pattern performance on aquifer with channel belt.

As far as the optimality of the optimal pattern is concerned, it is necessary to have a basis of comparison. To be more specific, the performance of the optimal flexible pattern should be compared with the performance of the optimal isotropic pattern in the heterogeneous channel belt aquifer and the performance of the isotropic pattern in the presumed homogeneous model (Figure 7.6). Therefore, the following steps will be compared:

- A synthetic geology is introduced with a naive and minimal case of assumed reservoir knowledge or information. The porosity is constant and everywhere $\phi = 12.5\%$. This is model A. For this geology, an optimisation experiment is run to find the optimal regular and isotropic well pattern that delivers the optimum NPV value. The optimal pattern size is called A (m). The suggested optimal NPV (A) performance is returned. This step aims to suggest the optimal regular and isotropic well pattern that delivers the optimum performance under lack of knowledge of the subsurface.
- Step B describes the optimisation process under full knowledge of the subsurface. It aims to find the optimal regular and isotropic well pattern that delivers the highest NPV. Thus the optimal well pattern (B) is found. The NPV (A) is compared with NPV (B). A comparison of optimal and isotropic well patterns, under full and lack of knowledge of geology is conducted: NPV (B) - NPV (A)

- The final step aims to address the optimal flexible well pattern (C) with full knowledge of subsurface geology. The performance of the optimal flexible pattern is NPV (C). The purpose of this experiment is to compare the NPV when applying a regular and isotropic pattern versus the NPV when adapting well configurations on local geological properties.

The optimal NPV from case A to B increases. Step A and B optimisation were conducted under the full search of the control. Again here all possible development strategies (well spacings) were evaluated analytically and the optimal well spacing that could deliver the highest possible NPV is presented in Figure 7.6. Therefore it is ensured that the results of A and B are reliable. The next step (C), with the optimal well density function, delivers a lower NPV than case B. Case C, is optimised numerically. 5 controls were required to be optimised so an analytical approach is computationally costly. The poor results reveals that the optimisation needs further tuning. If the optimiser was performing well, it would at least find a global optimum that at least delivers the same NPV as case B. So the comparison of B and C is not fair.

It was expected that the case C, would perform optimally with a more flexible pattern than the one showed here. The contrast of porosity 0.05-0.20, implies a contrast of 1:4 of warm brine volume present in the aquifer. The effect of volume directly would impact the well spacing as, the higher the present volume, the smaller the well distance, thus more wells need to inject and produce in order to sweep the aquifer. Therefore, a ratio of 4:1 was expected for the optimal well spacing, at the extreme porosity areas, but it was not found as optimal. The same concept was applied also here regarding the explicit modelling of the heat capacity. Shale and saturated sandstone were modelled the same way like in the model with the linear porosity. The extreme values of 950 and 2200 J/KG*K were used for shale and sandstone respectively.

Case B and C in Figure 7.7 compare again the performance of the isotropic and flexible well pattern on the same reservoir but with explicit modelling of heat capacity. Again case B operates under the optimal pattern (1.6 km) that was identified in figure 7.6 and has not been optimised. Also case C is not the optimal flexible well pattern but from this comparison it is shown that explicit modelling of heat capacity can better show the concept of flexible well patterns that perform better than isotropic well patterns for large scale geothermal developments. It is also shown that with the flexible well pattern, the producer wells tune more efficiently the timing of the thermal break-though. In case the timing of the breakthrough is less spread than case B. Therefore, the flexible well pattern is going to adapt, so that all producers more or less have thermal breakthrough at the same time.

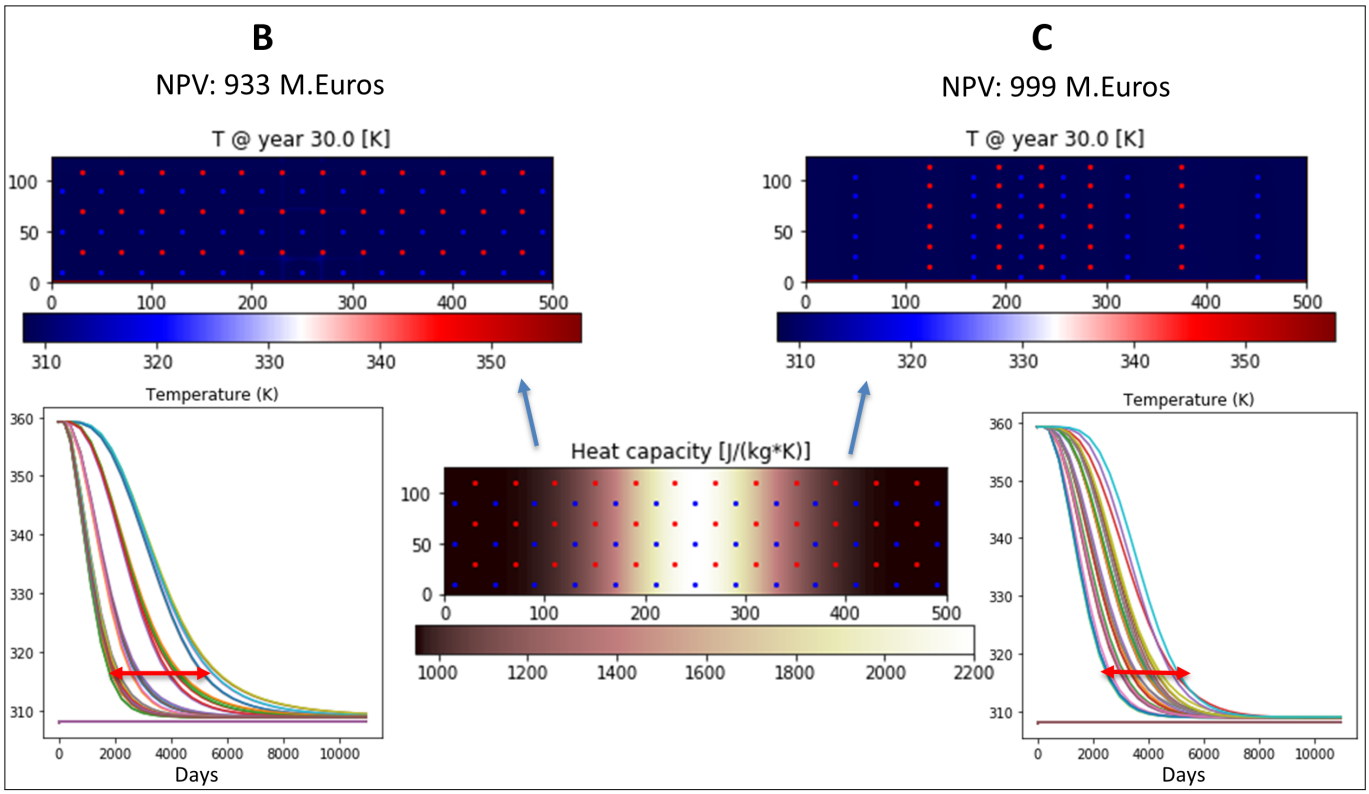

Figure 7.7: Heat capacity modelling of synthetic model with a channel belt, based on values derived from Willems et al. (2020). Case B and C compare the performance of the optimal isotropic well pattern of figure 7.6 versus flexible well pattern. Both cases are not optimised but show that there is room for improvement. The response of the flexible well pattern outperforms the isotropic well pattern strategy

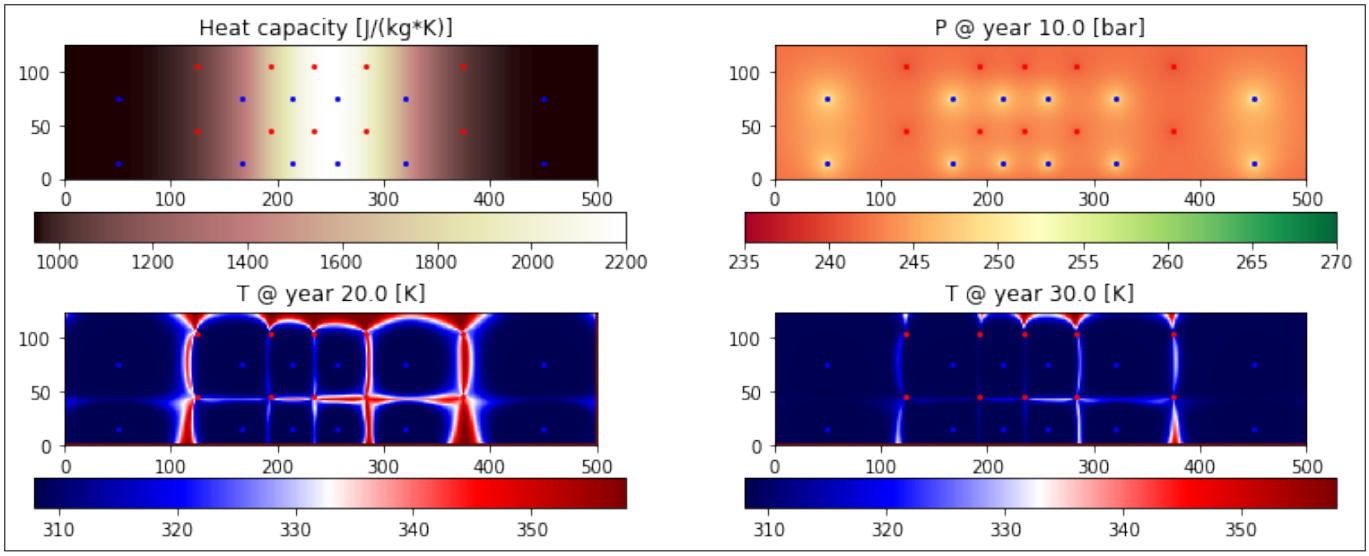

Figure 7.8: When modeling heat capacity explicitly, the thermal radius of the cold front changes being aligned with the porosity contrast and allows for the application of the flexible well pattern concept.

7.2 Optimal pattern sensitivity on aquifer thermal properties

Thermal properties remain largely unpredictable across potential geothermal target reservoirs. Thermal properties are crucial to predict water temperature during the foreseen lifetime of the geothermal wells, including the prediction of breakthrough and, therefore, the output of NPV. Knowledge of the thermal properties of the reservoir (Crooijmans et al. 2016, Kahrobaei et al. 2019, Willems et al. 2020) and the enveloping layers (de Bruijn et al. 2021) are invaluable for predicting and enhancing the sustainability of geothermal projects, as the thermal conductivity of these layers controls the thermal recharge of the aquifer.

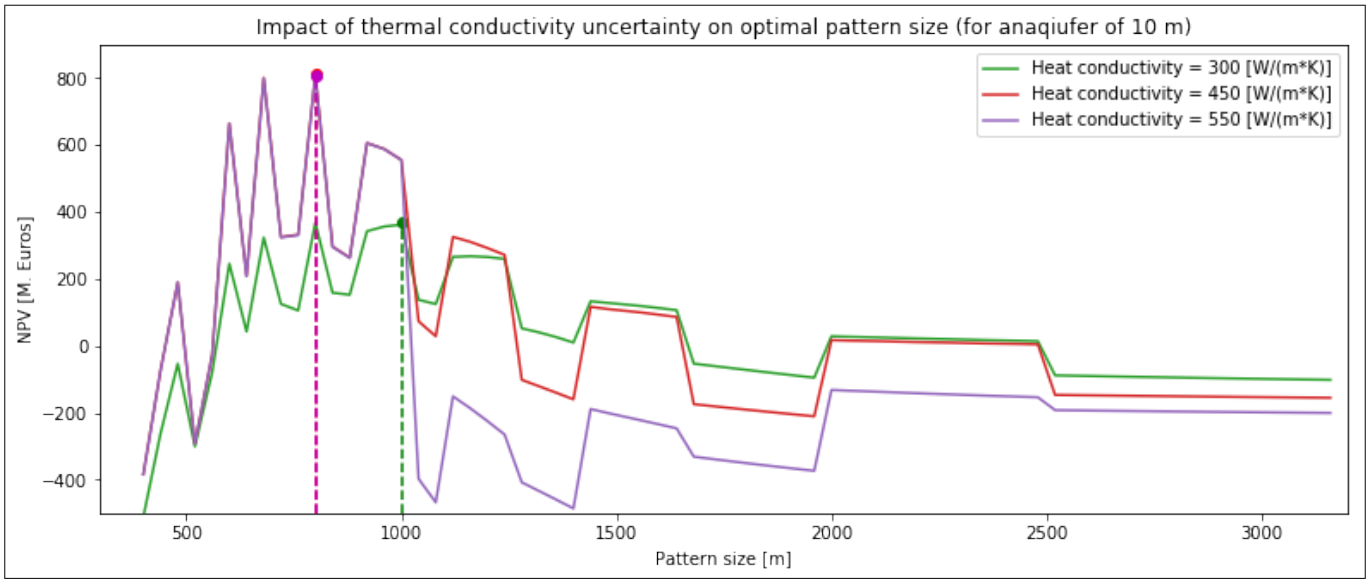

Figure 7.9: Full response curve of the objective function for three thermal conductivity aquifer scenarios (measured in $\frac{W}{m*K}$). The optimal pattern becomes smaller as the reservoir sandstone becomes more conductive.

The thermal recharge aspect from over- and under-burden in not taken into consideration for this project. A gap was identified in bibliography regarding the the Delft Sandstone thermal properties (Willems et al. 2020). Uncertainty for heat conductivity was identified. It was tested a full NPV curve in order to investigate if thermal conductivity uncertainty impacts the optimal pattern size. The values of 300 $\frac{W}{m*K}$ (low case), 450 $\frac{W}{m*K}$ (base case), and 550 $\frac{W}{m*K}$ (high case) are tested. The heat capacity is kept at the value of 2200. It is observed that the more conductive the aquifer becomes, the smaller the pattern size becomes to be able to fully sweep the more energy that is offered to the pore fluid. Therefore, the sandstone behaves as a thermal re-charger for the pore fluid, affecting the development strategies.

7.3 Sensitivity of the economic model under Dutch fiscal conditions the optimal pattern size.

Many pattern sizes were assessed, which can be analysed again in sensitivity analyses as a response surface. Hence the sensitivity of the objective function to the pattern size per NPV with well costs and all costs included at year 0 of production can be observed in Figure 7.10 in 2 different response surfaces. It is apparent that when introducing all development costs, the projects become economically unprofitable. It should be considered that all costs are included at the beginning of the project, thus having a greater impact. If costs are gradually introduced through time, the imposed discounting will affect the final NPV value. Therefore, it is imperative for these large scale geothermal projects that robust economic models be adopted. Only this way, an optimal well pattern can lead to a worthwhile investment.

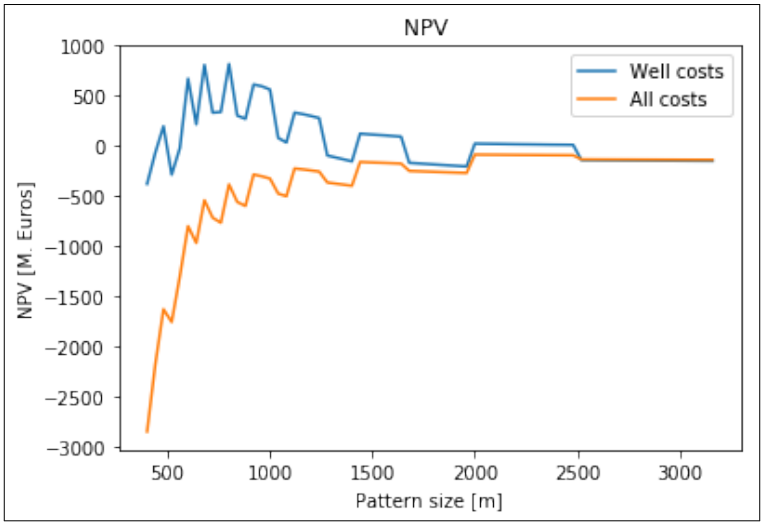

Figure 7.10: The curves represent full information about the objective function with one control with different economic models. Well costs only or all development costs are included in two scenarios. The development strategy is 5-spot. The optimal pattern changes as a function of development costs but they converge for larger pattern sizes.

7.4 Optimal pattern sensitivity on aquifer thickness

In the context of sensitivity of volumetrics on optimal pattern size, a sensitivity analysis of aquifer thickness is conducted to detect the changes. So it is inferred that when thickness doubles, the optimal pattern is halved accordingly. This proves the linear correlation between volume and pattern size.

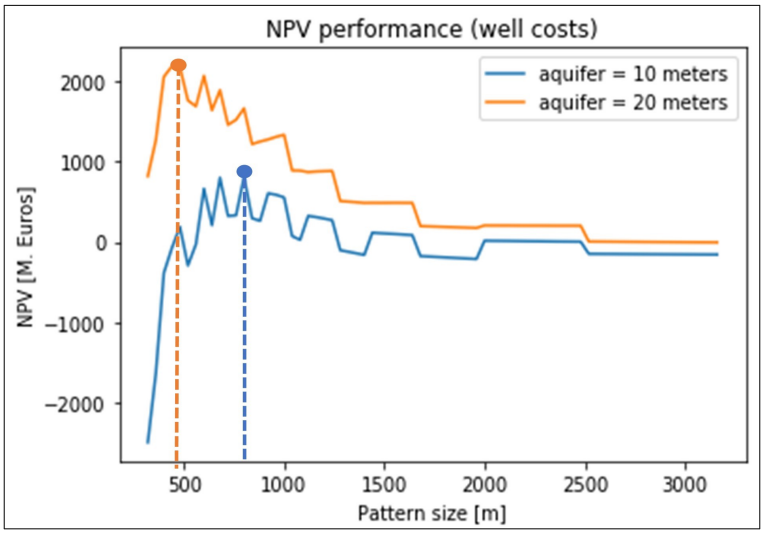

Figure 7.11: This curve represents full information about the objective function with one control for an aquifer of 10m and 20m. The development strategy is 5-spot. The optimal pattern decreases as a function of increasing aquifer thickness.

7.5 Performance of optimisation algorithm

The optimisation algorithm SHGO needs to be evaluated in terms of performance. This means tuning the algorithm per test case to deliver the optimal solution. This algorithm has been mainly parametrised by the meta-parameters of **sampling points** and a **maximum number of iterations** to perform. However, the iterations within the process of generating sampling points were tested in order to come up with the geometric information of the objective function. The objective function this project worked with is black-box meaning that the an equation is not provided. Endres et al. (2018) suggested that for black-box functions, the optimum number of sampling points to find all local minima, is unknown. Only if further information are available for the objective function, then the optimiser is able to perfume more efficiently when generating the geometrical information of the function. This concept was examined in this objective function. Indeed, the more sampling points were introduced, the algorithm could identify more local minima, thus more possible optimal solutions. This experiment is presented in Figure 7.12. The first function evaluation represents the global optimum.

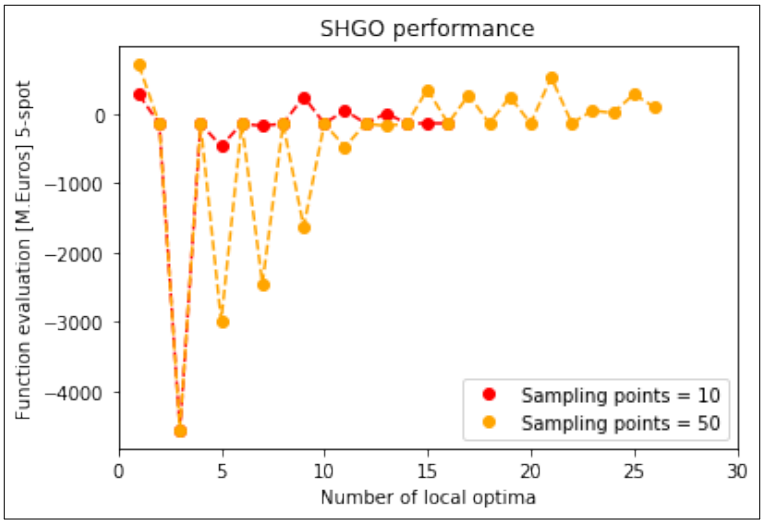

Figure 7.12: SHGO performance when the number of sampling points changes, The more sampling points are introduced, the algorithm is able to identify more locally convex areas, thus more local minima.

Furthermore, the algorithm can conduct iterations within the process of generating sampling points. Sampling initially 15 sampling points or imposing 3 iterations with 5 sampling points will generate 15 final sampling points. However, it is observed that introducing iterations in the optimisation process further refines the resolution enabling it to find more locally convex areas, thus local optima.

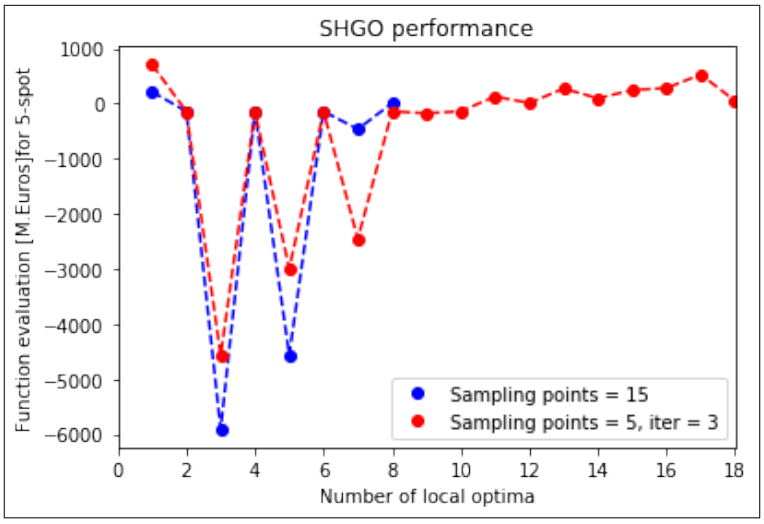

Figure 7.13: SHGO performance with ranging sampling points, The more samples are introduced, the more locally convex areas the algorithm is able to identify, thus more local minima.

The algorithm adopted was chosen in the context of the nature of the objective function. Since the geometry is rather non-monotonic, multiple local minima are present, and a local minimiser would have been inappropriate or too difficult to feed with initial guesses. This optimisation algorithm is still under construction and documentation. More features are added, plus detailed documentation is missing to fully grasp the performance of the objective function per

iteration, for example. Therefore, it is suggested that for geothermal field development modelling, this optimisation algorithm requires further investigation.

7.6 Implications of applied methodology

The current project named "Flexible well patterns and NPV optimisation on large scale geothermal field development" entails the introduction, description, development and application of two major innovative techniques. The first concept developed, is the **flexible well pattern** which is achieved by the introduction of **well density function**. Current methodologies (Onwunalu & Durlofsky 2009, 2010, 2011) modified only globally well patterns while this new introduced technique successfully adapted the pattern size based on the underling heterogeneity and anisotropy of the subsurface as a result of depositional and diagenetic processes. Moreover, there are no limitations of choosing a type of function as long as it represents a realistic trend on a geological formation. For the proof of this concept, only porosity was modelled with a well density function. It can be expanded in also on other properties like permeability that directly have an impact on the lifetime of a geothermal project. The spatial distribution of a property should be taken into account as well, as for this concept, porosity was modelled with well density functions in one direction but it can be extended in both direction. These modification allow for modelling more complex systems with the cost of feeding the well density function with more input variables.

The implications of applying this method include first of all the actual knowledge of the subsurface. It is required a prior modelling of properties (porosity, permeability trend) because the actual well density function will be adapted to the trend of the modelled geological property. Therefore, the more complex the subsurface, the more input variables are going to be introduced in the well density function. Subsequently, the number of decision variables is a key aspect that needs to be considered since the system becomes more complex. It is advised to be considered the modelling of only necessary geological trends and on a representative scale that are going to have an impact on the lifetime and profitability of a geothermal project.

The next concept that this project deals with, is the **optimisation of Net Present Value of large scale geothermal projects**. Finding the optimum development conditions to maximise geothermal NPV has already been developed by several authors (Willems, Nick, Goense & Bruhn 2017, Willems, Nick, Weltje & Bruhn 2017, Kahrobaei et al. 2019, Willems et al. 2020). The innovation of this project is the introduction to the large scale character of geothermal development and the implication it entails on the optimisation strategies. It was chosen an optimiser that globally searches for the optimal development conditions, contrary to the already applied methodologies adopting local minimisation techniques. This choice was made based on the fact that optimising objective functions with embedded reservoir simulations preserve a non linear character. The optimisation of large scale geothermal developments was successful when it comes to 1-2 controls. The chosen global optimiser is able to fully search the development options and detect the optimum conditions despite the non-linear character of reservoir simulations. Moreover, it is proved that a 5-spot pattern is always performing better than the already applied line-drive concept followed by previous researchers.

The suggestions of applying global optimisation on large scale geothermal development state that further investigation on optimising multiple decision variables is required. This is directly linked with the performance of the optimisation when feeding the objective function thus the reservoir simulation, with more complex geological models. This brings about the issue of the complexity of subsurface models, that the optimiser can deal with combined with optimisation under geological uncertainties. The latter would render the optimisation even costly as multiple geological realisations would be optimised simultaneously. Furthermore, the chosen synthetic geological field contrast of porosity was decided to reflect realistic conditions of the Dutch subsurface. Generally, a contrast of porosity of 0.05-0.20 or 0.12-0.20 would possibly represent geological formations as a result of depositional and diagenetic processes on siliciclastic systems and we focus on this system. It is inferred that the chosen porosity contrast is not fully able to result in a optimum flexible pattern with a ratio of 4:1 or 2:1 in pattern size as the given porosity contrast. It was proven that thermal recharge of injected cold water from the aquifer rock, had an impact on that. A more careful modelling of heat capacity based on porosity (facies) synthetic field is required as an input in order to come up with visually more flexible optimal patterns.

Chapter 8

Conclusions and recommendations

8.1 Conclusions

The objective of this research was to investigate the applicability of locally adapting well density to geological heterogeneity for large scale geothermal development operations and optimise the addressed well density with the main goal of maximum profitability of the development. The locally flexible well patterns of this project that globally adapted and warped different from the regular pattern sizes. The flexible well patterns are introduced by a well density function that honours subsurface geological properties. The well density function constructed is fed to an objective function with an embedded simulator, and the output represents the economic profitability of the given project. The objective function was optimised with a global optimisation algorithm that can capture the rather non-linear nature of the function with multiple local optima development strategies. Among them, a global optimum strategy is found. The **conclusions** of this thesis are presented by answering the research questions:

- **Is geothermal field development feasible on larger scales than what is currently applied?**

  This thesis suggests an introduction on a geothermal operation to a greater extent. The already suggested and applied field dimensions lie within the scale of 10s of km^2. This research proposes a wider application that falls in the range of 100s of km^2. The scale addressed here is 10*10 km and 10*20 km. The large-scale character enhances the profitability when operating thicker aquifers, so the NPV becomes higher. The current followed methodology proves that extensive fields could be brought into production. The 2D modelled aquifers introduced serve as a simplistic approach. Heterogeneity should be built up in small steps in order to comprehend and interpret the results.

- **What conditions make developments beyond well doublets desirable? Are well patterns used for oil and gas fields also applicable to geothermal field exploitation, and to what extent?**

  This research study attempts to bridge geothermal with oil and gas common development techniques. A proposal is made to introduce and expand oil and gas well pattern configurations for geothermal exploitation. The well patterns applied in geothermal operations already adopt a line-drive pattern, but further configurations are suggested in this study. Line drive and 5-spot pattern performance are compared, and it is inferred that 5 spot development strategy is more profitable. In all aquifer models tested, 5 spot prevailed over line drive in sweep efficiency while both configurations use the same number of wells. This fact had an impact on how profitable each development strategy proved to be. So the sweep efficiency is the driving factor that creates the discrepancy in the over-performance of the 5-spot over the line-drive pattern.

- **Can well patterns used for oil and gas field development be applied to geothermal field development, and if so, how could patterns adapt to local geological features?**

  This study constructed a flexible well density function that locally distorts regular well patterns. The flexible well density function is motivated by subsurface geological heterogeneity created by different depositional processes. Therefore, it is necessary to express properties like porosity or permeability in the form of a function that directionally expresses the modelled property trend. The geological property description function is converted into a well density function honouring production rules. For this study, pore volume fluid available controls the well density function and subsequently the number and location of wells necessary to operate the field. It was assumed that sweeping the great volumes of fluid in areas with higher porosity requires a relatively higher well density. A well density function was introduced that can increase or reduces the distance between wells (i.e. the pattern size) as a function of location in the field. The current methodology deals with directional parametrisation of heterogeneity and anisotropy.

- **How can a flexible well pattern development be modelled and what should be the controls and objective in optimizing the well pattern development?**

  An objective function is built that is fed with the well density function. The well density function is derived from a function that models a trend on a or more geological properties. So a basis of knowledge of the subsurface

is utilised. It is required the prior knowledge of any trend on different properties like porosity, permeability or heat capacity. When subsurface can be represented with a specific model, then a well density function can be developed. The well density function is fed to to the objective function. The objective function has an embedded simulator fed with the suggested pattern size and delivers energy recovery data. These are transformed to a full economic model under Dutch fiscal conditions. The profitability or net present value of the current development strategy is then addressed and set as the output of the function.

- **Is the well pattern problem optimisable, and can this be demonstrated in selected test cases?**

  The response surface of the objective function proposes a rather nor-linear behaviour with multiple local optima. The nature of the objective function for varying well pattern density (or well distance) suggests the need for a global, derivative-free, optimiser that cannot be trapped in local optima. These local optima that are observed, are introduced by the different wells and type of wells (injectors/producers) operating the field. The optimisation algorithm greatly depends on the number of controlling parameters of the well density function. The more parameters, the further tuning is required. More sampling points or more iterations required to find the global optimum development strategy render the experiments computationally expensive and time-consuming, even taking more than a day to conduct an optimisation run. The black-box nature of the function is an obstacle for fully tuning the optimiser to identify all local optima and, among them, the global optimum.

- **What is the performance of the selected optimizer, and how are results affected by properties of the reservoir model and by optimizer parameters?**

  Modelling and optimising large scale geothermal field development with the scope of proposing the optimal pattern size for different subsurface realisations is feasible but challenging. This strongly depends on the present geological complexity of potential geothermal targets. The more complex the subsurface, the more complex also becomes the set up of the well density function and the optimisation process of the objective function. The restrictions imposed on placing wells away from the boundaries of the licence area greatly impact the efficiency of energy recovered. Minor changes in these restrictions directly influence the number of wells that fit the field under a specific well density function.

8.2 Recommendations

This chapter discusses recommendations for future research based on the outcomes and uncertainties of the research done in this thesis.

- This research proved the applicability of adapting the density of well patterns in one direction locally. Further directions or more complex functions can be taken into consideration for future researchers. This implies considering more complex geological models.

- This research assumed known geology. In practice, permeability, porosity etc., will not be exactly known everywhere, which invites the idea of optimisation under uncertainty. This is typically done using multiple plausible geological realizations, which would pose serious challenges from a computational cost perspective on an optimization methodology. Optimising large scale developments under geological uncertainty is recommended to future researchers.

- Flexible well patterns should also consider flow patterns and thermal properties of the reservoir itself and enveloping layers, instead of only porosity variations to better adapt to realistic geological models.

- Further pattern types are suggested to be tested like 9-spot or 7-spot and compare their performance with the existing results.

- The negative outcome of the full economic model adopted in the sensitivity study motivates further tuning of the timing of introducing each expenditure type in the model. This implies a more flexible drilling strategy than the already adopted; thus, the concept itself could lead to an optimisation problem itself to develop the optimal profit of a project.

- In this approach, to keep things conceptually simple, we have assumed that all wells remain open as long as the produced temperature stays above injection temperature (i.e. always). This may not be economically attractive in practical applications if there are practical or economic top-side constraints on produced temperature. A more flexible approach to controlling over when to shut in wells is recommended.

- The capital initially available for a geothermal project is important to discuss. Having an A-amount to invest at the beginning of the project that would deliver B NPV is a different concept from having 2*A amount to invest at the beginning of the project that would deliver 4*B NPV. This concept directly implies the consideration of spreading development costs through time in order to avoid the lack of capital in the beginning of the project. Out strategy follows the second approach, thus focusing on the highest possible profits, but further investigation is required if there are funding constraints.

- The economic analysis of the current project attempts to incorporate realistic concepts on expenditures but simplistic approaches were adopted when costs presented variabilities or uncertainties due to market volatility. A more careful consideration of costs is suggested that aligns with reality and includes uncertainty of the market.
- Current optimisation strategy proves reliable in a small number of controls (1-2), but for more controls, further tuning of meta-parameters is required to ensure robustness in more complex geological models or well density functions fed to the algorithm. This could be implemented with surrogate models that behave in the same way as the adopted objective function. Further investigation of the behaviour and limitations of this optimizer will be needed.
- The optimisation experiments proved to be computationally and time expensive requiring extensive memory and time to run. A parallelisation of experiments would be more than advantageous.
- This project aimed to deliver a demonstration of the concept of optimisation of flexible well pattern designs for large geothermal developments. The flexible well pattern design results in spatial variability in the well density (or distance between wells), adapting to geological heterogeneity in reservoir and rock properties. Another approach could be to control the objective function with well rates which directly impacts NPV without introducing more wells in the project. Introducing more well, would sweep areas that are difficult to access but also comes this the cost of making the project more expensive, .Injecting more water can increase as well increase expenses but not at the same cost of wells. Generally speaking large companies prefer to drill a lot of wells right in the beginning of the project because it comes at a lower cost than drilling sporadically. Which strategy is better can be further investigated. Working with both pattern size and injection rates could be considered another optimisation strategy, and the context of optimisation needs further investigation.

Bibliography

Badru, O. & Kabir, C. (2003), 'Well placement optimization in field development. paper spe 8419 presented at the spe annual technical conference and exhibition, denver, colorado', *Denver, USA* .

Bouzarkouna, Z., Ding, D. Y. & Auger, A. (2013), 'Partially separated meta-models with evolution strategies for well-placement optimization', *SPE Journal* **18**(06), 1003–1011.

CBS Statline (2021), 'Natural gas and electricity, average prices of end users'.
URL: *https://opendata.cbs.nl/statline//CBS/nl/dataset/81309NED/table?fromstatweb*

Chen, B., Fonseca, R. M., Leeuwenburgh, O. & Reynolds, A. C. (2017), 'Minimizing the Risk in the robust life-cycle production optimization using stochastic simplex approximate gradient', *Journal of Petroleum Science and Engineering* **153**(April), 331–344.
URL: *http://dx.doi.org/10.1016/j.petrol.2017.04.001*

Crane, K. (2013), *Conformal geometry processing*, California Institute of Technology.

Crooijmans, R., Willems, C., Nick, H. M. & Bruhn, D. (2016), 'The influence of facies heterogeneity on the doublet performance in low-enthalpy geothermal sedimentary reservoirs', *Geothermics* **64**, 209–219.

Daniilidis, A., Alpsoy, B. & Herber, R. (2017), 'Impact of technical and economic uncertainties on the economic performance of a deep geothermal heat system', *Renewable Energy* **114**, 805–816.

Daniilidis, A., Nick, H. M. & Bruhn, D. F. (2020), 'Interdependencies between physical, design and operational parameters for direct use geothermal heat in faulted hydrothermal reservoirs', *Geothermics* **86**(September 2019), 101806.
URL: *https://doi.org/10.1016/j.geothermics.2020.101806*

De Boer, S., B. E. B. G. & et.al. (2016), Evaluatie algemeen instrumentarium geothermie, Technical report.

de Bruijn, E., Bloemendal, M., ter Borgh, M., Godderij, R. & Vossepoel, F. (2021), 'Quantifying the contribution of heat recharge from confining layers to geothermal resources', *Geothermics* **93**, 102072.

Endres, S. (2019), 'Simplicial homology global optimisation - github'.
URL: *https://stefan-endres.github.io/shgo/*

Endres, S. C., Sandrock, C. & Focke, W. W. (2018), 'A simplicial homology algorithm for Lipschitz optimisation', *Journal of Global Optimization* **72**(2), 181–217.
URL: *https://doi.org/10.1007/s10898-018-0645-y*

Endres, S. & Sandrock, C. (2021), 'Shgo documentation'.

Forouzanfar, F., Li, G. & Reynolds, A. C. (2010), A two-stage well placement optimization method based on adjoint gradient, *in* 'SPE annual technical conference and exhibition', Society of Petroleum Engineers.

Global Petrol Prices (2021), 'Netherlands natural gas prices'.
URL: *https://www.globalpetrolprices.com/Netherlands/natural*$_g$*as*$_p$*rices/*

Hatcher, A. (2002), 'Topology of numbers', *Unpublished manuscript, in preparation* .

Henderson, N., de Sá Rêgo, M., Sacco, W. F. & Rodrigues Jr, R. A. (2015), 'A new look at the topographical global optimization method and its application to the phase stability analysis of mixtures', *Chemical Engineering Science* **127**, 151–174.

Henle, M. (1994), *A combinatorial introduction to topology*, Courier Corporation.

ING Economics Department (2018), 'Focus on the Dutch climate challenge Insight into targets, certainties and uncertainties '.

Jones, E., Oliphant, T., Peterson, P. et al. (2016), 'Scipy: Open source scientific tools for python, 2001'.

Kahrobaei, S., Fonseca, R., Willems, C., Wilschut, F. & Van Wees, J. (2019), 'Regional scale geothermal field development optimization under geological uncertainties', *European Geothermal Congress* pp. 11–4.

Khait, M. & Voskov, D. (2018*a*), 'Adaptive parameterization for solving of thermal/compositional nonlinear flow and transport with buoyancy', *SPE Journal* **23**(02), 522–534.

Khait, M. & Voskov, D. (2018*b*), 'Operator-based linearization for efficient modeling of geothermal processes', *Geothermics* **74**, 7–18.

Kraft, D. (1994), 'Algorithm 733: Tomp–fortran modules for optimal control calculations', *ACM Transactions on Mathematical Software (TOMS)* **20**(3), 262–281.

Li, Z. & Scheraga, H. A. (1987), 'Monte carlo-minimization approach to the multiple-minima problem in protein folding', *Proceedings of the National Academy of Sciences* **84**(19), 6611–6615.

Mijnlieff, H. F. (2020), 'Introduction to the geothermal play and reservoir geology of the Netherlands', *Geologie en Mijnbouw/ Netherlands Journal of Geosciences* **99**.

Mijnlieff, H., Obdam, A., Kronimus, A. & Hooff, P. V. (2009), 'Inhoudsopgave'.

Ministerie van Economische Zaken en Klimaat (2019), 'Staatscourant van het koninkrijk der nederlanden, nr 9735'.
URL: *https://zoek.officielebekendmakingen.nl/stcrt-2019-9735*

Ministry of Economic Affairs and Climate Policy (2020), *Natural resources and geothermal energy in the Netherlands Annual review 2019*.
URL: *https://www.nlog.nl/sites/default/files/2020-11/annual*$_r$*eview*$_2$019$_n$*atural*$_r$*esources*$_a$*nd*$_g$*eothermal*$_e$*nergy*$_e$$n_1$8−11 − 2020*.pdf*

Ministry of Economic Affairs and Climate Policy (2021), *Pre-publication Chapter 8, Natural resources and geothermal energy in the Netherlands Annual review 2020*.
URL: *https://www.nlog.nl/sites/default/files/2021-03/pre-publ*$_c$*h8*$_y$*earbook*2020$_e$*n.pdf*

Onwunalu, J. E. & Durlofsky, L. J. (2009), 'Development and application of a new well pattern optimization algorithm for optimizing large-scale field development', *Proceedings - SPE Annual Technical Conference and Exhibition* **3**, 1926–1943.

Onwunalu, J. E. & Durlofsky, L. J. (2010), 'Application of a particle swarm optimization algorithm for determining optimum well location and type', *Computational Geosciences* **14**(1), 183–198.

Onwunalu, J. E. & Durlofsky, L. J. (2011), 'A new well-pattern-optimization procedure for large-scale field development', *SPE Journal* **16**(3), 594–607.

O'Sullivan, M. J., Pruess, K. & Lippmann, M. J. (2001), 'State of the art geothermal reservoir simulation', *Geothermics* **30**(4), 395–429.

Osundare, O. S., Teodoriu, C., Falcone, G. & Ichim, A. (2018), 'Estimation of plugging and abandonment costs based on different eu regulations with application to geothermal wells'.

Provoost, M., Albeda, L., Godschalk, B., van der Werff, B. & Schoof, F. (2018), 'Geothermal energy use, country update for the netherlands', *POLICY* pp. 3–1.

Rijksdienst voor Ondernemend Nederland (2019), 'Zon SDE+ na jaar 2019', (November).

Rijksoverheid (2019*a*), 'Climate Agreement'.
URL: *https://www.klimaatakkoord.nl/documenten/publicaties/2019/06/28/klimaatakkoord*

Rijksoverheid (2019*b*), 'Het Klimaatakkoord in (meer dan) 70 vragen'.

Roberts-Ashby, T. & Ashby, B. (2016), 'A method for examining the geospatial distribution of co2 storage resources applied to the pre-punta gorda composite and dollar bay reservoirs of the south florida basin, usa', *Marine and Petroleum Geology* **77**, 141–159.

Sarma, P., Chen, W. H. et al. (2008), Efficient well placement optimization with gradient-based algorithms and adjoint models, *in* 'Intelligent energy conference and exhibition', Society of Petroleum Engineers.

Savine, A. (2018), *Modern computational finance: AAD and parallel simulations*, John Wiley & Sons.

Schlumberger Oilfield Glossary (2021), 'Schlumberger Oilfield Glossary, Injection patterns'.
URL: *https://www.glossary.oilfield.slb.com/en/Terms/i/injection*$_p$*attern.aspx*

Schoof, F., van der Hout, M., van Zanten, J. & van Hoogstraten, J. (2018), 'Master plan geothermal energy in the netherlands', *Stichting Platform Geothermie: Delft, The Netherlands* .

Schoots, K. & Hammingh, P. (2019), 'Climate and energy outlook 2019', *The Hague: PBL Netherlands Environmental Assessment Agency* .

Sperner, E. (1928), 'Ein satz über untermengen einer endlichen menge', *Mathematische Zeitschrift* **27**(1), 544–548.

Stichting DAP (2021), 'Stichting DAP, DAP well'.
URL: *https://www.stichtingdap.nl/dapwell/*

Stichting Platform Geothermie (2019), 'Hoe duurzaam is aardwarmte?'.

Storn, R. & Price, K. (1997), 'Differential evolution–a simple and efficient heuristic for global optimization over continuous spaces', *Journal of global optimization* **11**(4), 341–359.

TNO (2019), 'Economic model (thermogis)'.
URL: *https://www.thermogis.nl/en/economic-model*

van den Bosch, R., Flipse, B. & Vorage, R. (2013), *Step-by-step plan for extracting geothermal energy for greenhouse horticulture*, Cash as Energy Source.

Van Dongen, B. (2019), The economic potential of deep, direct use geothermal systems in the netherlands, Master's thesis, Delft University of Technology.

van't Spijker (2016), 'Definition of Electro-submersible pump (ESP) design and selection workflow', (June), 1–38.

Voskov, D. V. (2017), 'Operator-based linearization approach for modeling of multiphase multi-component flow in porous media', *Journal of Computational Physics* **337**, 275–288.
URL: *http://dx.doi.org/10.1016/j.jcp.2017.02.041*

Wales, D. J. (2015), 'Perspective: Insight into reaction coordinates and dynamics from the potential energy landscape', *Journal of Chemical Physics* **142**(13).
URL: *http://dx.doi.org/10.1063/1.4916307*

Wales, D. J. & Doye, J. P. (1997), 'Global optimization by basin-hopping and the lowest energy structures of lennard-jones clusters containing up to 110 atoms', *The Journal of Physical Chemistry A* **101**(28), 5111–5116.

Wales, D. J. & Scheraga, H. A. (1999), 'Global optimization of clusters, crystals, and biomolecules', *Science* **285**(5432), 1368–1372.

Wang, Y., Khait, M., Voskov, D., Saeid, S. & Bruhn, D. F. (2019), 'Benchmark test and sensitivity analysis for Geothermal Applications in the Netherlands', *PROCEEDINGS, 44th Workshop on Geothermal Reservoir Engineering* **2**, 1–11.
URL: *https://pangea.stanford.edu/ERE/db/GeoConf/papers/SGW/2019/Wang6.pdf*

Wang, Y., Voskov, D., Khait, M. & Bruhn, D. (2020), 'An efficient numerical simulator for geothermal simulation: A benchmark study', *Applied Energy* **264**(October 2019).

Willems, C. (2017), *Doublet deployment strategies for geothermal Hot Sedimentary Aquifer exploitation.*

Willems, C. J. & Nick, H. (2019), 'Towards optimisation of geothermal heat recovery: An example from the West Netherlands Basin', *Applied Energy* **247**, 582–593.
URL: *https://doi.org/10.1016/j.apenergy.2019.04.083*

Willems, C. J., Nick, H. M., Goense, T. & Bruhn, D. F. (2017), 'The impact of reduction of doublet well spacing on the Net Present Value and the life time of fluvial Hot Sedimentary Aquifer doublets', *Geothermics* **68**, 54–66.
URL: *http://dx.doi.org/10.1016/j.geothermics.2017.02.008*

Willems, C. J., Nick, H. M., Weltje, G. J. & Bruhn, D. F. (2017), 'An evaluation of interferences in heat production from low enthalpy geothermal doublets systems', *Energy* **135**, 500–512.
URL: *http://dx.doi.org/10.1016/j.energy.2017.06.129*

Willems, C. J., Vondrak, A., Mijnlieff, H. F., Donselaar, M. E. & Van Kempen, B. M. (2020), 'Geology of the Upper Jurassic to Lower Cretaceous geothermal aquifers in the West Netherlands Basin - An overview', *Geologie en Mijnbouw/Netherlands Journal of Geosciences* **99**, 1–13.

Zaal Caroline (2020), Geothermal Field Development Strategies Based on Economic and Fault Stability Analysis, Master's thesis, Delft University of Technology.

Zaken, M. V. E. (2020), 'Alternatives to the gas reference price', (January).

Zhang, K., Chen, Y., Zhang, L., Yao, J., Ni, W., Wu, H., Zhao, H. & Lee, J. (2015), 'Well pattern optimization using NEWUOA algorithm', *Journal of Petroleum Science and Engineering* **134**, 257–272.
URL: *http://dx.doi.org/10.1016/j.petrol.2015.02.017*

Zhang, K., Li, G., Reynolds, A. C., Yao, J. & Zhang, L. (2010), 'Optimal well placement using an adjoint gradient', *Journal of Petroleum Science and Engineering* **73**(3-4), 220–226.